UNIVERSITÀ DI PARMA

UNIVERSITY OF PARMA

PhD in Biotechnology and Life Science

XXXII COURSE

Effects of metal-based nanomaterials on gametogenesis in different model organisms

Coordinator:
Prof. **Simone Ottonello**

Supervisor:
Prof. **Nelson Marmiroli**

Tutor:
Prof. **Roberta Ruotolo**
Prof. **Marta Marmiroli**
Prof. **Luca Pagano**

Candidate: **Riccardo Rossi**

2016/2019

Summary

Abstract

Nanotechnology is a rapidly growing field having potential applications in many areas. Metal-based nanoparticles (NPs), in particular, are receiving increased importance due to their diffuse industrial, medical, consumer and military applications. However, as particle size decreases, some metal-based NPs are presenting increased toxicity, even though the same material is relatively inert in its *bulk* form. One of the main concerns of these NPs is their potential genotoxicity, but the molecular mechanisms of action are still not well understood.

During the first part of my PhD in Biotechnology and Life Sciences, I studied the effect of a particular kind of NPs, Cadmium Sulfide Quantum Dots (CdS QDs), in the yeast *Saccharomyces cerevisiae*, focusing my research on the process of gametogenesis (called "sporulation" in yeast).

The presence of CdS QDs in the sporulation medium causes an alteration of the meiotic nuclear divisions in combination with a strong inhibition of spore morphogenesis, resulting in the formation of asci containing the meiotic products, but with the absence of refractile spores. The same effect was not seen using other types of metal-based NPs (ZnO, CuO, CeO_2) or a cadmium salt ($CdSO_4$). To determine whether the morphological alterations induced by QDs were accompanied by a transcriptional reprogramming of the gametogenesis process, a set of specific sporulation genes was analyzed by Real time PCR. In accordance with the phenotypic effects observed in response to CdS QD exposure, we found a down-regulation of regulatory genes expressed in the early-middle phase of the sporulation process and their downstream transcriptional targets.

Analysis of DNA content by Fluorescence-activated cell sorting (FACS) showed that sporulated cells exposed to CdS QDs presented an altered DNA content profile, in line with the phenotypic observations obtained by fluorescence microscopy.

To better understand the molecular mechanisms involved in NP effect in the sporulation process, we have studied and analyzed the composition of the “protein corona” formed on the surface of CdS QDs. Proteins corona have an important role in biological activity and environmental fate of metal-based NPs. NPs are known to selectively adsorb proteins, to form a ‘corona’ bound tightly to their surface. Corona proteins which show a high affinity for the NP surface are exchanged slowly, and these so-called “hard” proteins form the innermost layer.

To investigate if the formation of hard corona proteins is linked to the effects seen on gametogenesis, proteins were extracted from cells during sporulation and incubated with CdS QDs. Unbound proteins were removed and hard corona proteins were subjected to liquid

chromatography–mass spectrometry (LC-MS/MS) for protein identification. The most abundant protein found in the analysis are involved in the energetic metabolism and cell wall synthesis, the modulation of this proteins by the presence of CdS QDs suggests that energy metabolism is impaired by the ENP-induced stress, and could be a reason of the phenotypic observations.

The second part of this work has been done in collaboration with the Connecticut Agricultural Experiment Station (CAES, New Haven, CT, USA). In this case, my research was focused on another eukaryotic system, studying the physiological and molecular effects of different types of metal-based engineered nanomaterials (ENMs) on plant gametogenesis, with regards to the potential consequences on plant productivity of the crop *Cucurbita pepo* L. (zucchini). Literature is giving increased relevance to the beneficial effects that some ENMs may have on edible plants when used as fertilizer or pest control agents. However, the lack of knowledge to the potential environmental effects and health risks are still limiting the widespread commerce and application of ENMs. The ENMs taken into consideration in this project, together with their bulk counterparts, have potential application in agriculture as nanofertilizers or nanopesticides (CeO2, CuO). The study is performed in soil in order to bring to completion of the entire life cycle of the plants. The ENM concentrations used in the study are chosen to maximize the response, without hampering the complete plant growth and flower development. All of the treatments at the concentration tested showed no significant changes in the root or total plant biomass, as well as the morphological analysis of pollen performed by Environmental Scanning Electron Microscopy and pollen viability did not evidence any differences.

Inductively coupled plasma mass spectrometry (ICP-MS) analysis of metal content in flowers showed that Copper can translocate to the flowers, both in the bulk or in the nano form. Cerium content found in zucchini flowers is considerably lower than Copper, in agreement with past results showing a very low ability of Cerium to reach apical parts of the plant.

The main focus was placed on CuO NPs, performing a complete transcriptomic analysis of different plant organs and tissues in zucchini. Total RNA from roots, leaves and pollen of Zucchini treated with CuO NPS, CuO bulk and a salt form of copper was extracted and the samples were sent to IGA Technologies Services (Udine) for RNA-seq analysis. The preliminary results obtained from transcriptomic analysis in pollen showed a common response between the treatments performed, probably due to the physico-chemical properties of the materials. On the other hand, a side of the response can be considered more nano-specific and related to those mechanisms interested in oxidative stress prevention.

Introduction

Nanotechnologies

Nanomaterial (NM) is defined by the International Organization for Standardization (ISO) as a material with at least one external dimension on the nanoscale, or having an internal or surface structure in the nanoscale (ISO 2015). The nanoscale range is comprise between 1 and 100 nanometers (nm). Nanoparticles (NPs) are nanomaterials with all of three external dimensions on the nanoscale and with similar lengths between them. Other terms are adopted when dimensions are too dissimilar, generally higher than a factor of three: nanoplate (only one dimension in the nanoscale) or nanofiber (two external nano-dimensions). Size is the main factor to classify a NM, however, particulate materials can include particles with dimensions above 100 nm. Because of the reactivity of NPs, primarily due to their high surface to volume ratio, larger clusters often result from aggregation of NPs, and in several cases, the size distribution of NMs comprise a wide length range (EFSA 2018). To furnish a common regulatory basis within the EU areas, and considering the scientific and technological development, in 2011 the European Commission released a Recommendation for a definition of a NM. As stated in that recommendation, NM can be a natural, incidental or manufactured material including particles as an aggregate or in an unbound state, in which at least 50% of the particles have one or more external dimension in the nanoscale range. In particular conditions of environmental or health concern, the threshold of 50% may be reduced between 1 and 50% (EFSA 2018). In accordance with the definition, a first classification of engineered nanomaterials (ENMs) and non-engineered nanomaterials can be performed due to their natural or manufactured source. The first group comprise all the NMs produced by geological (e.g. chemical and physical degradation of rock materials, volcanic eruptions, neoformation) or biological processes. The ENMs are man-made nano-structures, designed to meet specific proprieties and characteristics and are synthesized through technological process. NMs have specific physico-chemical properties (optical, dielectric, of density, magnetic and mechanic resistance) and are now used in several areas such as electronics, pharmaceuticals, environmental analysis and remediation, biomedicine, cosmetics, catalysis and material sciences. For these reasons, the global market for nanocomposites totalled $2.0 billion in 2017 and is estimated to reach $7.3 billion by 2022, growing at a compound annual growth rate (CAGR) of 29.5% for the period of 2017-2022 (BCC report 2018). Several classifications for NMs are proposed based on their dimensions, on their origin, or most typically, by material:

- Carbon-based NMs: usually, these NMs include carbon, and have structures as hollow tubes, spheres or ellipsoids. Fullerenes (C60), carbon nanofibers, carbon nanotubes (CNTs), carbon black, graphene (Gr), and carbon onions are comprised in this group.
- Inorganic-based NMs: these NMs comprise metal and metal oxide NPs and nanostructured materials (NSMs).
- Organic-based NMs: NMs derived principally from organic matter, except for carbon-based or inorganic-based NMs.
- Composite-based NMs: multiphase NPs and NSMs with one phase on the nanoscale dimension that can either associate with other NPs bound with bulk materials (e.g. hybrid nanofibers) (Jeevanandam *et al. 2018*).

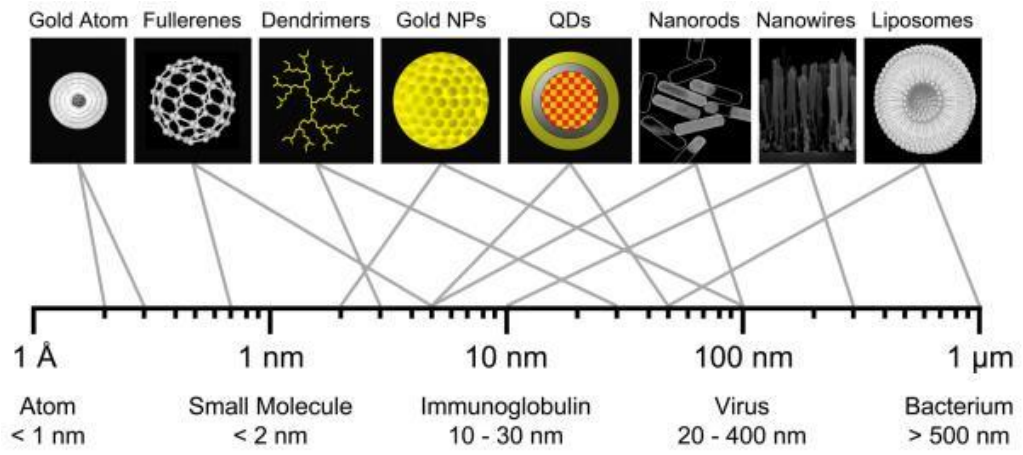

Figure 1. Relative Sizes of Nanoparticles: Hydrodynamic diameter (HD) ranges for nano-scale materials and naturally-occurring materials.

Engineered nanomaterials and risk assessment

NPs and NSMs represent a dynamic area of research and an economic field in great expansion in different application domains. ENMs have received increased importance in technological advancements due to their peculiar and tunable physicochemical characteristics such as electrical and thermal conductivity, melting point, light absorption and scattering, wettability, catalytic

activity, resulting in improved efficiency over their bulk analogues (Jeevanandam *et al*. 2018; Wani *et al.* 2017). Thus, the exposed population to ENMs keep growing as their application expands. On the other hand, because of their specific properties, their fate and mechanism of action are generally dissimilar from the ones of their bulk analogues. Toxicity of ENMs is based on several factors:

- Particle size effect: NPs exhibit size-dependent toxicity.
- Dose and exposure time effect: the concentration of NPs in the external medium and the time of exposure are directly correlated to the number of NPs that enter the cells (Buzea *et al.* 2007).
- Aggregation and concentration-effect: increasing the NP concentration seems to improve aggregation. NP aggregates can be micron-scale in size, so this aggregates may not penetrate cells and lose their toxicity.
- Surface area effect: generally, the toxicity of NPs increased as the particle size decreased.
- Particle shape effect: NPs exhibit shape-dependent toxicity.
- Functionalization: the surface properties of NPs can have extreme consequences relating to NPs translocation (Oberdörster *et al.* 2005).

Synthesis, utilization and disposal of products including NPs are the principal causes for the release of nanoparticulates in the environment. At the production level, the respiratory system is the major exposure way for ENMs (Borm *et al. 2006;* Savolainen *et al. 2010;* Shvedova *et al. 2005*) for workers. In the respiratory system, the particles size has a bigger impact on their systemic accumulation in the lungs or distribution in the body (Kreyling *et al. 2009*). The aerosol form, in fact, is the easiest way for entrance of the ENM, whereby they can reach the alveolar region. Consumer exposure to ENM has usually been evaluated less dangerous than workers exposure due to reduced concentrations and shorter time of exposure. Potential routes of exposure for consumers are dermal (use of cosmetic products), inhalation (for example spray products), while exposure by ingestion could become more frequent as the use of ENMs in food and food package materials is expanding (Dekkers *et al. 2016;* Vance *et al. 2015*).

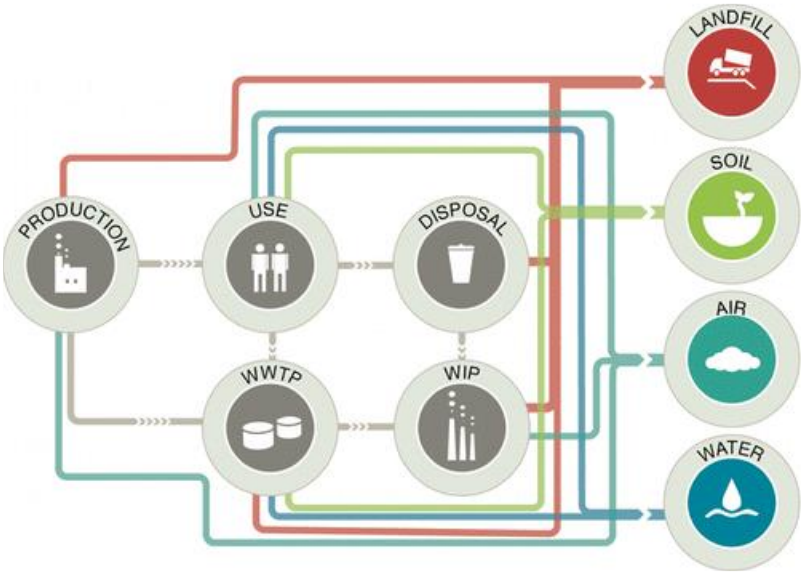

Figure 2. Routes of exposure and dispersion of ENMs in the environment (Keller *et al*. 2013).

Nanotoxicology and nanomaterial regulation

Nanotoxicology is a research field studying the interactions between NMs and biological matters at scales ranging from molecules, macromolecular complexes, organelles, cells, to whole organisms, such as animals or plants. The unique physicochemical characteristics of NMs may determine health benefits but could also be related to harmful consequences on cells and tissues, interfering with vital cell functions, resulting in toxicity. Some ENMs, such as metal-based NPs, can promote chromosomal fragmentation, DNA strand breaks or point mutations, or alterations in gene expression. The study of the genetic effects of ENMs is known as "geno-nanotoxicology." ENM toxicity is an emerging subject because the mechanisms and of nanotoxicity are not entirely testable or predictable with common toxicology tests, but the comprehension of this bio-nano interaction is essential for the safe and design of NMs for their different applications. Interactions between ENMs and cells, through unspecific contacts or ligand receptor interactions, along with the intracellular mechanisms involved in the distribution of these materials inside the cell, need better characterization (Silva *et al. 2016*). The physicochemical properties of ENMs and their interactions with an organism can induce divergent consequences. These interactions, indeed, define the stability, biocompatibility and side effects of ENMs (Marmiroli *et al.* 2019). In this context of risk characterization and analyses, nanotoxicology could be an important tool for the investigation of

the effect of ENMs on biological organisms. In recent years, ENMs risks have been tested using both *in vitro, in vivo* and in *silico* techniques. Considering the widespread diffusion of ENMs, their physical and chemical diversity as well as the urgency to reduce the use of animals, the identification of testing platforms alternative to the expensive and ethically questionable testing strategies becomes crucial. Amongst the key improvements in this new toxicology, vision is the widely accepted 3Rs principle, which aims to replace, reduce, and refine animal testing (Burden *et al. 2017*). The in vitro tests comprehend the use of single cells type cultures, co-cultures, three-dimensional models of tissues and cell- free assays (Stone *et al. 2016*), usually from humans but also other mammals. To limit the number of in vivo tests, not only mammalian cell lines can be utilized but also alternative whole model organisms. Due to their easy use as molecular tools for toxicological screening, simplicity but also genetic similarity with higher organisms, eukaryotic model systems widely employed for nanotoxicity tests are for example the yeast *Saccharomyces cerevisiae* and the nematode *Caenorhabditis elegans*. Model plants such as *Arabidopsis thaliana*, or crop plants such as *Cucurbita pepo* and *Oryza sativa* are used for ecotoxicological studies (Marmiroli *et al. 2015;* Pagano *et al. 2016*). In the next years, in vitro assessments or the application of nonmammalian organisms may provide specific information and novel insights concerning the toxicity mechanisms of ENMs. However, although animal testing should be reduced to a minimum, in vivo studies are still fundamental to comprehend a set of effects connected to the whole organism, such as the distribution of the ENMs between different organ systems or the potential accumulation of the NPs in the body. Furthermore, mammalian models are crucial to determine any dosimetry limit. A method to deduce several NPs characteristics, like the toxicity of newly designed NPs, are in silico models. Computational techniques, and in particular (Quantitative) Structure-Activity Relationship ([Q]SAR) modelling, give hazard estimations, crucial for risk assessment. The basic idea of (Q)SAR model is that, when the structural properties (descriptors) are known for a group of compounds, but the experimental activity data are accessible just for a part of them, it is possible to create a mathematical model based on the available data and deduce the unknown activities for the remaining compounds (Dearden *et al.* 2017; Cherkasov *et al.* 2014). Moreover, omics tools, such as genomics, proteomics, transcriptomics, and metabolomics, can be coupled with computational approaches (bioinformatics) to identify pathways that can be quantitatively modelled.

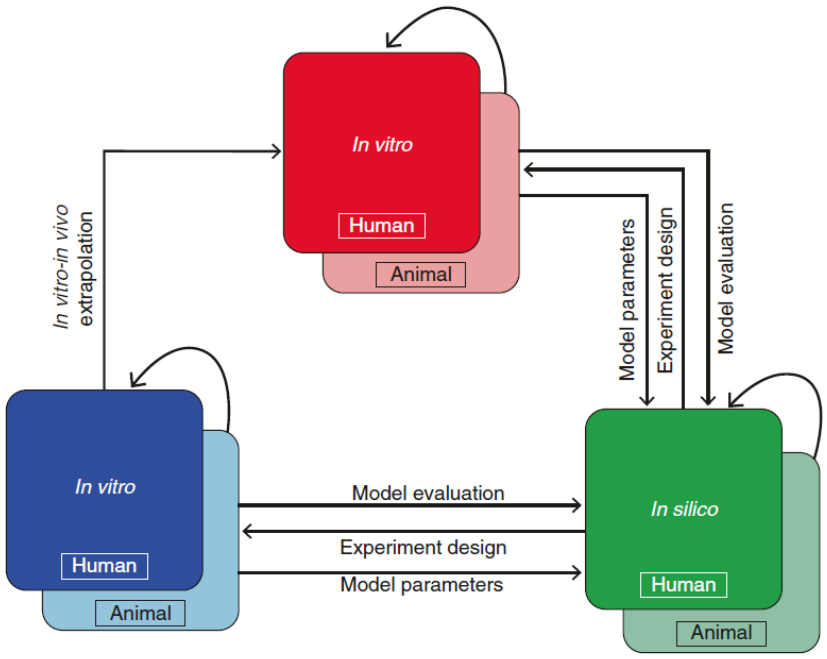

Figure 3. Correlation among in vivo, in vitro and in silico investigations (Saquib *et al.* 2012)

Transcriptomic profiling is useful in toxicogenomics as a discovery tool for identifying the biochemical mechanisms underlying compensatory responses to xenobiotics, the potential mechanisms of toxicity, and the biomarkers for drug safety evaluation. Microarrays are still an elective technology for transcriptome profiling, though emerging alternatives is the utilization of next-generation massively parallel sequencing (NGS) to sequence and count transcripts directly from samples (RNAseq or digital transcriptomics) (Wang *et al.* 2009). In the EU, NMs are protected by the same regulatory framework that establishes the utilization of all chemicals, the REACH and CLP regulations. This implies that risk assessment of nanoforms still have to be assessed and their safety needs to be ensured.

Synthesis of engineered nanomaterials

ENMs are prepared by a plethora of different methods that can be classified in different ways. One of the classifications, top-down/bottom-up, is based on the "size" of the starting material. Top-down methods start with bulk materials and are shattered or etched until reaching sizes in the nanorange.

These are mainly based on physical phenomena including attrition, milling, and laser ablation (Marmiroli *et al.* 2019). Various methods of lithography are used in the top–down approach, including serial and parallel techniques for patterning two-dimensional nanoscale features, but also scanning probe lithography, nanoimprint lithography and block co-polymer lithography (Gates *et al.* 2005*;* Mailly *et al.* 2009). Bottom-up strategies are based on physical and chemical processes to build up from atoms or molecules to crystals and NMs. These include chemical synthesis, self-assembly, positional assembly, and lithography (Fig. 4). Chemical synthesis is mainly carried through sol-gel, oxidation-reduction, and biological processes. To produced zero-dimension NPs, dimensional synthesis uses homogenous and heterogeneous nucleation, and kinetic confinement (Ariga et al. 2008).

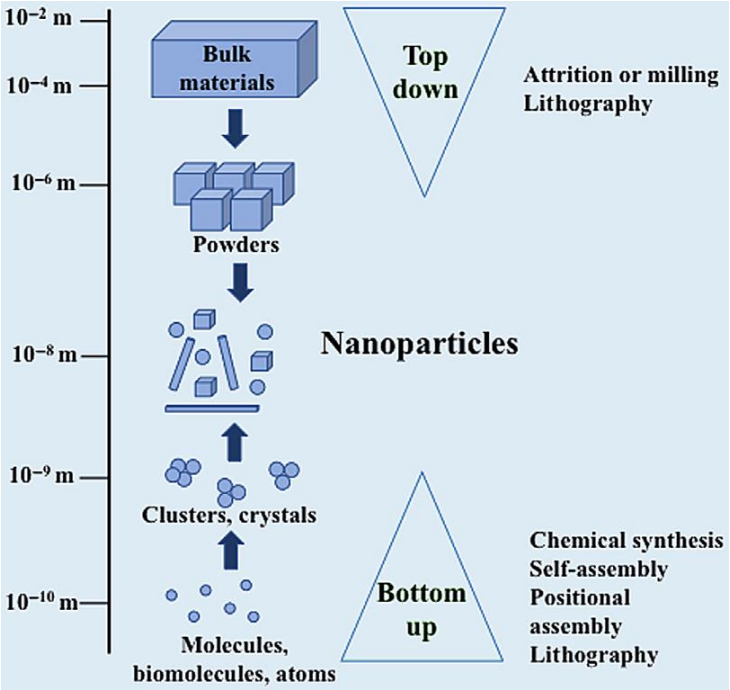

Figure 4. Engineered NMs can be fabricated starting with bulk materials (top-down) or by chemical reactions (bottom-up) (Marmiroli *et al.* 2019).

Quantum dots

The term “quantum dot” (QD) was used to describe nanocrystalline semiconducting fluorophores, composed by metals belonging to groups II-V or III-V of the periodic table, with a typical size of 2-20 nm. They are double systems containing a core of semiconducting material surrounded by a shell formed by another material. QD fluorescence is related to the bandgap between the valence and the conduction electron bands, and absorption of a photon higher in energy than the spectral bandgap of the core semiconductor results in electron excitation to the conduction band, generating an electron-hole pair. Because of the physical size of the bandgap determines the photon’s emission wavelength, it is possible to achieve the fluorescence wavelength by the NP size (Cheki *et al.* 2013). Thanks to the to their narrow emission waveband, high photostability, intense fluorescence and broad UV excitation, QDs find applications for tracking of intracellular process, in vitro bioimaging and real time monitoring (Bailey *et al.* 2004). Moreover, they can be coupled with ligands and applied as highly sensitive probes (Oh *et al.* 2016). Because of their tuneable absorption spectrum and the high extinction coefficient, QDs have application in the production of new generation aerogel components of photovoltaic panels (Xing et al. 2016). They are also exploited in the production of batteries, high resolution led screens and precision tunable lasers (Zhai *et al.* 2010).

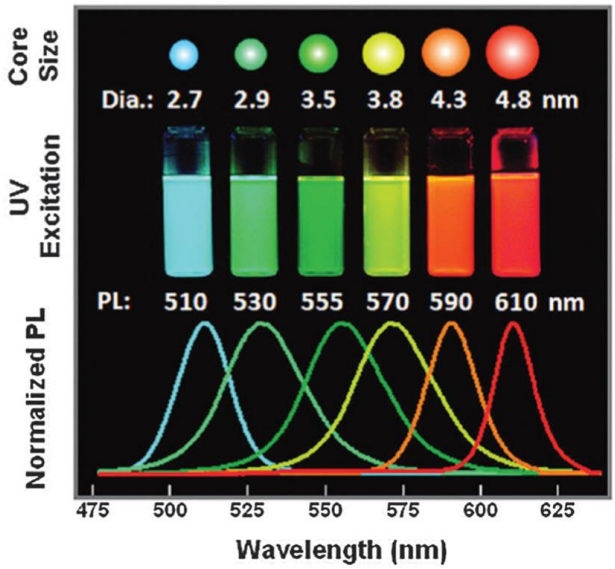

Figure 5. Schematic representation of the “quantum confinement” effect on the energy level structure of a semiconductor material. The larger band-gap energy of smaller QDs of the same material leads to lower PL wavelengths (large QDs are red and small QDs are blue). Copyright 2011 American Chemical Society.

The Cadmium sulfide quantum dots (CdS QDs) used in this study were synthetized by IMEM-CNR (Istituto dei materiali per l'Elettronica e il Magnetismo, Parma, Italy). CdX (X = S, Se, Te) QDs are part of the group II-VI QDs. They were synthetized through a wet-chemistry approach, according to Villani *et al.* 2012, Cadmium acetate 99,99% ($Cd(CH_3CO_2)$), N,N-dimethylformamide 99% (HCON(CH3)2) and thiourea 99.5% (NH2CSNH2). These QDs have an average diameter of 4-5 nm, a density of 4,82 g cm^{-3} and an average weight of 2,5 10^{-18} g. They have the crystal structure of wurtzite (Villani *et al.* 2012). CdS QDs, as one of the most widely used quantum dots, have demonstrated their great performances both *in vitro* and *in vivo* imaging. Still, the toxicity of QDs, widely limits the applications of these NPs and is one of the most important issues that should be evaluated when analyzing the potentials of these materials (Fan *et al.* 2016). A number of publications have indicated contradictory results concerning the mechanisms of Cd-based QDs toxicity: several studies primarily explain the CdS QDs toxicity to the release of Cd^{+2} ions upon oxidation of particles surface (Derfus *et al.* 2004) but under other circumstances, particle characteristics like shape and size seem to be more relevant (Wu and Tang 2014; de Carvalho *et al.* 2017; Marmiroli *et al.* 2014, 2016). Moreover, the importance of exposure duration on Cd-based QDs toxicity is poorly known (Oh *et al.* 2016; Yan *et al.* 2019). To date, few studies have explored and compared the influence of CdS QDs and Cd ions on whole organisms, organs, as well as tissues and cellular structures (Wang and Tang 2018; Rocha *et al.* 2017; Majumdar *et al.* 2019). Marmiroli *et al. (*2014*)* compared the effects of CdS QD treatment on wild type (wt) and two mutant strains of *Arabidopsis* , *atnp01* and *atnp02*. The mutants were selected because of their tolerance to CdS QDs at concentrations that significantly affect the growth of the wild type. It was shown that *atnp01* and *atnp02* had a different response between them and to the wt, and the tolerance response was characterized at a proteomic and transcriptomic level (Marmiroli *et al*. 2015). Paesano *et al*. (2016) defined the cytotoxic and genotoxic effect of CdS QDs on HepG2 cells to highlight the mechanisms associated in the cellular response and to determine potential markers of exposure. Fan *et al.* (2016) explored the biological mechanism of QDs induced toxicity *in vitro* and *in vivo*. It was shown that QDs could induce toxicity in different human cell lines, where autophagy was induced by the production of ROS. Furthermore, injection of Cds QDs caused liver injury, nephrotoxicity, splenic injury, and hematopoietic disorders in mice.

Metal oxide nanoparticles

Metal oxide NPs are one of the most extensively used ENMs for industrial applications. The large heterogeneity of oxide compounds available for their synthesis together with the ease of tunability and modification of their chemical and physical characteristics, makes them applicable for use in construction materials (e.g. paint, insulators, semiconductors; Lee *J.et al.* 2010), agriculture (e.g. CuO and ZnO used as biocides, Bondarenko *et al. 2013*), in the biomedical field (e.g. antibacterial iron oxide NPs, Javanbakht *et al. 2016*) and cosmetics (e.g. ZnO and TiO_2 used in sunscreen, Lu *et al. 2015*). Metal oxide NMs have a large variety of different properties, so that it might be complex to have a comprehensive conclusion on the material toxicity. Even for the same compound and same testing protocols, different results on toxicity could be obtained. In particular, the NM surface properties are extremely important factor affecting their toxicity and interaction with living organisms (Djurisic *et al. 2015).* The toxicity of metal oxide NPs is principally associated with the dissolution of the metal ion from the NP when in contact to cells or biological fluids. The entry through endocytosis can exert greater toxicity to the cell if compared to non-endocytosis internalization. The cells transport the metal oxide NPs to the lysosome and metal ions can be released in the cytoplasm as a consequence of to the acidic pH of the lysosome, interact with proteins and generate superoxide radicals (Sabella *et al.* 2014). The generation of reactive oxygen species (ROS) can lead to a plethora of consequences, depending on several factors (for example the metal, the organism, the localization inside the cell, the concentration and the size of the NPs).
Zinc oxide (ZnO) NPs are one of the most used semiconductor metal oxide which exhibits several applications like ultra violet light (UV) blocking property, photocatalytic and antibacterial properties (Chang *et al* 2012). The cytotoxicity and genotoxicity potential of ZnO NPs has been shown both in vitro and in vivo (Popov *et al.* 2010). ZnO NPs reduced cell viability in a time-dependent and dose-dependent way. ZnO NPs also enhance the expression of the metallothionein gene, which is recognized as a biomarker in metal-induced toxicity (Gao *et al.* 2017).
Titanium oxide (TiO_2) NPs are widely used as a thickener, a pigment, and a UV absorber in skin care and cosmetic products. Several studies have shown in vitro cytotoxicity and genotoxicity of TiO_2 NPs in different cell lines, plants, and brains of mice via oral administration (Sahu *et al.* 2014; Smijs *et al.* 2011).
Synthetic amorphous silica has been used as a common food additive for decades. It is extensively utilized to processed foods and registered by the European Union as a food additive with the code

E551. The toxicity of amorphous SiO_2 NPs on human lung submucosal cells is correlated with inflammation, release of ROS inducing to apoptosis, and decreased cell survival (McCarthy *et al.* 2012). The decreased viability of human epithelial cell line exposed to SiO_2 NPs was demonstrated in a time-dependent and concentration manner (Seabra *et al.* 2015).

Iron oxide NPS, such as magnetite (Fe_3O_4) and hematite (Fe_2O_3), have some relevant industrial and biomedical applications (Haddad et al. 2012). The toxicity of iron oxide NPs can be due to the ROS induction of oxidative stress (Wu *et al.* 2014), and it is determined by the particle surface, size distribution and the zeta potential (Seabra *et al.* 2014).

Copper oxide (CuO) NPs are a semiconductor metal with specific electrical, magnetic and optical properties and it has been applied for several applications, for example the production of batteries, high temperature superconductors, catalysis, gas sensors, field emission emitters, solar energy converters, etc. (Grigore *et al.* 2016). CuO NPs have also biological applications, such as antimicrobial agents for preservation of wood, antifouling paints, agricultural biocides. CuO NPs can interact with the negatively charged cell wall of microorganisms, get internalized and cause several negative effects on DNA, membranes and other organelles (Hou *et al.* 2017). Lately, CuO NPs are evaluated as promising candidates for agrochemical fertilizer to increase plant production, due to its beneficial effects in plant photosynthesis (Wang *et al.* 2019; Adhikari *et al.* 2016). Cu is also an essential plant micronutrient, promoting growth as well as defence in response to pathogenic infections (Elmer *et al.* 2018). Cu is a cofactor for three important proteins: peroxidases, plastocyanins and multi Cu oxidases (Evans et al. 2007). Besides its toxicity to microorganisms, several studies reported toxicity of CuO NPs in different organisms. In human cell lines, CuO NPs induced the production of ROS and decreased cell viability (Karlsson *et al.* 2009), there are also several studies on CuO NPs toxicity exerted on neuronal cell lines and Alzheimer disease (Ryu *et al.* 2008).

Cerium oxide (CeO_2) NPs, also known as nanoceria, are extensively used as semiconductors in solar cells, UV blockers, polishing agents and their photocatalytic properties are exploited in chemical and mechanical cleaning methods (Balavi *et al*. 2013). The increased use of nanoceria and the consequent risk of exposure makes a priority to test its toxicity. Contradictory results were found concerning the toxicity of nanoceria and the valance state of Ce atoms in the nano preparation may be the cause of differential outcomes. The transition of Ce^{+4} to Ce^{+3} generates subsequent oxygen vacancies, producing superoxide anions which further originates hydroxyl ions that are toxic to cells; whereas, Ce^{+3} can react with hydroxyl ions and behave as an antioxidant. In this manner, the

oxidation state of Ce in CeO_2 NPs can determine if it will exert a toxic or protective effect to the cells (Dunnick *et al.* 2015).

Cucurbita pepo as a model organism for nanomaterial exposure in crop plants

Cucurbita pepo L. is a plant belonging to the family of Cucurbitaceae. It is the most cultivated species of pumpkin and is considered a great dietary source of vitamins, minerals and fibres (Obrero *et al.* 2011). The production of *C. pepo* reached 27.5 million tons in 2017, with more than 2 million cultivated hectares (http://www.fao.org/faostat/en/#data/QC/visualize). Different varieties exhibit a great diversity of flowering and fruit qualities, and between them, cultivars of the zucchini group are one of the most worldwide value crop (Formisano *et al.* 2012). Despite the agronomic importance of the species, before 2017, few genetic and genomic resources were accessible. Montero-Pau *et al.* (2017) firstly presented a complete description of the zucchini genome: its size is 263 Mb, organized in 20 pseudomolecules and 34240 predicted gene models, of which 27780 are protein coding genes. Moreover, the *C. pepo* genome is most likely the result of a whole-genome duplication (WGD). Despite the WGD, the size of the zucchini genome is comparable to other sequenced cucurbits, and the number of genes is similar. This indicates that most genes were deleted after the WGD event. Due to its popularity and massive distribution, in recent years *C. pepo* is obtaining an increasing interest as a model organism for toxicology and nanotoxicology studies: Stampoulis *et al. (2009)* reported that Cu NPs reduced emerging root length by 77% and 64%, compared to untreated control and bulk Cu treatment; Musante and White (2012) showed that Cu and Au NP treatments in *C. pepo* result in a decrease in biomass and transpiration; E. Xun *et al.* (2017) presented that squash could translocate Cu into its floral organs and could potentially affect the pollen viability. In the same way, Cu NPs can reach the edible part of the plant, with no harmful effects observed (C. Tamez *et al.* 2019). Recently, the focus is mainly on the transcriptional response after ENMs exposure (Pagano *et al.* 2016*;* Pagano *et al.* 2017), however, most studies have only examined metal accumulation in vegetative organs of plants, in spite of the evidence that flowering plants usually spend more defensive responses in their reproductive organs (Brown *et al.* 2003).

C. pepo is a monoecious species, with distinct male and female flowers on the same plant. Early in development, the plant produces male flowers in the node axis and only after several cycles of male flower development, the female flowers grow in the following nodes (Carvajal *et al.* 2013). The

pollen grain in *C. pepo* is bicellular, with a generative cell enclosed inside the vegetative cell (Digonnet-Kerhoas *et al.* 1989). The mature pollen grain is spherical, with a diameter of 180–200 µm, and has 12 operculate pores covered by the intine or inner wall and a resistant outer wall or exine. Male gametogenesis requires many specific genes for the production and release of pollen grains for germination. Several genes specifically expressed during male gametogenesis have been identified in different plants, like petunia and willow (Futamura *et al.* 2000*;* Garrido *et al.* 2006). In *Arabidopsis* , many pollen-specific genes have been isolated using various molecular approaches (Da Costa-Nunes & Grossniklaus 2003; Becker *et al.* 2003; Honys & Twell 2003). Excessive metal accumulation in aboveground tissues of plants not adapted to soils with elevated heavy metals might negatively affect plant reproductive success through decreasing pollen and seed viability or seed production (Vogel-Mikuš *et al.* 2007; Breygina *et al.* 2012). Because of poor data of metal translocation into flowers (Meindl and Ashman *2014*; Meindl *et al.* 2014a*,* 2014b*;* Sánchez-Mata *et al.* 2014), it is unclear what fitness repercussion may emerge from non-hyperaccumulator plants that are capable of translocating heavy metals to their reproductive organs.

S. cerevisiae as a model system for the investigation of ENMs toxicity during gametogenesis

S. cerevisiae is considered as one of the most commonly used model systems, representing a eukaryote organism whose genome can be easily manipulated. Some of the characteristics that make yeast specifically appropriate for biological studies are rapid growth fast life cycle (one division every 90 minutes), dispersed cells, a well-known genetic system, the facility of replica plating and mutant isolation, and most relevant, a greatly versatile DNA transformation system. Yeast is non-pathogenic, so can be managed with little precautions. It is also a cheap source for biological studies (Dos Santos *et al.* 2015). Unlike the majority of other microorganisms, strains of *S.* cerevisiae have both a stable haploid and diploid form, so recessive mutations are easily manifested in haploid strains, while complementation tests can be performed with diploid strains. *S. cerevisiae* has a haploid set of 16 chromosomes, ranging in size from 200 to 2,200 kb. The total sequence of chromosomal DNA, forming 12 Mb, was completely sequenced and annotated in 1996 (Goffeau *et al.* 1996). According to the Saccharomyces Genome Database (SGD; http://www.yeastgenome.org/), as of August 2019, the number of “verified open reading frames

(ORFs)" in the reference strain S288C stood at 5179. Many human genes associated to disease have orthologues in yeast, and the high conservation of regulatory and metabolic pathways has contributed to the extensive use of *S. cerevisiae* as a model eukaryotic system for the assessment of the mechanisms underlying the response to environmental pollutants as ENMs (Dos Santos *et al.* 2015).

Sporulation in yeast provides an excellent model system to study the meiotic developmental pathway. In response to nitrogen starvation and in the presence of a poor carbon source, yeast diploid cells undergo meiosis and package the four haploid nuclei produced into stress-resistant spores (Fig. 6). This process is tightly regulated by a precise transcriptional program and the timing of gene expression strongly correlates with the sporulation progression. Three main groups of genes are sequentially activated and can be distinguished in "early", "middle" and "late" sporulation genes.

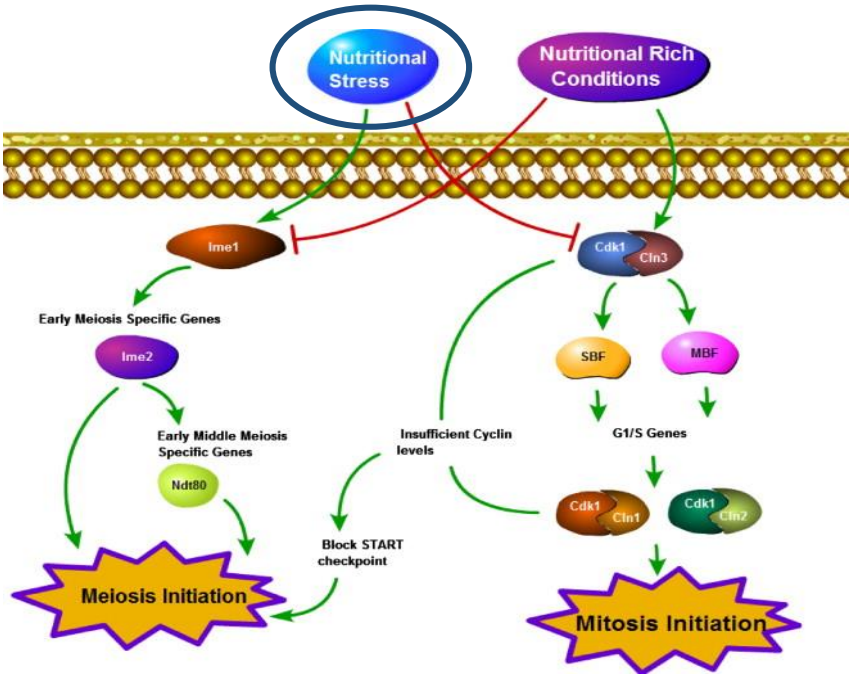

Figure 6. Nutritional dependence of mitosis and meiosis initiation of budding yeast diploid cells (Wannige *et al.* 2014).

The early genes are required for premeiotic S phase and progression through meiotic prophase I. Their induction is controlled by the master regulator Ime1, which expression is activated by nutritional signals such as glucose repression and alkaline-sensing, and encodes a transcription factor that activates the expression of the so-called early meiotic genes (van Werven and Amon

2011) (Fig. 7). Another fundamental gene expressed in the early phase of gametogenesis is *RIM4*. Rim4 is a putative RNA binding protein, the absence of which results in substantially reduced expression of several early meiotic genes including *IME2*. Overexpression of *RIM4* results in the formation of cells presenting four nuclei but the absence of refractile spores (Deng *et al.* 2001). Moreover, multi-site phosphorylation of Rim4 is critical for its regulated disassembly and degradation, and failure to clear Rim4 assemblies interferes with meiotic progression (Carpenter *et al.* 2018). Middle genes are expressed when cells initiate the first meiotic division. The principal regulator of mid-sporulation is Ndt80, which autoactivates its own expression and induces middle gene expression. The middle phase comprehends the principal cytological events of sporulation, where the meiotic divisions produce four haploid nuclei that are then packaged into newly formed prospore membranes. Smk1 is a meiosis-specific MAP kinase homolog that controls spore morphogenesis after the meiotic divisions have taken place. It was demonstrated that *SMK1* is required for the execution of multiple steps in spore morphogenesis that demand increasing thresholds of *SMK1* activity, a downregulation of this gene can result in the formation of ascii with different level of spore membrane disorganization (Wagner *et al.* 1999; McDonald *et al.* 2009). Late genes are involved in post-meiotic differentiation, and encode proteins required for the assembly of the thick coat, or spore wall, a critical step for the spore maturation. Upon activation, Ndt80 triggers a positive autoregulatory loop that brings to the expression of genes promoting exit from prophase, the meiotic divisions, and spore formation. The pathway is controlled by multiple feed-forward loops that give switch-like properties to the commitment transition.

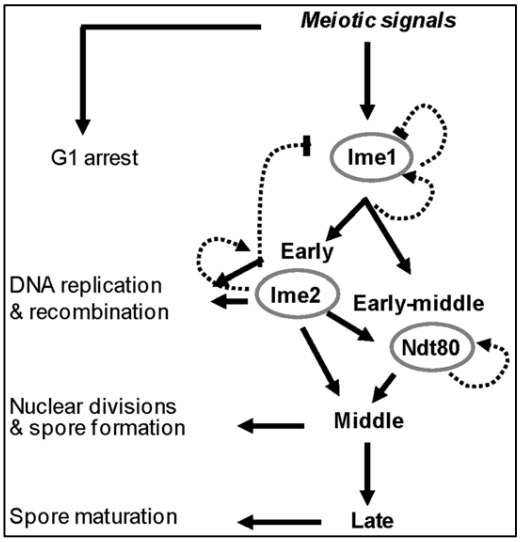

Figure 7. A schematic model illustrating the transcriptional cascade that governs meiosis in *S. cerevisiae* (Gurevich *et al.* 2010).

Similarly, in plants little is known about the biological effects of ENM exposure in yeast. In addition, the variety of ENMs behaviour and the different types of exposure applicable to yeast, increase the complexity of the potential consequences. Different studies on yeast showed high variability of effects among different categories of ENMs. Pasquali *et al.* (2017) showed that the CdS QDs exposure in yeast increased the level of ROS and decreased the reduced vs oxidized glutathione (GSH/GSSG) ratio. Moreover, Fan *et al.* (2016b) proposed that the exposure of CdTe QDs induced toxicity also inhibiting autophagy. Strtak *et al.* (2017) also showed that chronic exposure to CdSe QDs can exert a selective pressure in yeast population causing irreversible genetic changes leading to adaptation, founding, in particular, a mutation in the ubiquitin ligase gene *bul1.* Another mechanism suggested to induce toxicity of QDs is on a proteomic level: Ruotolo *et al.* (2018) found that CdS QD treatment in yeast induced the formation of hard corona proteins on the NP surface. Some of the proteins forming the hard corona were found to be implicated in crucial metabolic pathways, and as a consequence, the free amount of these proteins were strongly reduced, even if a compensatory transcriptional modulation may take place. Moreover, it is known that Cadmium has several harmful effects on the reproductive system and the embryo. Incorporation of Cd into the chromatin of the developing gamete has also been shown, and Cd accumulation in ovaries has been associated with failure of oocyte progression. Higher dosage exposure of Cd inhibits development to the blastocyst stage, and can induce degeneration and decompaction in blastocysts development, with apoptosis and breakdown in cell adhesion (Thompson *et al.* 2008). Furthermore, it was demonstrated that exposure to Cadmium Oxide NPs, which are a precursor used to synthesize also CdS QDs, can results in renal injury in pregnant mice females and their newborn offspring (Blum *et al.* 2015).

Aim of the project

The aim of this work was to evaluate ENMs impact on two organisms phylogenetically distant, as *C. pepo* and *S. cerevisiae,* focusing on the meiotic processes and its products. Meiosis is a peculiar type of cell division which is fundamental for sexual reproduction in most eukaryotes. Unlike mitosis, regulation and molecular mechanisms of meiosis are less understood. To best mimic the potential conditions of exposure and environmental accumulation, the toxicity of nanomaterials were evaluated in conditions of chronic exposure (low concentrations and long times of exposure).

In the first part of the project, it was used the yeast *Saccharomyces cerevisiae*, as a model for eukaryotes, to determine the toxic effect on the gametogenesis process due to CdS QDs exposure. Similar to gamete formation in higher organisms, meiosis (also called sporulation) in yeast is tightly regulated on a transcriptional level, and can be roughly divided into three major phases. Fluorescence microscopy firstly provided a general overview of the morphological consequences due to CdS QDs exposure during sporulation. To determine if the morphological alterations caused by QDs were connected to a transcriptional reprogramming of the process, a set of specific sporulation genes was analyzed by Real-time PCR. Moreover, viability and DNA content of the meiotic products was analyzed throughout the development, as well as the potential role of corona proteins formation.

The second part of the study aims to characterize the physiological and molecular responses in zucchini (*Cucurbita pepo* L.), a plant species of relevance in food production and agro-industry, treated with copper oxide (CuO) and cerium oxide (Ce_2O) NPs, from germination to flowering. The literature on beneficial effects of some engineered nanomaterials on edible plants is increasing, both as fertilizer and disease/pest control agents. However, there are some factors which are still limiting the widespread development and application of ENMs including regulatory differences, and the underlying potential for unknown environmental effects and health risks. Furthermore, the understanding of the chronic low dose ENMs effects on edible tissues is still very limited. The physiological analyses have been accompanied by a complete transcriptomic analysis of the different plant tissues and organs. The application of high-throughput transcriptomics, coupled with analytical and physiological data, can bridge the gap between genotypic and phenotypic evidence when investigating plant response to ENMs exposure. Furthermore, the study will try to develop new methods potentially used for risk assessment procedures in food and agriculture, in conditions ENMs exposure.

Materials and Methods

Part I. Effects of metal-based nanomaterials in *Saccharomyces cerevisiae*

Preparation and characterization of the nanoparticles

CdS QDs were synthesized at IMEM-CNR (Parma, Italy), according to the method reported in Villani *et al.* (2012). The bulk density of the QDs was 4.82 g cm^{-3} and their mean diameter was 5 nm. From X-ray diffraction analysis, Cd represented 78% of their dry weight (Marmiroli *et al.* 2014). CeO_2 NPs (<25 nm, particle size), CuO NPs (<50 nm, particle size), ZnO NPs (<100 nm, particle size) and their relative bulk powders (99.99% purity) were purchased from Sigma-Aldrich (Merck). Before their use, an aqueous suspension of these NPs was exposed for 15 min to sonication in a Transonic T460/H device (Elma Electronic GmbH) to reduce agglomeration of the NPs. Zeta-potentials and hydrodynamic diameter were obtained by dynamic light scattering (DLS) analysis at 25 °C using a Zetasizer Nano ZSP (Malvern Instruments Ltd). Transmission electron microscopy (TEM) analysis was performed using a Talos F200S G2 (Thermo Fisher Scientific).

Yeast strains and growth conditions

All the experiments discussed in this study were performed using the diploid homotallic strain Z239-6B-6B (genotype: *α/a D lys2-1 ade2-1 ura3-3 his1 leu1-2 canR1*; the symbol D indicates the presence of the wild-type set of genes *HO*, *HMR* and *HML*) of *S. cerevisiae*. Vegetative growth were propagated in YPD (Yeast extract Peptone Dextrose) medium, containing 1% w/v yeast extract, 2% (w/v) peptone, 2% (w/v) dextrose. Spot assays (see below) were performed on selective SD (Synthetic Defined) agar plates, containing 6.7 g L^{-1} yeast nitrogen base, 2% glucose (w/v), 20 mg L^{-1} histidine, 30 mg L^{-1} leucine, 30 mg L^{-1} adenine, 30 mg L^{-1} lysine, 50 mg L^{-1} uracil and 15 g L^{-1} agar.

Spot assay and growth analysis in liquid media

Z239-6B-6B strain was pre-grown in YPD medium for 24 h at 28 °C; yeast precultures were then diluted to an OD_{600} (optical density at 600 nm) of 1, and 10-fold serial dilutions were made and spotted onto SD agar plates supplemented (or not) with CdS QDs (5-100 mg L^{-1}). After 72 h of incubation, the yeast growth at each cell dilution was examined.

To evaluate the toxicity of the NPs, growth analysis in liquid media were also made. Yeast precultures in YPD medium were diluted to an OD_{600} mL^{-1} of 0.1 in SD medium supplemented (or

not) with the NPs at different concentrations (1-10 mg L^{-1}), and incubated at 28 °C with shaking (160 rpm) for 24 h.

Sporulation assay

To determine the effect of NP exposure on the sporulation of *S. cerevisiae*, yeast cells were pre-grown overnight in respiratory conditions using YEPA medium (1% yeast extract, 2% peptone, 2% potassium acetate). Cells were then collected by centrifugation, washed in PBS (Phosphate-Buffered Saline) buffer, and resuspended in sporulation medium (2% potassium acetate, 20 mg L^{-1} histidine, 30 mg L^{-1} leucine, 30 mg L^{-1} adenine, 30 mg L^{-1} lysine, 50 mg L^{-1} uracil) to a concentration of OD_{600} mL^{-1}=2 in the presence or not of NP treatments. Yeast growth was then monitored at 28° C for 72 hours.

Fluorescence microscopy assays

To analyze the progression of gametogenesis process, 1 x 10^7 cells were collected, washed, fixed in 70% ethanol for 45 minutes. Cells were then stained with 4',6-diamidino-2-phenylindole (DAPI) at a final concentration of 1 µg mL^{-1} and washed in water two times prior to microscopy analysis. DAPI is a blue-fluorescent DNA stain (emission at 470 nm) that binds AT-rich regions on dsDNAs. It is excited by the violet (405 nm) laser line and is commonly used as a nuclear counterstain in fluorescence microscopy and flow cytometry.

For the fluorescence analysis of spore walls, cells were collected, washed in water and stained with Calcofluor white (CFW; excitation/emission at 365 nm and 435 nm) at a concentration of 25 µM. CFW is a chitin/chitosan-binding dye used to stain the yeast cell walls.
To analyse the percentage of death cells after exposure to NPs, cells were collected and stained with 100 mg L^{-1} of Propidium Iodide (PI; excitation/emission at 536/617 nm), a membrane impermeant dye that binds to double stranded DNA by intercalating between base pairs, PI is generally excluded from viable cells, but internalized by dead cells.

Random spore analysis

To evaluate the viability of single spores, a random spore analysis test was performed. Spores were collected from asci formed in the presence of doses (1 mg L^{-1}) of CdS QDs that don't strongly compromise the gametogenesis process. Yeast cells (50 µl) were collected after 72 h in sporulation medium w/wo the CdS QD treatment (see before) and washed in water. A solution containing lyticase (2.4 KU/ml, final concentration; Sigma-Aldrich) and 2-mercaptoethanol (143 mM, final concentration) was then added and samples were incubated over-night at 30 ºC with gentle shaking. TWEEN® 80 was added at a final concentration of 0.1 % (v/v) and samples were subjected to several cycles of sonication (eight times for 1 minute) using a water bath sonicator (Transonic T460/H device) and vigorous vortexed (four times) for 1 minute followed by 1 minute incubation on ice using a Thermo Savant FastPrepR Cell Disrupter (Qbiogene Inc.). Lytic digestion of vegetative cells and asci was verified using optical microscopy analysis and the procedure was repeated until the percentage of single spores reached 90%. The concentration of single spores in the samples was then determined with a hemocytometer, and 200 spores were seeded in YPD agar plates. The growth of germinated spores was evaluated after 3 days of growth at 28 º C.

Gene expression analysis

Yeast cells grown in sporulation medium in the presence (or not) of CdS QDs (4 mg L^{-1}) were collected at different times (3, 8 and 24 h), and total RNA was isolated using an RNeasy Mini Kit (Qiagen), following the manufacturer's instructions. 1 µg of each RNA sample was retrotranscripted using QuantiTect® Reverse Transcription Kit (Qiagen) and single stranded cDNA was quantified by Real-time PCR using a PowerUp SYBR™ Green Master Mix (Thermo Fisher Scientific) on a ABI PRISM 7000 Sequence Detection System (Applied Biosystems). Relative quantification of gene expression was obtained using the "comparative C_T method" and *ACT1* as housekeeping gene. The primer sequences used in this work are included in Appendix.

Fluorescence-activated cell sorting (FACS) analysis

To analyse the DNA content of yeast cells exposed to CdS QDs during the sporulation process, pre-cultures in YEPA medium were collected by centrifugation, washed in PBS buffer and resuspended to a concentration of 2 x 10^7 cells mL^{-1} in sporulation medium in the presence (or not) of CdS QDs

(4 mg L^{-1}). Cells were collected at different times (0, 6, 24 and 48 h), sonicated to break up cell clumps, fixed in ice-cold ethanol (70%) and conserved at -20 °C. Samples were then washed, resuspended in 50 mM Tris-HCl buffer (pH 7.5) and treated with RNase A (10 µg mL^{-1}, final concentration) for 2 hours at 37 °C. Cells were then resuspended in the FACS buffer (180 mM NaCl, 100 mM Tris-HCl pH 8) and PI (2 µM) was added to samples 30 minutes before analysis. As a positive control for the quantification of dead cells, an aliquot of each sample was put at 95 °C for 10 minutes prior to the addition of PI. As a negative control, an aliquot of each sample was also analysed without the addiction of PI.

Protein extraction

Pre-cultures in YEPA medium were collected by centrifugation, washed in PBS buffer and resuspended at a concentration of 2 x 10^7 cells mL^{-1} in sporulation medium. Yeast cells were then grown for 72 h at 28° C without CdS QD treatment. Yeast cells (10^8 cells) were collected, washed in PBS buffer and then resuspended in ice-cold breaking buffer [50 mM Tris-HCl (pH 8.0), 100 mM NaCl, 10% glycerol, with protease inhibitor cocktail] with an equal volume of acid-washed glass beads. Cells were broken with six rounds of vigorous vortexing for 45 seconds followed by 3 minutes incubation on ice using a Thermo Savant FastPrepR Cell Disrupter. The lysate was then clarified by centrifugation (14000 rpm for 30 minutes at 4 °C). The protein concentration was determined using both the Bradford Assay (Bio-Rad) and the BCA Protein Assay Kit (Thermo Fisher Scientific), following the manufacturer's instructions.

In vitro protein-NP binding assay

To identify the yeast proteins adsorbed with high-affinity to the NP surface, the cell lysate (7 g L^{-1}, final concentration) obtained from (untreated) sporulated cells (see before) was incubated with CdS QDs (0.5 g L^{-1}, final concentration) in binding buffer [50 mM Tris HCl (pH 7.4), 100 mM NaCl, 10% (v/v) glycerol, 5 mM $MgCl_2$] for 24 h with gentle agitation at 4 °C, according to Sund *et al.* (2011) and Ruotolo *et al.* (2018). The CdS QDs, together with their adsorbed (corona) proteins, were recovered by centrifugation (14000 rpm, 5 min, 4 °C), and unbound proteins were discarded by washing the pellet five times in salt-free buffer [20 mM Tris-HCl (pH 7.4)], followed by three times in salt-buffered solution [20 mM Tris-HCl (pH 7.4), 0.1 M NaCl]. After each wash, the pellets were gently vortexed

and centrifuged (14000 rpm, 5 min, 4 °C). Hard corona proteins were recovered from the CdS QD surface by a 1 h incubation in resuspension buffer [60 mM Tris-HCl (pH 6.8), 2% (w/v) SDS, 10% (v/v) glycerol] at room temperature, then held at 95 °C for 5 min.

For visualization, proteins were denatured in sample buffer [62.5 mM Tris-HCl (pH 6.8), 2.5% (w/v) SDS, 2% (v/v) β-mercaptoethanol, 0.02% (w/v) bromophenol blue, 10% (v/v) glycerol] for 5 minutes at 95 °C, then separated electrophoretically through 12% (w/v) SDS polyacrylamide gels. The concentration of released corona proteins was quantified using the BCA Protein Assay Kit.

LC-MS/MS analysis

Hard corona proteins were denatured in 6 M urea in 25 mM ammonium bicarbonate. Disulphide bonds were reduced by adding 35 mM dithiothreithol (DTT) and holding for 1 h at room temperature; reduced cysteine residues were alkylated by iodoacetamide to a final concentration of 32 mM and incubating for 1 h at room temperature in darkness. Urea concentration was then lowered to 0.6 M by dilution with 25 mM ammonium bicarbonate, trypsin (Sigma Aldrich, Merck) was added in a 1:30 (w/w) ratio and the digestion was allowed to run for 18 h at 37 °C. The reactions were stopped by adding formic acid to a final concentration of 0.5% (w/v) and incubating with gentle agitation at 37 °C for 15 min; the solutions were then lyophilized with a Speedvac device (Savant). The dried samples were re-suspended in 0.1% (w/v) formic acid and analyzed by liquid chromatography-mass spectrometry (LC-MS/MS), using a Dionex Ultimate 3000 micro HPLC device coupled to an LTQ-Orbitrap XL mass spectrometer, equipped with a conventional electrospray ionization source (Thermo Fisher Scientific).

Statistical analysis

For Real-time PCR each reaction was conducted in triplicate, and included a no template control. Relative transcript abundances were derived using the 2-ΔΔCT method. Cytofluorimetric data were analysed with NovoExpress software (Agilent Technologies). For corona protein identification, information regarding known yeast protein sequences was retrieved from the UniProt database (www.uniprot.org). The experiments were carried out as two biological replicates and three technical replicates.

Part II. Effects of metal-based nanomaterials in *Cucurbita pepo* L.

Exposure Assay

The seeds were pre-germinated in vermiculite for 10 days prior to transplanting to soil. The soil was collected from top 50 cm of the Connecticut Agricultural Experiment Station (CAES) in New Haven, CT. The Individual solutions of bulk and NP in water (volume =30% water capacity of soil/vermiculite) were probe sonicated to maximize dispersion. The bulk, NP or salt stock dispersions were then slowly added to 500g soil and were mixed manually in an attempt to achieve homogeneity. The amended soil was then transferred to each experimental pot. The final concentration of Cu and Ce for each bulk, NP and salts replicate pot was 100 mg/kg. The zucchini seedlings were planted (one per pot) and grown indoor under supplemental fluorescent lighting (60 µE/m2/sec) at approximately 22−28 °C until complete flowering (about 60 days). The plants were top watered as needed and amended every two weeks with Hoagland's Solution (10%) during the 30-d growth period. For every condition, 5 plants were planted.

ICP-MS

Flower biomass samples for elemental analyses are rinsed with tap water, MilliQ water and two 30-sec HNO3 (0.01 M) rinsing is done to remove soil and surface-attached NPs. To determine Cu and Ce content in the replicate tissues, wet vegetation is oven-dried at 100 °C for 72 h and digested for 25 min on a hot block with concentrated HNO3 at 115 °C. After 30 min, 1 mL of H_2O_2 is added to each digestion tube and the samples were digested for an additional 30 min and diluted to 50 mL with MilliQ water. The digests are analysed by inductively coupled plasma mass spectrometry (ICP-MS) (Agilent 7500ce) for Cu (mass 63) and Ce (mass 140). The samples are quantified against a four-point calibration curve (1- 100 µg L^{-1}) that had been previously evaluated for linearity and accuracy. Analytical blanks, matrix blanks, and calibration verification samples are included in each sequence.

Preparation of tissue for light microscopy

Anthers, collected at different stages (ex. 1 and 3) and mature pollen fixed in 4% formaldehyde and 2% glutaraldehyde in phosphate-buffered saline (PBS) pH 7.4, rinsed four times in PBS and dehydrated in a graded ethanol series. Tissue is then embedded in Embed 812 resin, and sections

of 1.0‑1.5 µm cut with a microtome and stained with 1% toluidine blue in borax. For mature pollen gently scraping the anther with a micro-spatula, and immediately transferred to a 1.5-ml tube in fixative. Light micrographs can be taken using a light microscope with a digital camera.

Pollen viability

A simplified version of Alexander's staining was used to test pollen viability. Free anthers were collected when pollen was mature but anthers were still non-dehiscent (stage 12-13), and fixed in Carnoy's fixative (6 alcohol:3 chloroform: 1 acetic acid) for a minimum of 2 hours. Buds can be stored in fixative for 12 months at either room temperature or cold room. Mature pollen is collected and stained using protocols described by Peterson *et al.* After staining, all aborted and non-aborted pollen was counted using a Zeiss compound microscope at 200× magnification.

Environmental Scanning Electron Microscope (ESEM)

Pollen grains were analysed fresh with no fixation or staining; they were collected from mature flowers and positioned on 2 cm diameter stainless-steel sample holder (stub) covered with adhesive carbon tape. The scanning microscope ESEM FEG2500 FEI (FEI Europe, Eindhoven, The Netherlands), operating in low-vacuum (60 Pa) with LFD (Large Field Detector) allowed optimal Secondary Electron (SE) imaging. The cone PLA (Pressure Limiting Aperture) 500 µm improved the signal available to the Bruker X-ray detector, QUANTAX XFlash®6 | 30 Detector with energy resolution ≤ 126 eV FWHM at Mn Kα., and a highly efficient, versatile mid-size 30 mm^2 SDD (Silicon Drift Detector) for nano-analysis and high count rate spectral imaging (Bruker Nano GmbH, Berlin, Germany). SE imaging was performed at 10 KeV with a beam size of 2.5 µm, EDX analysis at 20 KeV acceleration voltage, final lens aperture of 40 µm, and beam size of 4 µm. The working distance was about 10 mm, and the scanning time was 60 s. The software xT microscope Control, xT microscope Server and FEI User Management software were used for imaging, Esprit 1.9 package was used for X-ray spectra acquisition and analysis was conducted during two acquisition modes: Point/Area analysis and Linescan. X-ray spectra deconvolution and standard-less quantification were performed using the P/B-ZAF (Peak/Background evaluation matrix with atomic number (Z), absorption (A), and secondary fluorescence (F) correction) interactive method supported by Esprit 1.9 "Quantify Method Editor" option (Goldstein *et al.*, 2003). SE images and EDX spectra were collected for

samples treated with CuO NPs, CuO bulk, CeO_2 NPs, CeO_2 bulk, as well as for the untreated controls. The detection limit in our working conditions was of 0.01% for elements with N≥21 and 0.005% for N<21.

RNA sequencing

Library preparation and sequencing:
TruSeq Stranded mRNA kit (Illumina, San Diego, CA) has been used for library preparation following the manufacturer's instructions. RNA samples were quantified and quality tested by Agilent 2100 Bioanalyzer RNA assay (Agilent Technologies, Santa Clara, CA). Final libraries were checked Agilent Bioanalyzer DNA assay (Agilent Technologies, Santa Clara, CA). Libraries were prepared for sequencing and sequenced on single-end 75 bp mode on NextSeq 500 (Illumina, San Diego, CA).

RNA-Seq bioinformatics analysis:
Base calling and demultiplexing. Processing raw data for both format conversion and de-multiplexing by Bcl2Fastq 2.0.2 version of the Illumina pipeline. Adapters masking. Adapter sequences are masked with Cutadapt v1.11 from raw fastq data. Trimming. Removing lower quality bases and adapters by ERNE software.
Alignments on the reference genome. Aligning reads on reference genome/transcriptome available at the link http://cucurbitgenomics.org/organism/14 with STAR (default parameters), a splice junction mapper for RNA-Seq reads. It aligns RNA-Seq reads to genomes and then analyzes the mapping results to identify splice junctions between exons. Execute transcripts count. Assembling and quantitation of full-length transcripts representing multiple spliced variants for each gene locus by Stringtie (default parameters). Quality control. RSeqQC package is used to perform statistics on "strandness" of reads, on genome coverage and read distribution

Data analysis

For Real-time PCR each reaction was conducted in triplicate, and included a no template control. Relative transcript abundances were derived using the 2-ΔΔCT method. A one-way ANOVA with Tukey's (HSD) pairwise multiple comparison test, was used for biomass and metal content analysis. For RNAseq data, differentially expressed genes were identified using a 2.3 threshold of FPKM (in log2). Student T test was applied for analysis of homogeneity of variance, statistical analysis for

scatter plots and box and whiskers graphs were performed with R statistical software (www.r-project.org). Venny bioinformatics tool (http://bioinfogp.cnb.csic.es/tools/venny/) was used for the generation of Venn diagrams. Gene Ontology (GO) network analysis was performed by the Cucurbitgenomics data service (http://cucurbitgenomics.org/), the GO term enrichment analysis was conducted using a cut-off p-value of 0.05 for cellular components and biological processes, 0.03 for function ontology for significant represented GO Terms.

Results and Discussion

Nanoparticle characterization

The NPs used in the present work were resuspended in milliQ water and sonicated prior to use (see "Materials and Methods" for details). Average particle size (nm) determined by TEM analysis (Fig. 8a), Z-potentials (Fig. 8b) and hydrodynamic diameter (nm) of the NP aggregates determined by DLS analysis were estimated as described in "Materials and Methods". Zeta potential (Fig. 8b) is the potential difference between the mobile dispersion medium and the stationary layer of the medium attached to the dispersed particle. Zeta potential values of ±30 mV are representative of NPs stable in suspension. Different parameters that characterize NPs used in the present work were indicated in Fig. 8c.

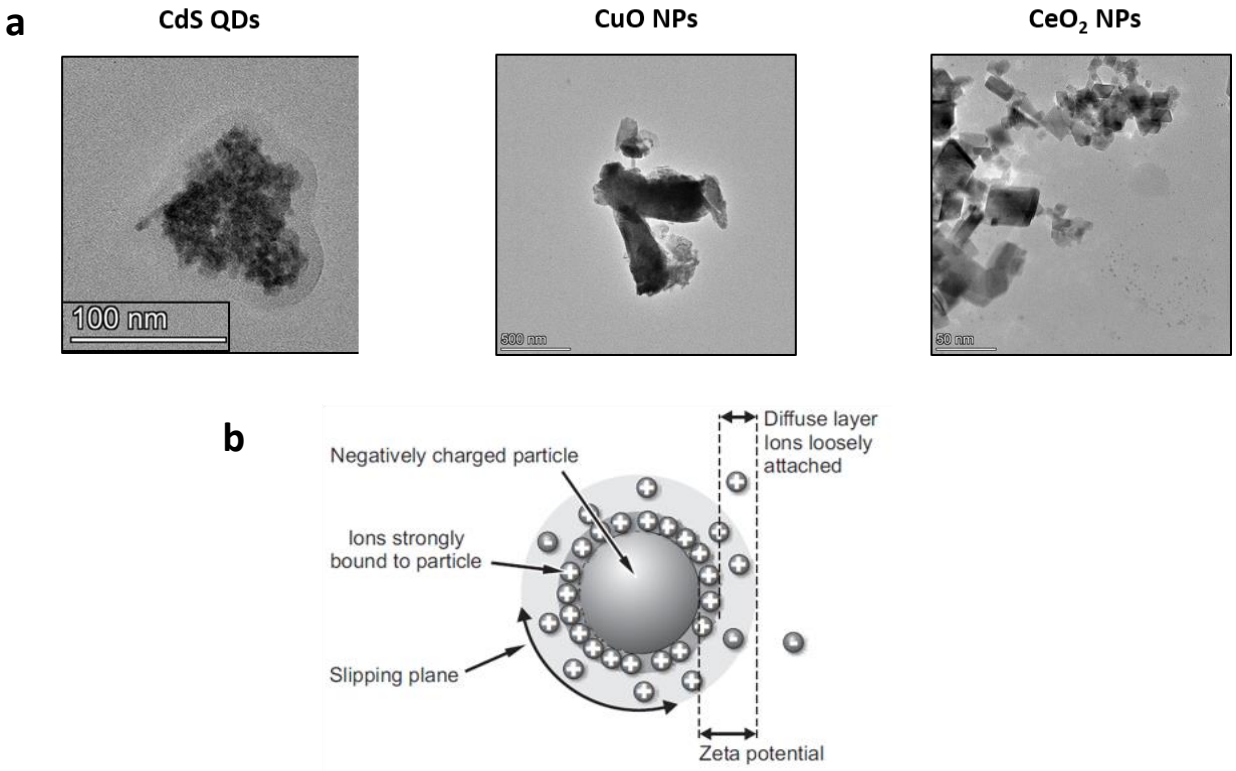

c

NPs	Size (nm) (manufacturer data)	Zeta potential (mV)	Hydrodinamic diameter (nm)
CdS QDs	<5	-22	196.5
CeO_2 NPs	<40	40	246.9
CuO NPs	<25	-25	533.9
ZnS QDs	<5	12	302.9

Figure 8. (a) Representative TEM images for CdS QDs, CuO NPs and CeO_2 NPs. (b) Schematic representation of Z-potential, (c) Characterization of NPs used in the present work.

Part I. Effects of metal-based nanomaterials in *Saccharomyces cerevisiae*

Toxicity of CdS QDs in different growth conditions

Serial dilution spot assays were performed to evaluate the fitness of a diploid yeast strain (Z239-6B-6B) in the presence (or not) of CdS QD treatments. Ten-fold dilutions of yeast pre-cultures were performed and aliquots (4 µl) of each dilution were spotted onto SD-agar plates in the presence or absence of CdS QDs (5-100 mg L^{-1}; see "Materials and Methods" for details). As observed for haploid cells (Ruotolo *et al.*, 2018), high concentrations of CdS QDs (≥ 10 mg L^{-1}) suppress the viability of the diploid strain (Fig. 9).

To better define the range of CdS QD concentrations (≤ 10 mg L^{-1}) that cause a growth impairment in diploid cells, a growth analysis in liquid culture conditions in SD medium was conducted (Fig. 10). The higher concentration tested for the growth curves (10 mg L^{-1}) causes a decrease of the yeast growth higher than 50% compared to the control (Fig. 10), for this reason for the next experiments it was not taken into consideration.

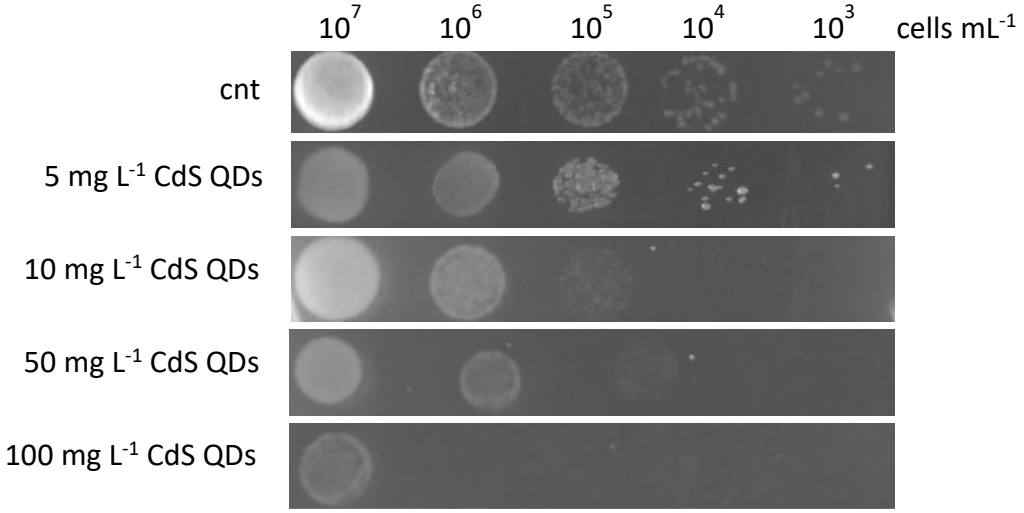

Figure 9. The growth of the diploid strain was affected by the QD treatment in fermentative conditions. Serial dilution spot assays of diploid cells grown in the absence (CNT) or in the presence of CdS QDs (5, 10, 50, 100 mg L^{-1}) on standard synthetic media supplemented with glucose (2%) as carbon source (SD medium). Cell concentration (cells mL^{-1}) of each dilution plated was indicated in the upper part of this figure. Cnt, untreated control cells.

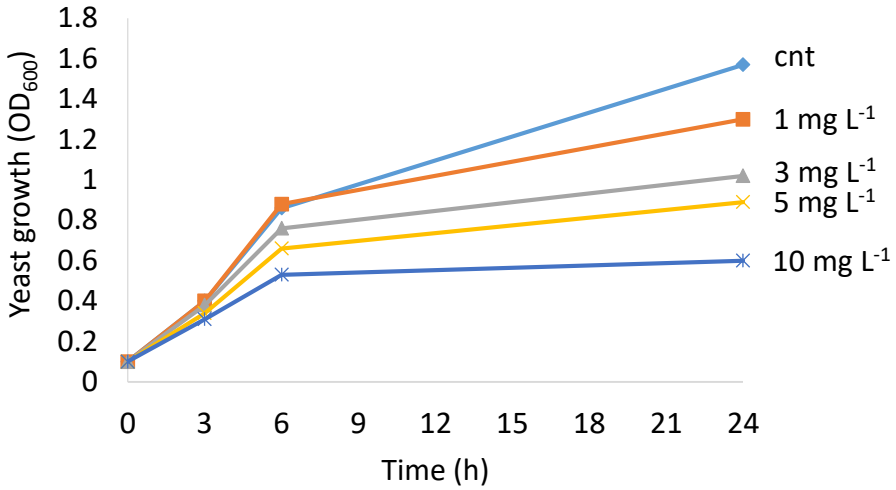

Figure 10. CdS QDs strongly affect the viability of the diploid strain in liquid growth conditions conducted in SD medium. Growth curves were recorded for 24 h in SD medium in the presence (or not) of different concentrations of CdS QDs (1-10 mg L^{-1}). Cnt, untreated control cells.

Then, we have evaluated the inhibitory effects of CdS QDs on the yeast viability in the sporulation medium (Fig. 11). Unlike fermentative conditions, the exposure of yeast cells to CdS QDs in sporulation medium does not cause an appreciable inhibition of the yeast growth. In fact, it is known that the sporulation process produces cells (spores) more resistant to environmental stresses.

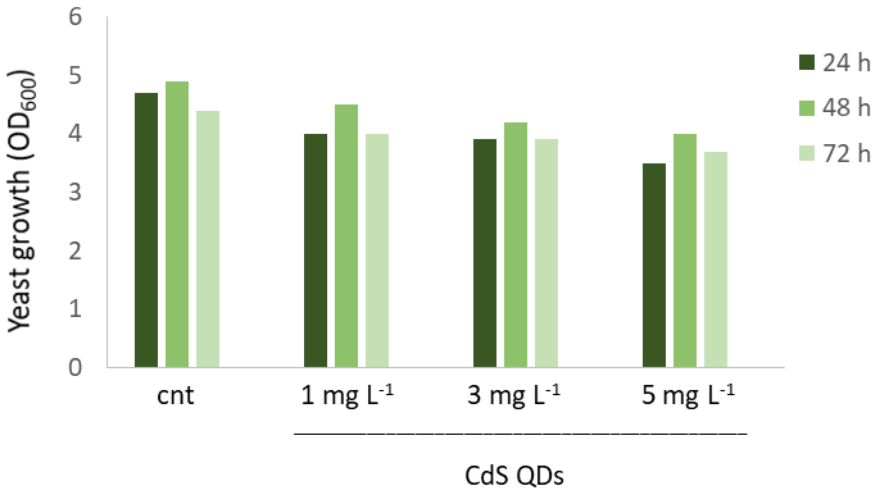

Figure 11. CdS QDs affect the growth in sporulation medium. See "Materials and Methods" for details in growth conditions for sporulation assay.

To evaluate if the treatment with CdS QDs did not reduce the viability of the cells under sporulation conditions, yeast cells were stained with the Propidium Iodide (PI; Fig. 12), a dye that allows the discrimination of living (PI^-) and dead (PI^+) cells. The percentage of living cells in the control (untreated cells) throughout the gametogenesis process, obtained by fluorescence microscopy observations, is about 96% of total cells (Fig. 12). The treatment with CdS QDs at 5 mg L-1 slightly reduced the percentage of viable cells (about 90%), suggesting that CdS QDs are not toxic within this concentration range in starvation condition (Fig. 12).

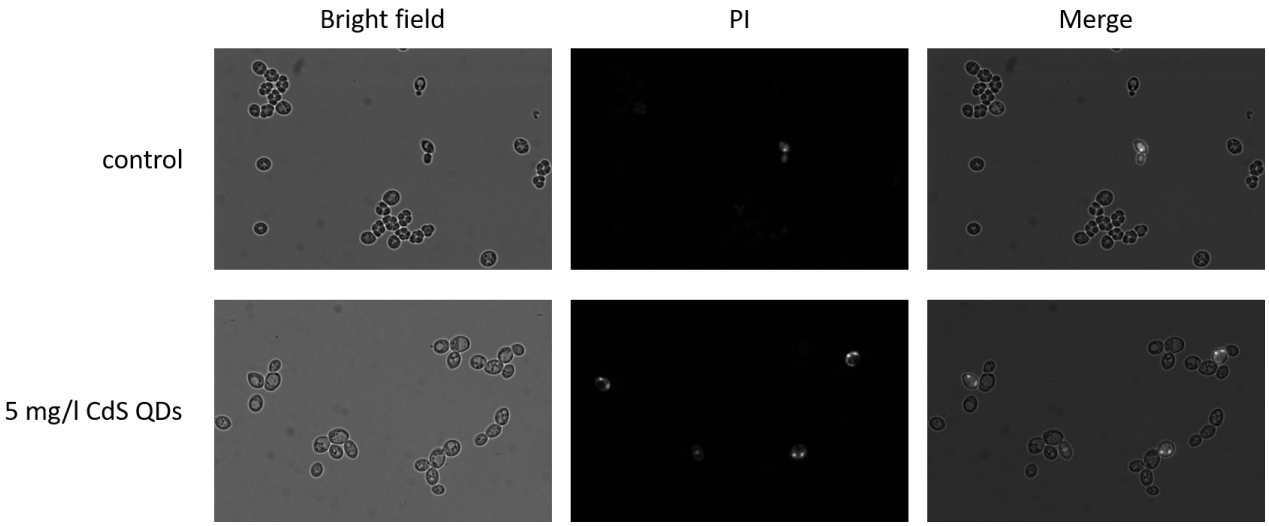

Figure 12. CdS QD treatment does not increase the number of dead cells in sporulation conditions. Yeast diploid strain Z239-6B-6B stained with the fluorescent intercalating dye Propidium Iodide (PI), to identify dead cells in untreated and treated (5 mg L^{-1} CdS QDs) samples.

Fluorescence microscopy assays

To test the effects of CdS QD exposure in meiotic cell cycle progression and spore formation, yeast diploid cells were treated with different concentrations of CdS QDs (1-5 mg L^{-1}) in sporulation medium and analyzed with optical microscopy. After 72h treatment in the presence (or not) of CdS QDs, *S. cerevisiae* cells were stained with DAPI and Calcofluor white to identify, respectively, the nuclei and the spore walls of the yeast cells using fluorescence microscopy. This analysis revealed that low concentrations of CdS QDs (1 mg L^{-1}) do not alter the sporulation process, in fact the asci

formed appeared apparently indistinguishable from those found in wild-type tetrads in untreated cells, with a predominance of asci containing four refractile spores (Fig. 13). Conversely, higher concentrations of CdS QDs (3 and 5 mg L^{-1}) cause an alteration of the meiotic nuclear divisions in combination with a strong inhibition of spore morphogenesis, resulting in the formation of asci containing the meiotic products, but with the absence of refractile spores (Fig. 13).

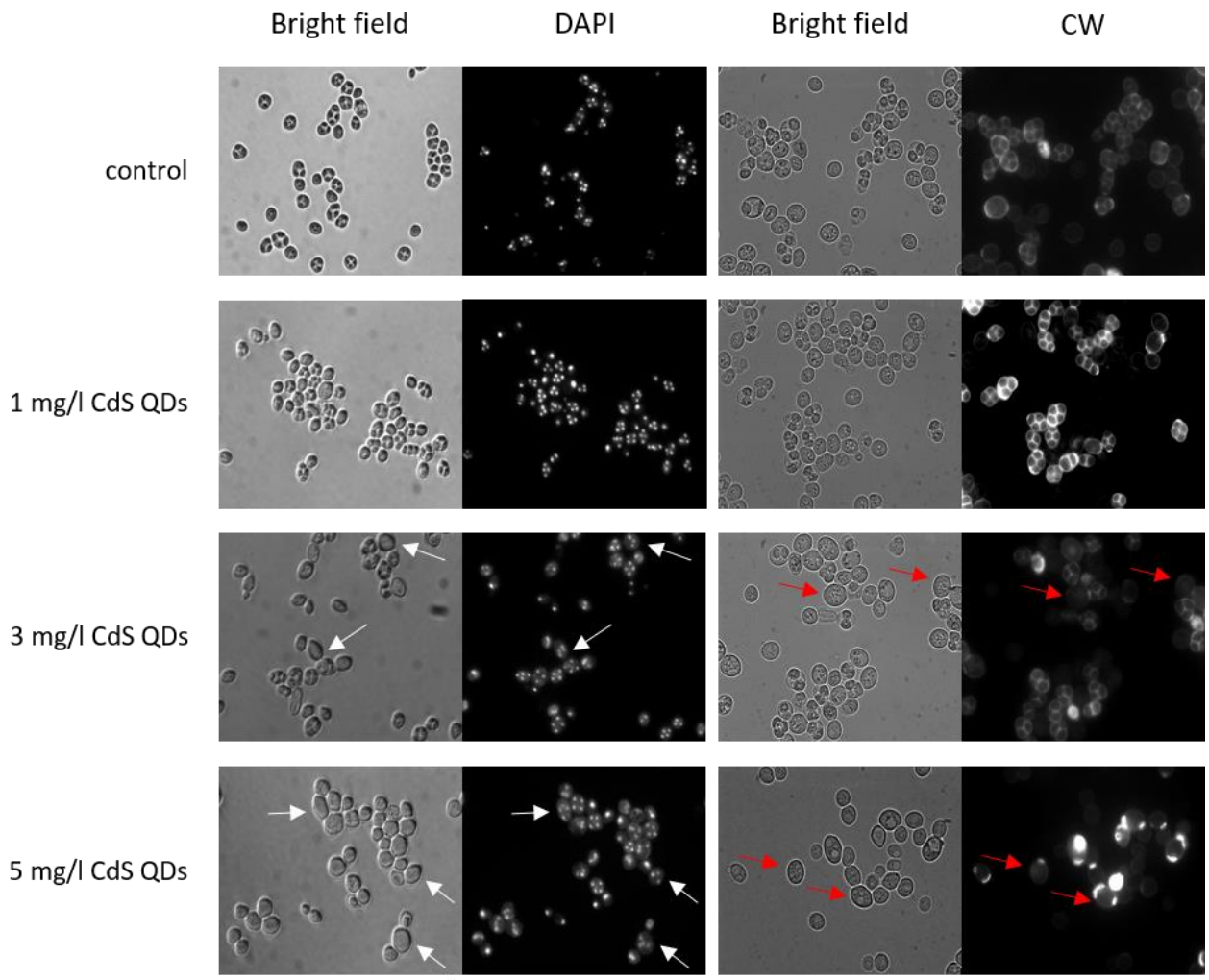

Figure 13. CdS QDs affect the sporulation process. Yeast strain Z239-6B-6B was grown in sporulation conditions (see "Materials and Methods" for details) in the presence (or not) of different CdS QD concentrations for 72 h; cells was stained with DAPI and Calcofluor White (CW), and analyzed using fluorescence microscopy. Note the predominance of asci containing four refractile spores formed in the control (untreated) cells and in the cells treated with low concentration of CdS QDs (1 mg L^{-1}). Higher concentrations of CdS QDs cause the formation of asci containing three or four meiotic products (white arrows; multinucleated cells) and the absence of refractile spores (red arrows).

The graph in Figure 14 resumed the phenotypes observed in fluorescence microscopy images. They were grouped into four different categories: cells which had correctly completed the gametogenesis process, presenting asci with four spores and their relatives haploid nuclei; cells presenting the meiotic products but the absence of spores (multinucleated cells); cells containing just two nuclei, cells which did not switch in the meiotic process (multinucleated cells); cells that presents one nucleus.

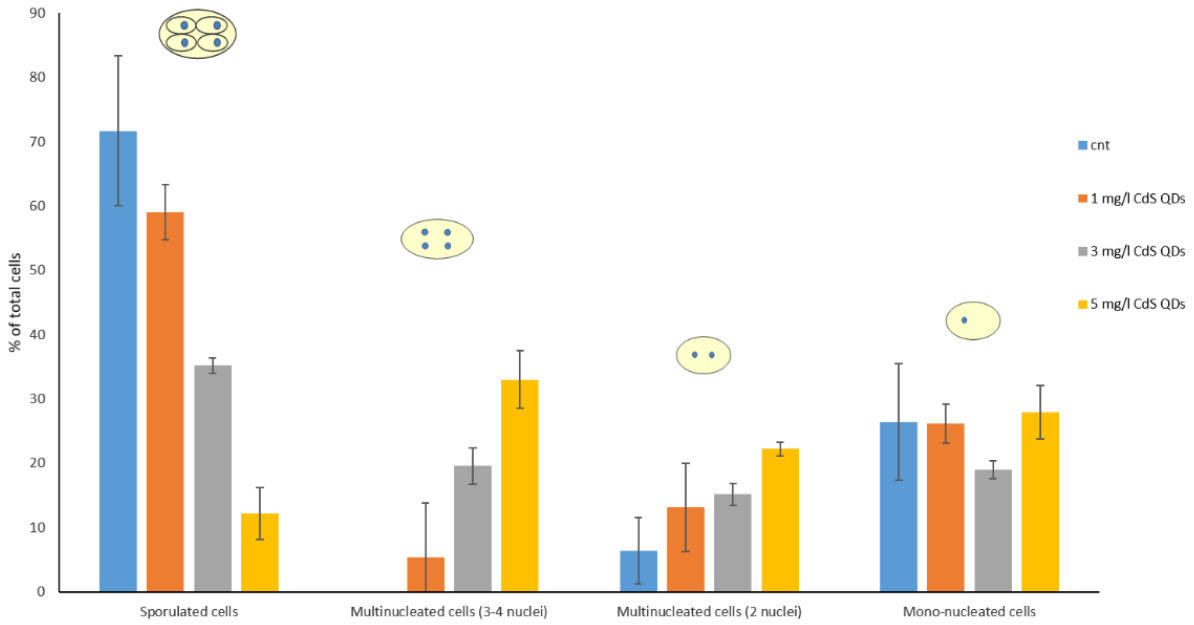

Figure 14. CdS QD treatment strongly affects the spore morphogenesis. Morphological observations were made with microscope fluorescence analysis (At least 100 cells were counted for each condition). Higher concentrations of CdS QDs (3-5 mg L^{-1}) cause the formation of multinucleated cells.

The same exposure assay was also carried out using other NPs (CeO_2 NPs, CuO NPs, ZnS QDs), characterized by different sizes, shapes and zeta potentials, in order to elucidate if the morphological and nuclear alterations of the gametogenesis process observed with the CdS QD treatment were a general effect (or not) of NPs. Different concentrations of these NPs were tested, but no phenotypical differences were observed (Fig. 15). Finally, we have also evaluated the effect of cadmium salt ($CdSO_4$), using equivalent concentrations of metal ions applied in the QDs form (Cd represented 78% of the dry weight of each CdS QD (Marmiroli *et al.*, 2014)].

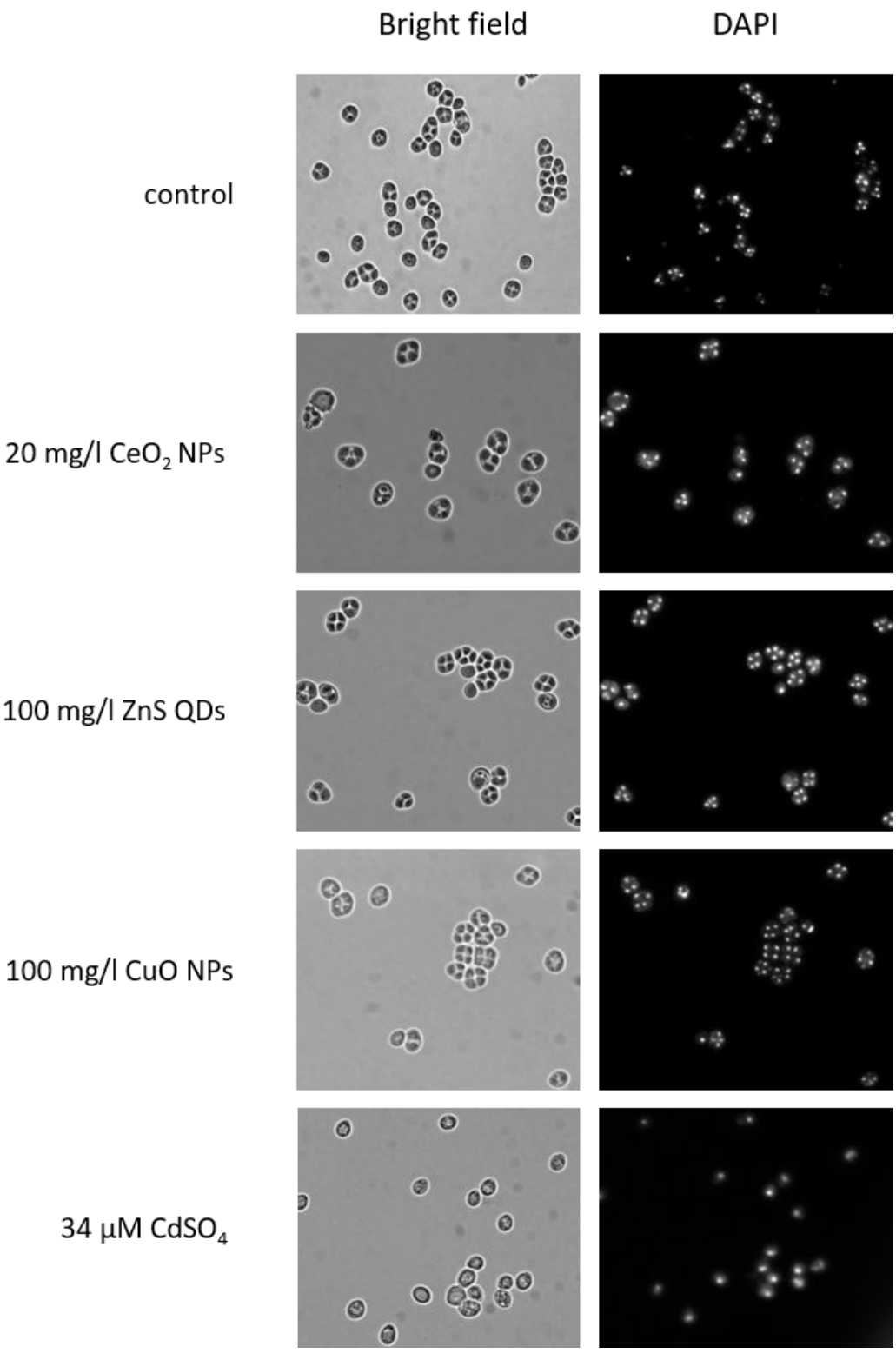

Figure 15. Effects in sporulation process induced by other NPs and cadmium ions. Yeast strain Z239-6B-6B was grown in sporulation conditions in the presence of CeO_2 NPs, ZnS QDs, CuO NPS and $CdSO_4$; cells were stained with DAPI and photographed using fluorescence microscopy. None of the tested NPs alters the process of gametogenesis. In figure are reported images obtained by the exposure of yeast cells in

sporulation medium with higher concetration tested: 20 mg L^{-1} for CeO_2 NPs, 100 mg L^{-1} for CuO NPs, 100 mg L^{-1} for ZnS QDs. Very high concentrations of CeO_2 NPs did not morphologically affect the gametogenesis process, but these NPs form aggregates that accumulates on the surface of sporulated cells. Cadmium ions strongly affect the sporulation process with the absence of asci with refractile spore, but the presence of mononucleated cells after 72 h of treatment.

None of the NPs used interfere with the meiotic process, as the newly formed asci appear indistinguishable from those found in wild-type tetrads (Fig. 15). In contrast, $CdSO_4$ exposure strongly affects the meiotic process, but in a different manner: in this case gametogenesis is inhibited, as the vast majority of the cells presented one nucleus, and the absence of budded cells implies a strong toxicity induced by this heavy metal. These results suggest that the morphological abnormalities observed during sporulation after the exposure of yeast cells with CdS QDs are specific for this NP.

Random spore analysis and spore germination

To examine the integrity and viability of single spores formed as a consequence of the meiotic process in the presence of doses (1 mg L^{-1}) of CdS QDs that not strongly compromise the gametogenesis process (Fig. 13), a random spore analysis test was performed. Untreated asci and treated with these doses of CdS QDs were collected after 72 h in sporulation medium, and spores were recovered using enzymatic and mechanical methods (see " Materials and Methods" for details). Given not all cells undergo meiosis, the analyzed samples may contain vegetative cells (mononucleated cells) in addition to asci. To eliminate the vegetative cells and at the same time to release spores from asci, the sporulation mixture was treated with lyticase, a hydrolytic enzyme that selectively degrade the cell wall of vegetative cells and asci, without affecting the viability of spores, in a buffer containing a detergent (Tween 80) and a reducing agent (2-mercaptoethanol). The concentration of single spores in the samples was then determined with a hemocytometer, and 200 spores were seeded in YPD agar plates to evaluate their competence to form colonies. The growth of germinated spores was evaluated after 3 days of growth at 28 ^{o}C (Fig. 16).

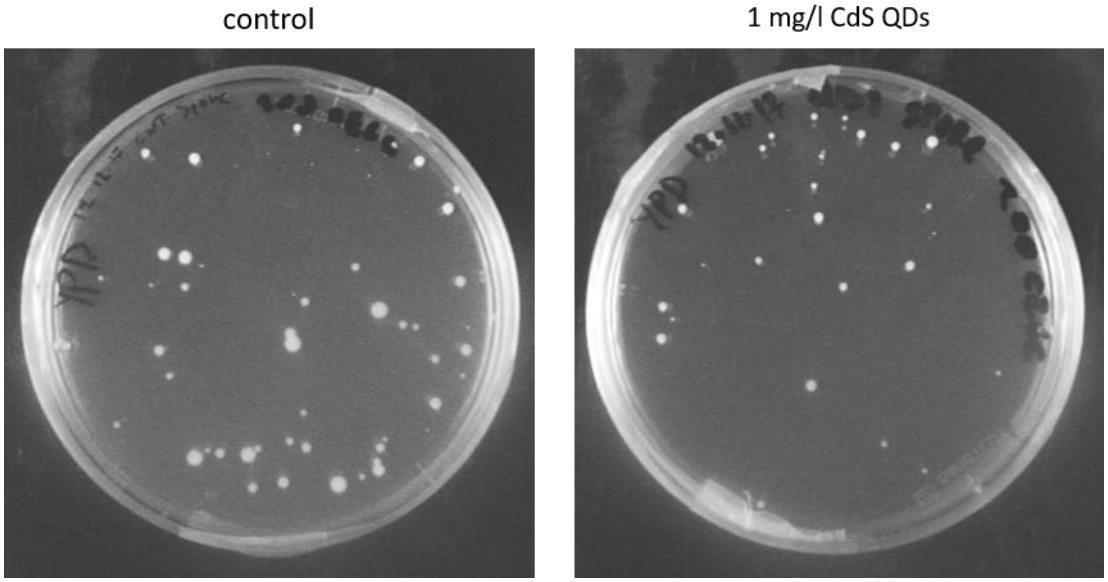

Figure 16. Germination of spores was affected by low doses of CdS QDs (1 mg L^{-1}). 200 spores were seeded in YPD agar plates to evaluate their competence to form colonies. The growth of germinated spores was evaluated after 3 days of growth at 28 °C.

The rate of germination of single spores was higher in the control in comparison to treated cells (61 and 30 colonies respectively). These results indicate that even if at low concentrations of CdS QDs *S. cerevisiae* correctly completed the gametogenesis process, with no evident morphological differences observed by fluorescence microscopy, the single spores formed were anyhow affected by the NPs exposure. Unfortunately, it was not possible to perform this analysis with cells exposed to higher concentrations of QDs, simply because in these cases the spore formation process was strongly affected. Moreover, it is interesting to note that more prolonged mechanical steps were necessary for the process of isolation of single spores from control (untreated) cells if compared to the CdS QD-treated cells, suggesting a defect in the composition of the spore wall in CdS QD-treated cells. The spore wall has in fact at least two different fundamental aspects if compared to the vegetative cell wall: it includes more elements, and it is formed de novo. The external chitosan and dityrosine layers not only protect the internal spore but they also form bridges that connect the spores of the tetrad together. These links help the spores to stay associated even when the external ascus is removed (Coluccio *et al.*, 2004).

Gene expression analysis

To determine whether the morphological alterations induced by QDs were related to a transcriptional reprogramming of the gametogenesis process, a set of specific sporulation genes, chosen by their function and the phase in which they are expressed, was analysed by Real time PCR (Fig. 17).

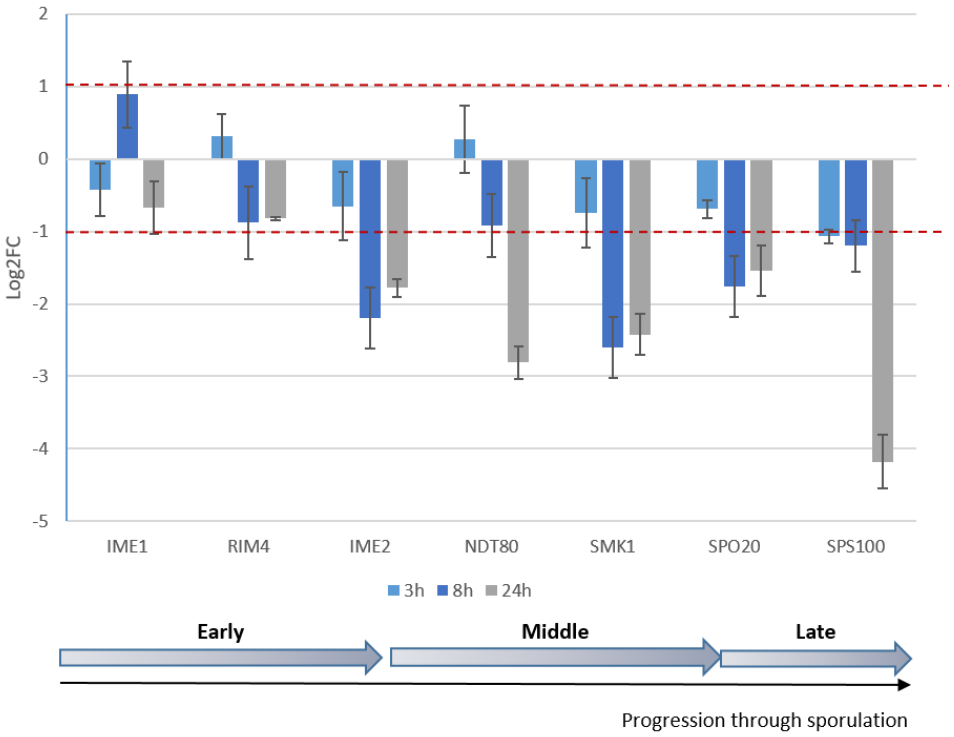

Figure 17. CdS QDs affect the expression of sporulation-specific genes after induction of sporulation. Cells were grown in sporulation media at different times (3, 8 and 24 h), total RNA was extracted from each condition and retrotranscribed. Results are represented as Log2(fold change). FC, fold change.

Yeast cells were treated for different times (3, 8 and 24 h) in sporulation medium with or without CdS QDs (4 mg L^{-1}), total RNA was extracted from these samples and cDNAs were synthesized (see "Materials and Methods" for details). Real-time PCR analysis was performed on cDNA prepared from treated and untreated samples, using *ACT1* as housekeeping gene.

Gene expression analysis showed a general down-regulation of sporulation regulatory genes (*IME2*, *NDT80* and *SMK1*; Fig. 17) expressed in the early-middle phase of the sporulation process and encoding for their downstream transcriptional targets (*SPO20* and *SPS100*; Fig. 17). Meiosis is a specialized form of nuclear division that involves a single round of DNA replication followed by two rounds of chromosome segregation and *IME2* encoding a meiosis-specific cyclin-dependent kinase

(CDK)-like kinase regulates multiple steps in meiotic development. It is known that *IME2* expression blocks DNA replication between the meiotic nuclear divisions, primarily by preventing the core enzyme of the replicative helicase to be loaded onto origins of replication (Phizicky *et al.* 2018; Hua *et al.* 2013). A downregulation of *IME2*, and as a consequence of his downstream transcriptional targets, may explain the alterations observed microscopically in the nuclear division processes. Ime2 is a positive regulator of "middle sporulation genes", as *NDT80*, encoding a meiosis-specific transcription factor, that induces the transcription of other middle sporulation genes, including *SMK1*, encoding a MAP kinase required for proper spore morphogenesis. It was shown that Smk1 is required for the execution of multiple steps in spore morphogenesis that demand increasing thresholds of its activity. A downregulation of *SMK1* can result in the formation of ascii with different level of spore membrane disorganization (Wagner *et al.* 1999; McDonald *et al.* 2009), phenotypically similar to multinucleated cells, without refractile spores, formed after CdS QD treatment. Therefore, it is possible that the treatment with CdS QDs may interfere with the action of Ime2 or with Ime2-dependent regulation of Ndt80, causing a blockage of the spore morphogenesis process.

DNA content

To directly assess the effect of CdS QDs exposure on cell cycle distribution, flow cytometric DNA content analysis was performed on cultures undergoing meiosis (Fig. 18). Wild-type yeast cells display a characteristic pattern in which after the meiotic induction all cells firstly present a 2C DNA content (where C is the DNA content of a haploid genome), then most of them undergo DNA duplication and are recognizable by the tetraploid DNA content peak (4C), while only a small portion of cells remain in an intermediate phase. In contrast, cells exposed to CdS QDs exhibit a significant increase in the proportion of cells in the intermediate premeiotic S phase of DNA duplication between 2C and 4C. The increase in the premeiotic S-phase fraction suggests that NP exposure cause a block of treated cells in this step of the development, in which DNA is duplicated but the spore maturation has not yet occurred, and is in line with the downregulation of middle sporulation genes involved in this process previously described (Fig. 17).

As observed with fluorescence microscopy (Fig. 12), FACS analysis showed that CdS QDs does not affect the viability of sporulated cells. As already seen, the percentage of dead cells after exposure to CdS QDs (5 mg L^{-1}) was about 11% (Fig. 19).

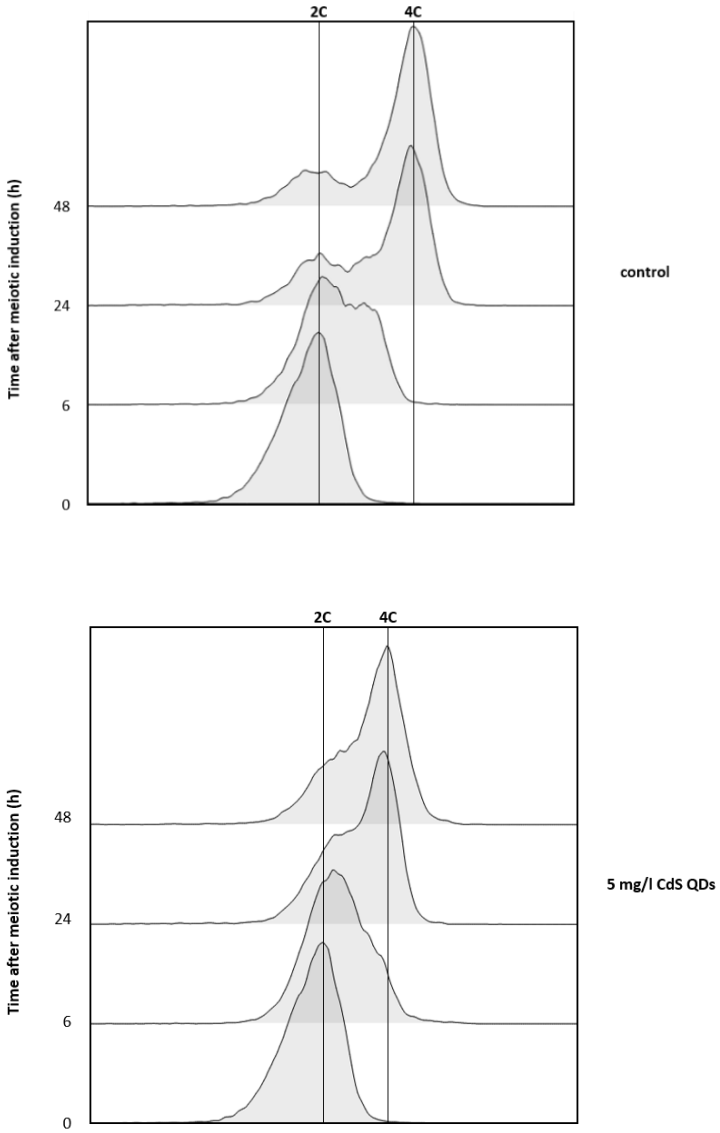

Figure 18. DNA content distribution of untreated cells and cells exposed to CdS QDs (5 mg L^{-1}) for different times in sporulation medium.

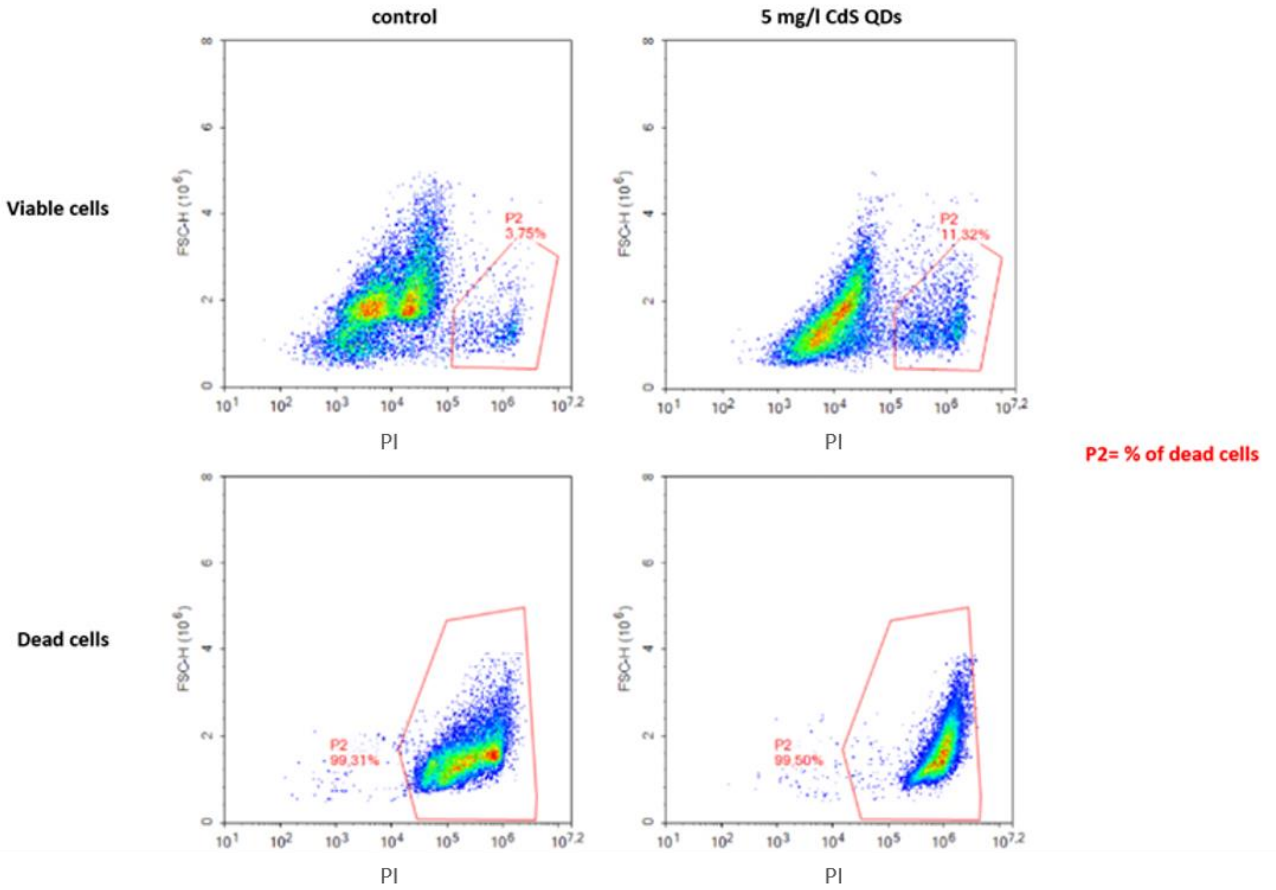

Figure 19. CdS QDs not affect the viability of sporulated cells. Cells were plotted based on forward scatter signals (FSCH) and Propidium Iodide intensity (PI), and the population of dead cells was gated using as a positive control an aliquote of cells previously killed, both for untreated and treated cells.

Identification of hard corona proteins

To better understand the potential molecular mechanism involved in CdS QD inhibition of the sporulation process, we have studied and analysed the composition of the “protein corona” formed on the surface of CdS QDs (Table 1). Proteins corona have an important role in biological activity and environmental fate of metal-based NPs. NPs are known to selectively adsorb proteins, to form a ‘corona’ bound tightly to their surface. Corona proteins which show a high affinity for the NP surface are exchanged slowly, and these so-called “hard” proteins form the innermost layer.

NPs can induce unfolding and a reduced activity of the identified proteins, but CdS QD binding to hard corona proteins could also mediate non-specific interactions with other cellular components. Misfolded corona proteins can aggregate with itself or other proteins causing cytotoxicity (Ruotolo *et al.* 2018).

Corona protein	Description (UniProt Accession N.)	Score	Coverage (%)	Biological process
Cdc19	Pyruvate kinase (P00549)	192,37	73%	Energy metabolism
Idp2	Isocitrate dehydrogenase (P41939)	174,19	67%	Metabolic process
Tdh3	Glyceraldehyde-3-phosphate dehydrogenase (P00359)	149,31	62%	Energy metabolism
Tdh2	Glyceraldehyde-3-phosphate dehydrogenase (P00358)	137,40	45%	Energy metabolism
Atp1	ATP synthase subunit alpha (P07251)	132,45	42%	Energy metabolism
Tdh1	Glyceraldehyde-3-phosphate dehydrogenase (P00360)	119,27	33%	Energy metabolism
EF-1α	Elongation factor 1-alpha (P02994)	93,01	9%	Translation process
Leu2	3-isopropylmalate dehydrogenase (P04173)	81,46	33%	Biosynthetic process
Atp2	ATP synthase subunit beta (P00830)	77,28	9%	Energy metabolism
Pdb1	Pyruvate dehydrogenase E1 component subunit beta (P32473)	73,89	11%	Energy metabolism
Psa1	Mannose-1-phosphate guanyltransferase (P41940)	63,16	12%	Cell wall biosynthetic process
Lat1	Dihydrolipoyllysine-residue acetyltransferase component of pyruvate dehydrogenase complex (P12695)	59,57	13%	Energy metabolism

Table 1. Hard corona proteins identified on the surface of CdS QD. Coverage (%): the ratio between the number of residues in all found peptides and the total number of amino acids in the entire protein sequence. Score: the probability (*P*) that the observed match between the experimental data and the database sequence was not a random event.

Notably, some proteins that bind with high affinity to the surface of CdS QDs (Cdc19, Tdh3, Tdh2, Tef1) were already identified in a previous work performed with the same organism and the same NPs but in fermentative conditions (Ruotolo *et al.* 2018): Cdc19, catalyses the conversion of phosphoenolpyruvate to pyruvate, which is the input for aerobic (TCA cycle) respiration in sporulation. The three isoforms of Glyceraldehyde-3-phosphate dehydrogenase [(GAPDH), Tdh1, Tdh2 and Tdh3], are glycolytic enzymes which catalyses the conversion of glyceraldehyde-3-phosphate to 1,3 bis-phosphoglycerate, but also display non-glycolytic activity in certain subcellular locations (Sirover 2005). EF-1α is involved in polypeptide chain elongation (Sandbaken *et al.* 1988), and is also thought to target damaged proteins to the proteasome (Spahn *et al*. 2004). It was shown that some of these proteins (in particular Cdc19 and Tdh3, the only yeast GAPDH isoform of which the structure is available) present a ring-shaped structure characterized by a ring cavity of 5-7 nm diameter that could enfold ENPs and give them high stability in aqueous media (Ruotolo *et al.* 2018). Moreover, yeast mutant strains carrying deletions in genes encoding Tdh2 and Tdh3 showed tolerant phenotypes also in the presence of high concentrations of CdS QDs, suggesting that the formation of the protein corona may be crucial in the *in vivo* response to QDs in yeast.

Other corona proteins identified are involved in respiratory metabolism (Table 1). Exposure to CdS QDs has been shown to increase the synthesis of reactive oxygen species (ROS), disrupt mitochondrial membrane potential and affect mitochondrial morphology in yeast (Pasquali *et al.* 2017). The binding of these proteins on the surface of CdS QDs suggests that the energy metabolism could be impaired by the NP-induced stress and this observation could partly explain our phenotypic observations; in fact, the respiratory metabolism is crucial for gametogenesis progression.

Finally, Psa1 (Table 1), a protein required for normal cell wall structure and involved in cell cycle progression through cell-size checkpoint was also found. Spores collected from a yeast diploid strain presenting one copy of Psa1 disrupted showed decreased viability when placed on YPD plates (Hashimoto *et al.* 1997). A similar outcome was obtained with the analysis of the spore germination performed in this work, suggesting that the interaction of CdS QDs with this protein can contribute to spore morphogenesis defects.

Part II. Effects of metal-based nanomaterials in *Cucurbita pepo* L.

Physiological, morphological analysis and metal content

Plants after complete flowering were harvested and fresh mass of roots and shoots was measured. None of the different treatments of CuO, CuO NPs, CeO2, CeO2 NPs at the concentration tested had an effect on zucchini biomass (fresh weight) as compared to untreated control (Fig. 20). These findings agree somewhat with previous works, where several reports show that exposure to CeO2 NPs did not impact physiological parameters in agricultural crops (Pagano *et al.* 2016; Ma *et al.* 2015). Moreover, Tamez *et al.* 2019 saw no significant changes in the root and leaf biomass of zucchini, treated with similar concentrations of CuO NPs, when compared to control. These results are anyway considerably different from similar studies conducted under hydroponic conditions. When yellow squash was grown in Hoagland medium, exposed with up to 500 mg kg^{-1} concentrations of CuO NPs or its micron-sized counterpart (bulk), plant biomasses decreased by 99% and 74% respectively (Musante and White 2012), whereas in Pagano *et al.* (2016) CuO NPs had no effect on zucchini total biomass as compared to untreated controls, even at higher concentrations tested, whereas in tomato, plant biomass significantly decreased, indicating a differential response dependent on plant type. Other studies in model organism *Arabidopsis thaliana* in hydroponic conditions also show a strong reduction in root length after exposure to CuO NPs (Tang *et al.* 2016). The varying results suggest that effects caused by nano copper compounds are influenced by growth medium, plant species, and exposure time. The time of treatment in this work in fact was particularly long if compared to similar experiments.

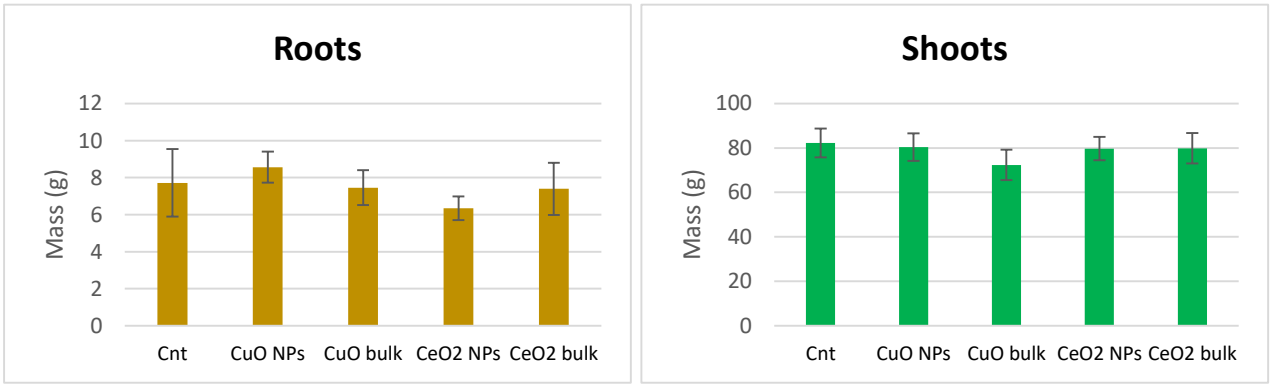

Figure 20. Fresh tissue mass of root (left) and shoot (right) of zucchini exposed to CuO NPs, CuO bulk, CeO_2 NPs, CeO_2 bulk at 100 mg kg^{-1}. Values displayed as mean ± SE of 8 replicates per treatment.

Pollen grain morphology was analysed by Environmental Scanning Electron Microscopy (ESEM) from transverse sections of developing mature anthers. No differences were observed between treatments (Fig. 21): the pollen grain is large (150-200 µm in diameter) if compared to other plants, spherical, with radial symmetry, polyantoporate with circular anulate pores. On the surface it presents macro-spikes (echinate), often covered in pollenkitt. During its development, the grain increases greatly in volume and does not dehydrate until anthesis.

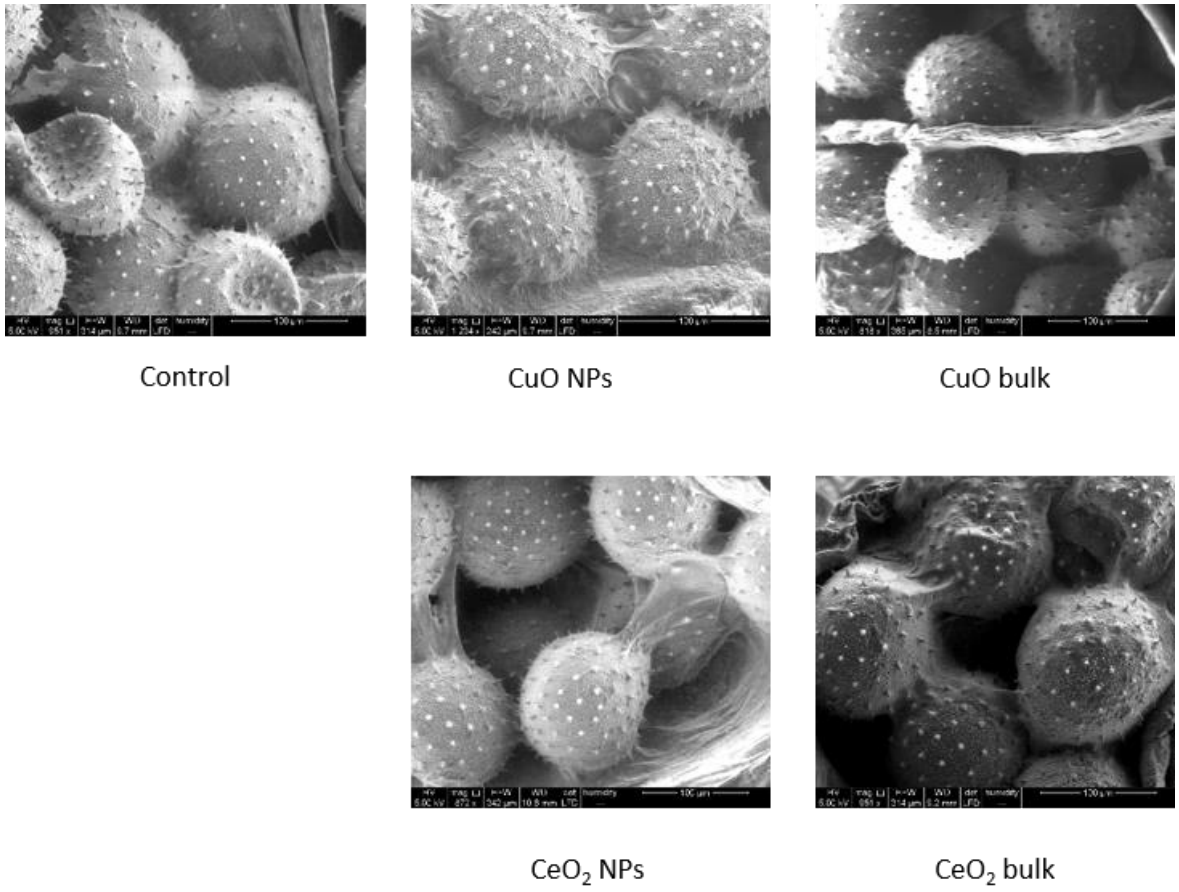

Figure 21. ESEM micrographs of fresh pollen grains from *C. pepo*

In addition to morphology, knowledge of the viability of pollen is crucial for the study of the development of male gametophyte and to the preservation of reproductive fitness of plant species. To determine if pollen development was affected in the different treatment tested, pollen viability

was examined using Alexander's stain. Again, no differences were found among treatments, with pollen viability always around 100% (Fig. 22).

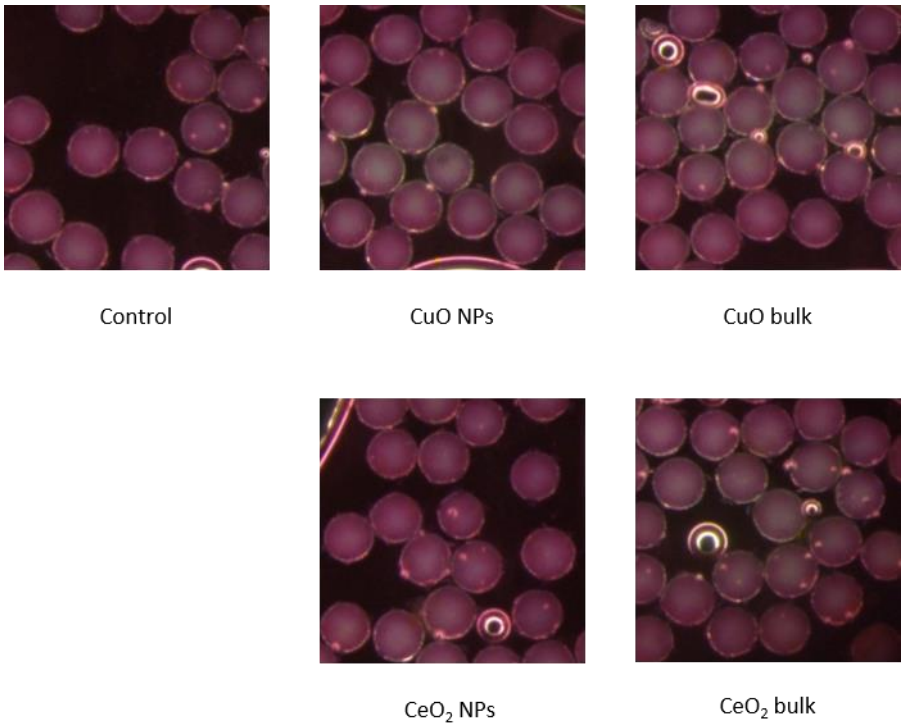

Figure 22. Viability by histochemical test of pollen. Non-aborted pollen grains are stained magenta-red. Any abortive pollens would be stained blue-green.

Previous studies had demonstrated that copper is one of the most toxic metals on seed and pollen germination, pollen viability and tube growth: Sharafi (2014) showed that high concentrations of copper lead to almost complete abolition of pollen germination and pollen tube length in Almond cultivars. The same results were seen in other plants, such as *Pisum sativum* (Sabrine *et al.* 2010). Furthermore, copper is one of the most toxic elements on pollen germination in tobacco plant (Breygina *et al.* 2012). However, dissimilar effects of heavy metal applications have been reported in fruit trees, in which copper weakly affected pollen germination and tube growth. These controversial observations may be due to distinct toleration of different plants to heavy metal stress. Very few works have been done to evaluate the potential effects on pollen caused by nanoformulation of copper: Kumbhakar *et al.* (2016) showed that both copper and cadmium sulphide NPs reduced pollen fertility in black cumin, which signifies potential hindrance exerted by these NMs either during pollen formation or in developmental maturation process or both.

Similarly, in *Coriandrum sativum* L., CdS NPs and CuO NPs are potentially effective to induce physiological alterations and cytological aberrations in meiotic cells, and as a consequence decreased viability of pollen grains (Pramanik *et al.* 2018). The aberration types and frequency induced in meiotic cells of *C. sativum* by NPs treatments are lesser than that reported before in *Nigella sativa* L.. Those variations reflect differential genotype sensitivity as well as NPs effectivity in a biological system. Copper has a primary role in many physiological pathways in plants, including respiration, photosynthesis, protein metabolism and carbohydrate distribution, so it is possible that only at higher concentrations it exerts his toxic effects. Some plants have a great tolerance to increased concentrations of copper and this element can accumulate to extremely high amounts in their tissues. The Cu and Ce content in zucchini flowers is shown in figure 23. Previous studies (Pagano *et al.* 2016, 2017), already performed ICP-MS metal content analysis on different plant tissues (roots, stems, leaves) and highlighted that zucchini effectively translocated Cu from roots to both stems and leaves, while Ce does not accumulate in leaf tissues. Flower content of copper was significantly increased by the NPs and bulk treatment (13816 mg kg^{-1} and 11260 mg kg^{-1}, respectively). The data shows that the Cu is able to reach the flowers, both in the bulk or in the nano form when compared to untreated plants. On the contrary, the relative movement from the soil to the flowers of Ce was minimal. These Ce data are in accordance with previous findings, showing a low translocation of this metal from roots to leaves. The nanocrystal structure and the lower dissolution rate of CeO_2 NPs could be a reason for the decreased level of translocation to the leaves (Ma *et al.* 2015).

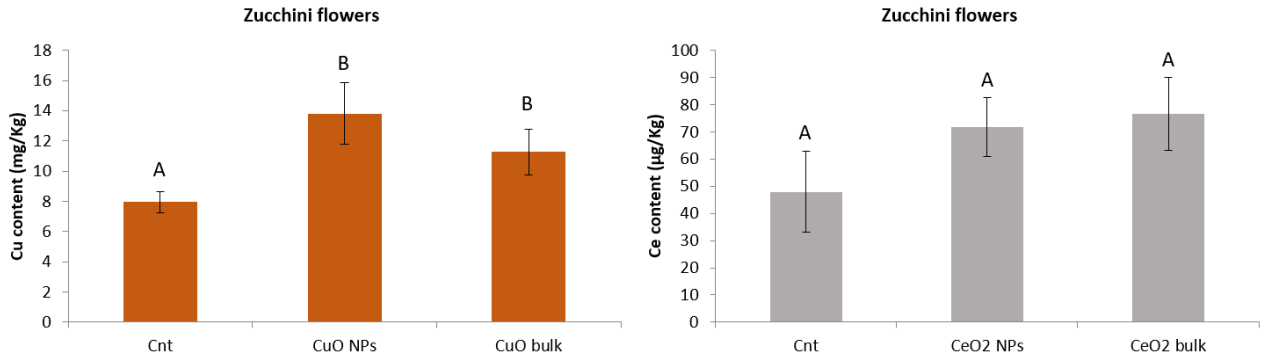

Figure 23. ICP-MS data related to Cu (mg/kg) and Ce (µg/kg) content from treatment with 0 or 100 mg L^{-1} NP or bulk CuO (left) or CeO2 (right) in flowers. Within a tissue and element, bars with different letters are significantly different (One-way ANOVA followed by a Tukey Multiple Comparison test)

RNA Sequencing

In consideration of the active translocation of Cu into flowers and previous studies indicating Cu as a strong inhibitor of pollen development and viability, the main focus was placed on the plant response to Cu exposure, performing a complete transcriptomic analysis of the different plant organs and tissues in zucchini. Total RNA from roots, leaves and pollen of plants treated with CuO NPS, CuO bulk and relative copper salt ($CuSO_4$) was extracted and the samples were sent to IGA Technologies Services (Udine, Italy) for RNA sequencing analysis. Recently, a high-quality draft of C. pepo genome with a sequences length of about 263 million base pairs (Mbp) was made accessible on Cucurbitgenomics database (http://cucurbitgenomics.org/) as well as a few C. pepo transcriptomes have been examined (Blanca *et al.* 2011; Wyatt *et al.* 2015; Xanthopoulou *et al.* 2016; Montero-Pau *et al.* 2017). Still, little is known about the genetic diversity of this important crop and even less has been done to analyze its proteome.

This first overview of RNA-seq data revealed the number of genes expressed in each sample (Fig. 24). Statistical analysis of RNA-seq showed data homogeneity between treatments in the different tissues, with similar averages and dispersions (Fig. 25 and 26). A log2 fold change ≥2.3 was used as the threshold value to highlight the significance of the differential expression. Comparison between CuO NPs, CuO bulk and $CuSO_4$ treatments showed that in roots genes with differential expression were 4420, 6540, 4747 respectively. In the leaves, CuO NPs treatment showed less variability in differential expression if compared to other treatments: 3122 genes were up- or down-regulated while in CuO bulk and $CuSO_4$ 9924 and 9103, respectively. The number of differentially expressed genes in pollen was less than half compared to other tissues (almost 6000). This greater diversity of genes expression, is probably due to the more diverse cell types present in roots and leaves than in pollen, but can be also related to the differential effect of the Cu forms taken into account in the different tissues analysed.

In the scatter plots are represented the ratio between the log2 transformed dataset profile of treated samples, compared with the untreated. Most values on the scatterplots fall along the y=x line, supporting consistency of data, on the other hand, CuO bulk and $CuSO_4$ treatment performed a more disperse response in comparison to CuO NPs, this is particularly true for the leaves.

Roots

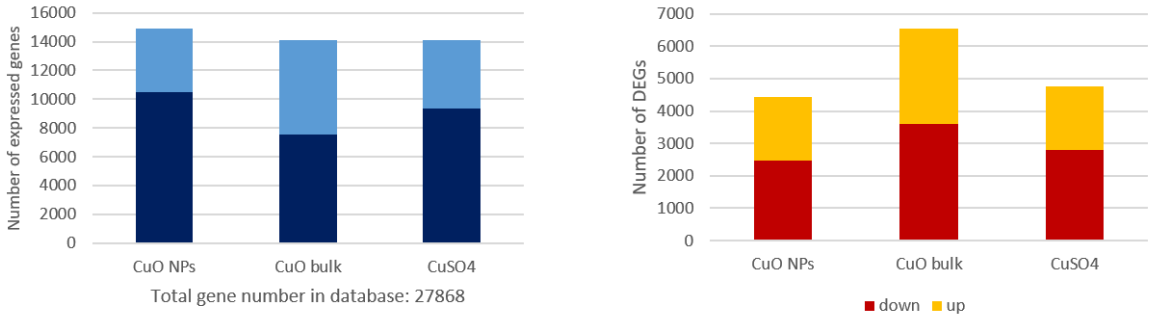

Leaves

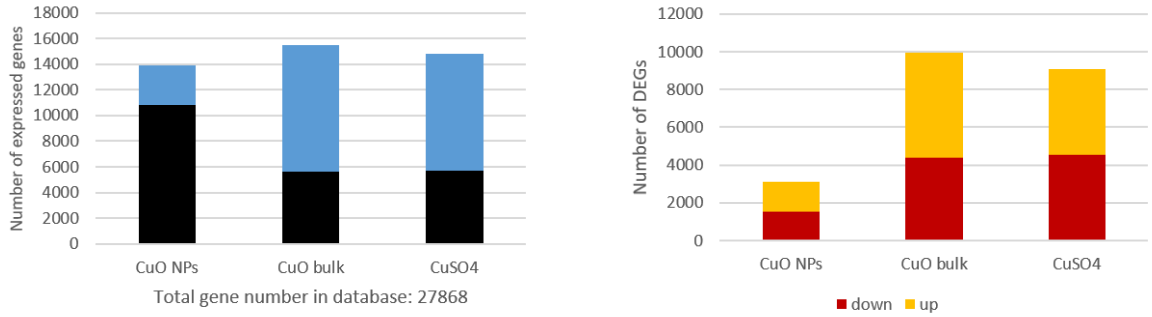

Pollen

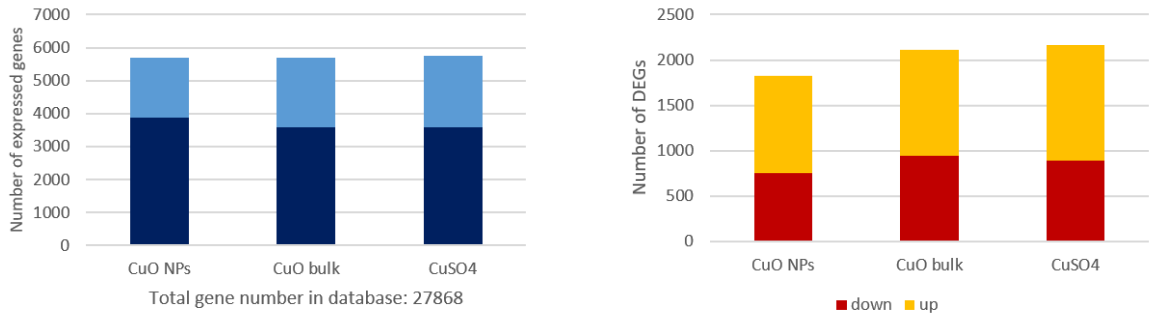

Figure 24. Statistics of expressed genes in different tissues exposed to 100 mg kg^{-1} of CuO NPs, CuO bulk and $CuSO_4$. (Left) Number of detected expressed genes for each sample compared to untreated plants (light blue: different genes expressed, dark blue: common genes expressed). (Right) Number of up- and down-regulated DEGs (differentially expressed genes) compared to untreated plants.

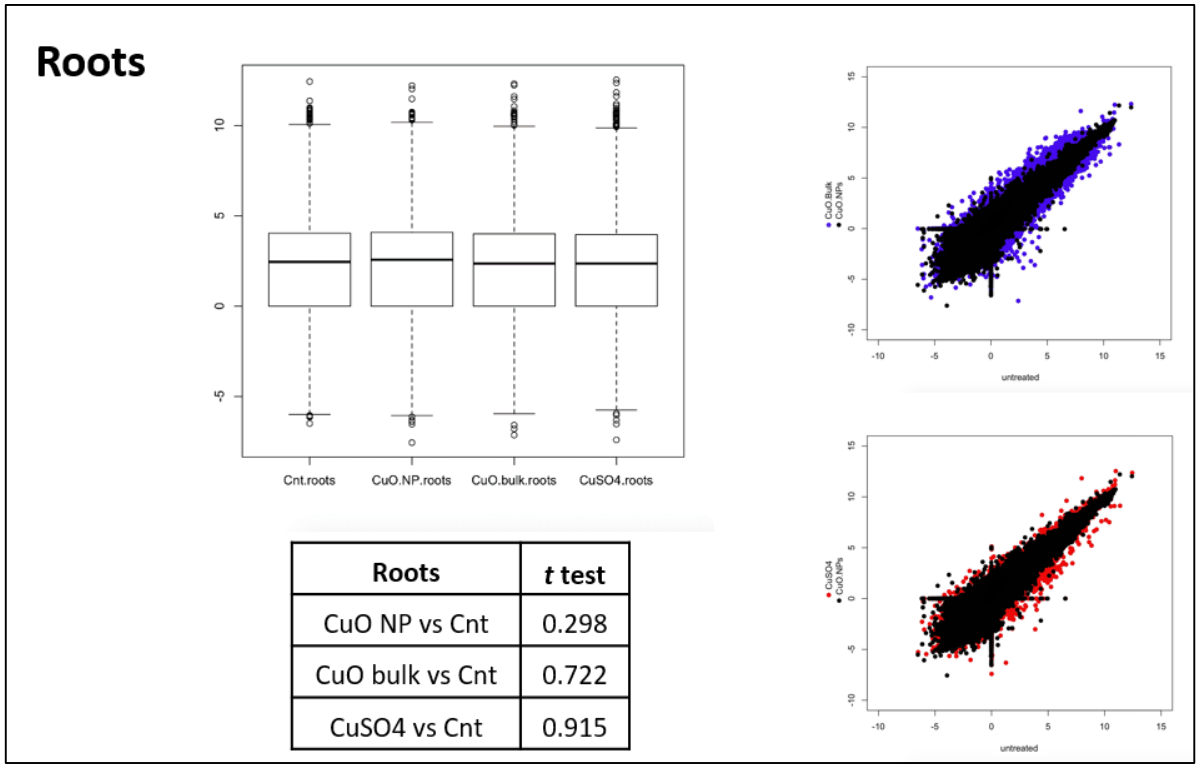

Roots	*t* test
CuO NP vs Cnt	0.298
CuO bulk vs Cnt	0.722
CuSO4 vs Cnt	0.915

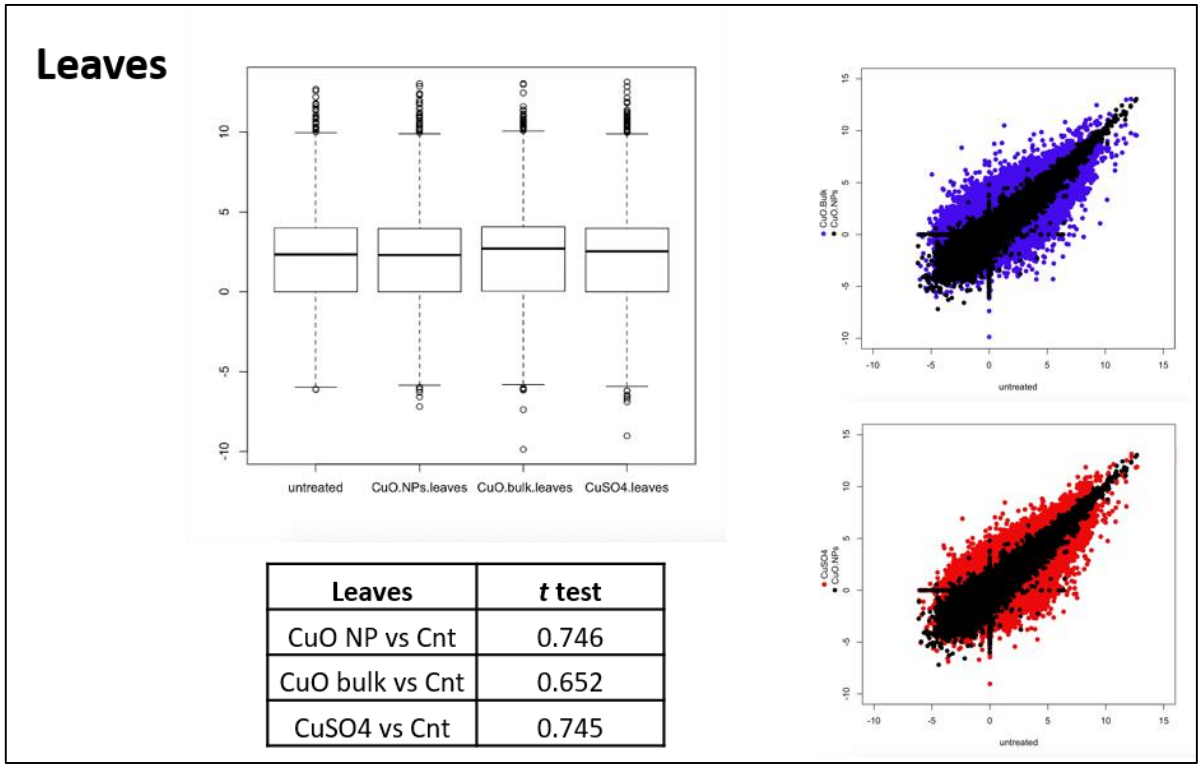

Leaves	*t* test
CuO NP vs Cnt	0.746
CuO bulk vs Cnt	0.652
CuSO4 vs Cnt	0.745

Figure 25. Statistics of expressed genes in roots and leaves exposed to 100 mg kg of CuO NPs, CuO bulk and CuSO4. (Left) Box plots and *t* tests, (Right) Scatter plots.

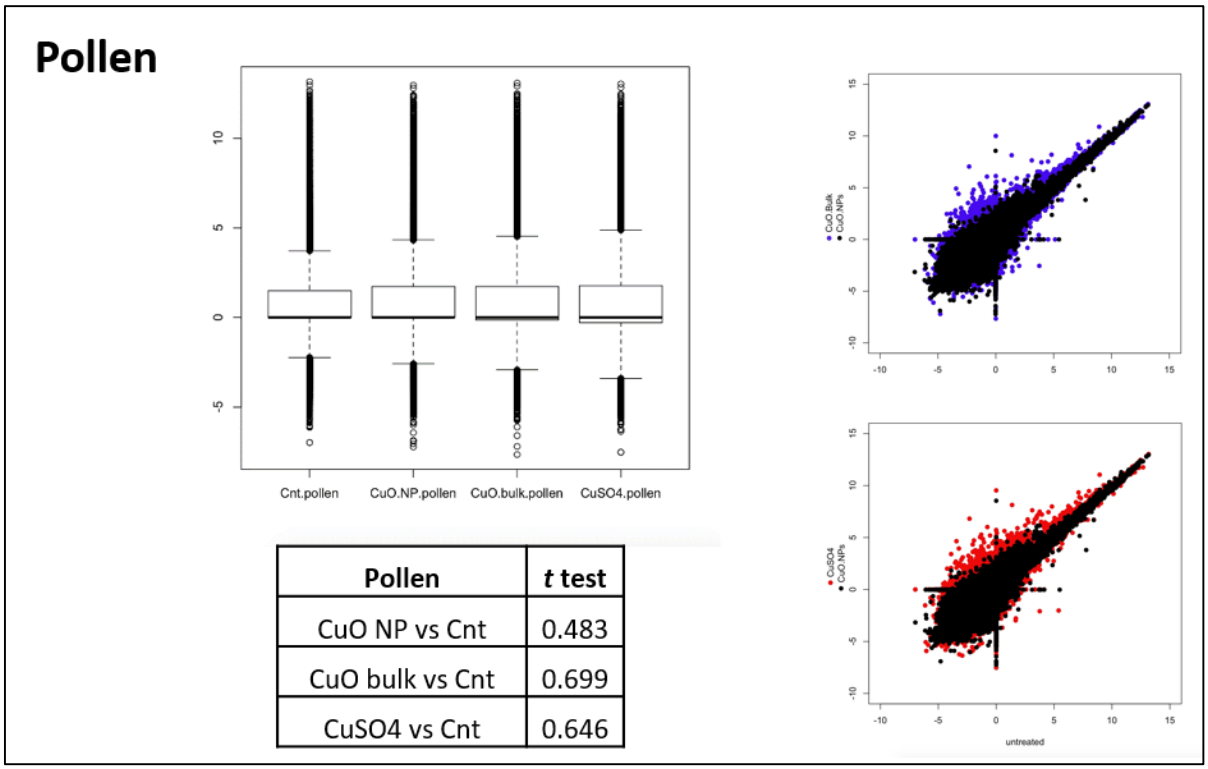

Pollen	*t* test
CuO NP vs Cnt	0.483
CuO bulk vs Cnt	0.699
CuSO4 vs Cnt	0.646

Figure 26. Statistics of expressed genes in pollen exposed to 100 mg kg of CuO NPs, CuO bulk and CuSO4. (Left) Box plots and *t* tests, (Right) Scatter plots.

Roots

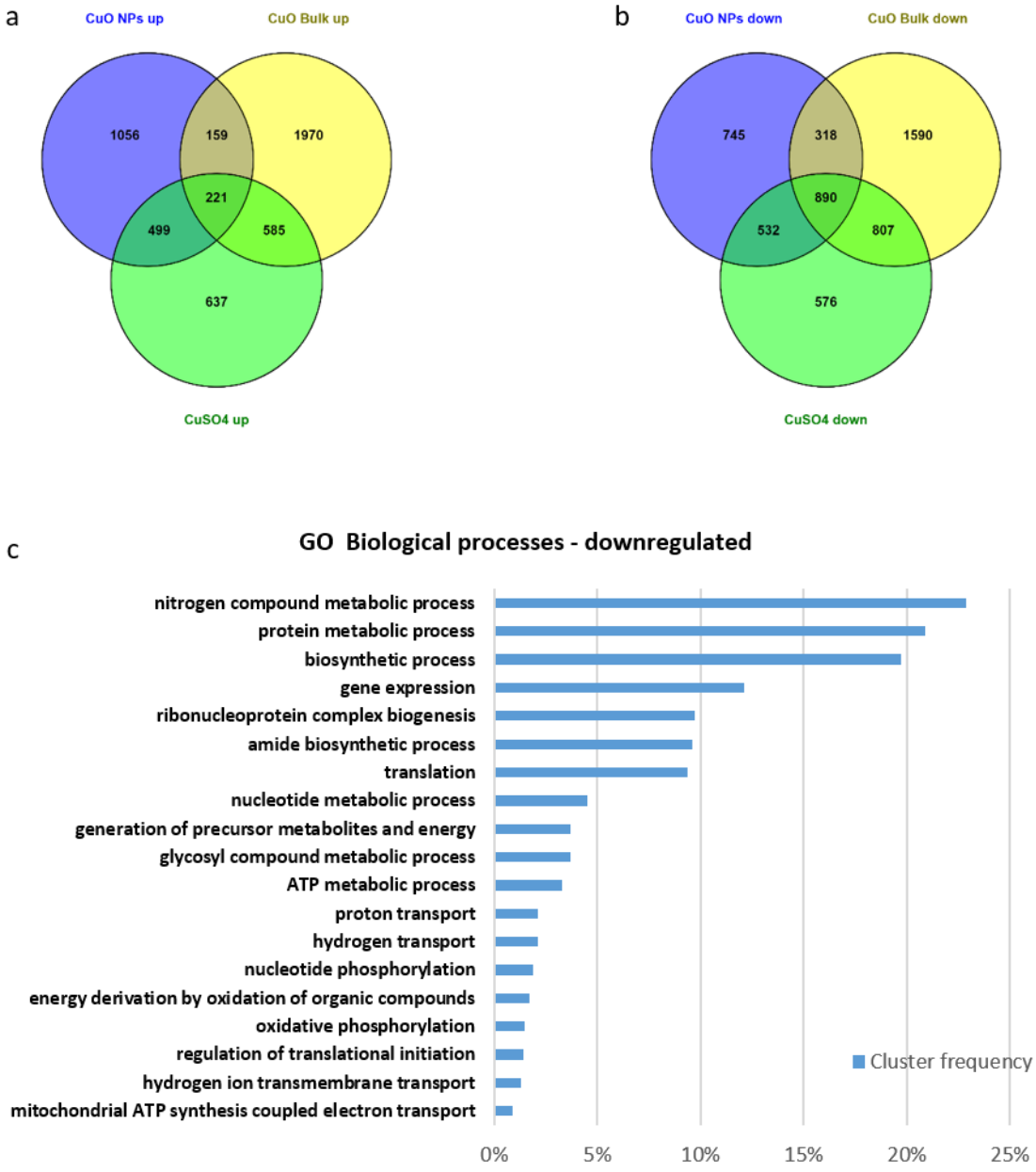

Figure 27. Venn diagrams of DEGs upregulated (a) and downregulated (b) in roots: CuO NPs treatment (blue), CuO bulk (yellow), CuSO4 (green). (c) GO enrichment in the category of biological process of DEGs down-regulated in CuO NPs treatment.

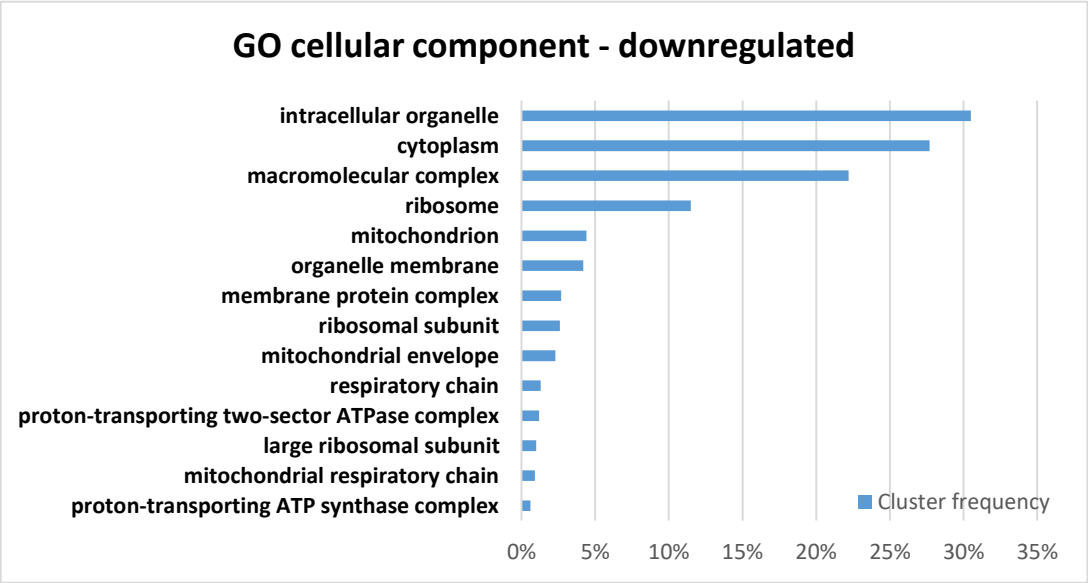

Pathway name	P-value
aerobic respiration I	3.31e-09
adenosine ribonucleotides de novo biosynthesis	2.67e-07
aerobic respiration III	1.69e-05

Figure 28. (Top) GO enrichment in the category of cellular component of DEGs down-regulated in CuO NPs treatment. (Down) Highly represented pathways.

In figures 27 and 28 are represented the Venn diagrams of DEGs upregulated and downregulated in roots and the gene ontology enrichment related to the downregulated genes found with CuO NPs treatment (GO for other treatments are reported in Appendix). For none of the conditions in roots were found GO enrichment particularly representative at the threshold used (p-value higher than 1e-05), it is also worth noting that C. pepo genome was first described only in 2017, and as a consequence GO annotations often lacks in details. The common response between all conditions was relatively low, especially if compared to other tissues (Fig. 28 and 31), only 11% and 35% of total genes up- and down- expressed in CuO NPs treated plants were in common with other conditions respectively. Metabolic processes and ribosome translation were the most highly represented groups in biological processes (Fig. 26). Biological processes involved in mitochondrial activity were also found. In contrast to NPs and bulk, in the Cu salt data also a nuclear component is represented, and this is probably due to the specific Copper ion genotoxic activity (Dutta *et al.* 2018).

Leaves

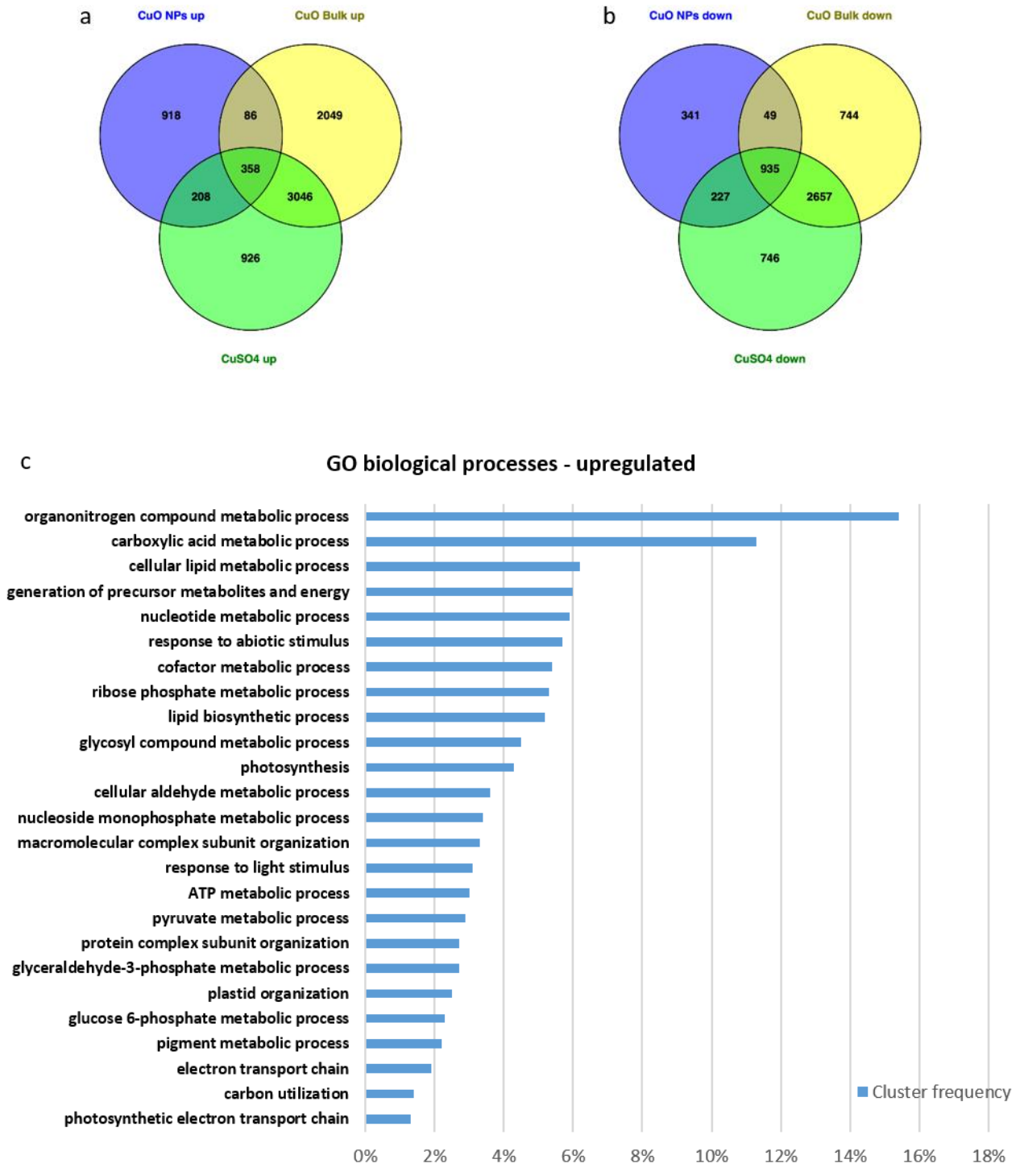

Figure 29. Venn diagrams of DEGs upregulated (a) and downregulated (b) in leaves: CuO NPs treatment (blue), CuO bulk (yellow), CuSO4 (green). (c) GO enrichment in the category of biological process of DEGs overexpressed in CuO NPs treatment.

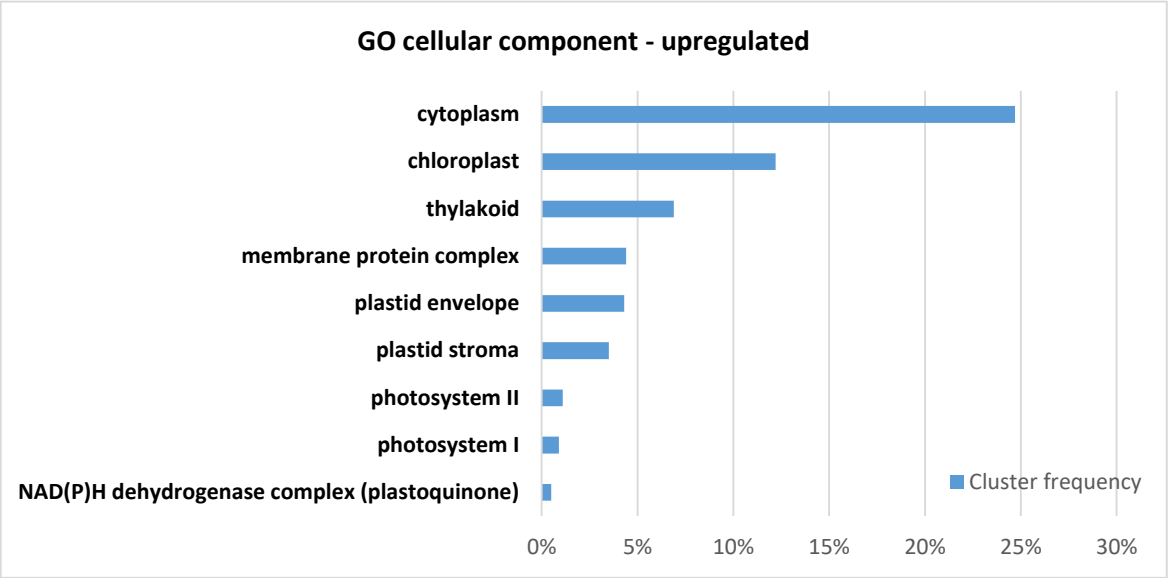

Pathway name	P-value
Calvin-Benson-Bassham cycle	2.72e-08
gluconeogenesis I	1.46e-07

Figure 30. GO enrichment in the category of cellular component of DEGs overexpressed in CuO NPs treatment and highly represented pathways.

In leaves, the percentage of genes commonly up- or down-regulated increased compared to roots: 22% and 60% respectively (Fig. 28a). This increased in common response is probably due to the higher dissolution of Cu ions from the nano and bulk forms. CuO NPs reduction and sulfidation has been observed within plant cells. The transformed products were detected as Cu_2O, Cu_2S and Cu-acetate. This processes significantly influence NP bioavailability and toxicity in plants (Dai *et al.* 2019; Servin *et al.* 2017). Genes involved in metabolic and energetic processes are still the most enriched, while in the case of cellular component, GO terms related to chloroplast are well represented, together with genes implicated in response to abiotic stimuli (Fig. 29 and 33). Previous studies in *A. thaliana* highlighted the primary role of chloroplast as a potential target of ENMs exposure (Ruotolo *et al.* 2018). CuO NPs strongly up-regulate ZAT12, a transcription factor implicated in abiotic stress response, that play a key role in ROS signalling pathway. Moreover, ZAT12 is co-expressed with

ORF31, a chloroplastic electron carrier involved in photosynthesis that has been identified as a potential biomarker of ENM exposure (Pagano *et al.* 2016). Wang *et al.* (2016) showed that CuO NPs arrested the electron transport from quinone A (QA) to quinone B (QB), and from plastoquinone (PQ) to cytochrome, but did not interact with the electron transport from Fe−S to Ferredoxin (Fig. 31). This blockage of electron transport could bring to excessive ROS accumulation and oxidative stress, causing oxidative damage of biological molecules and disruption of cellular metabolism.

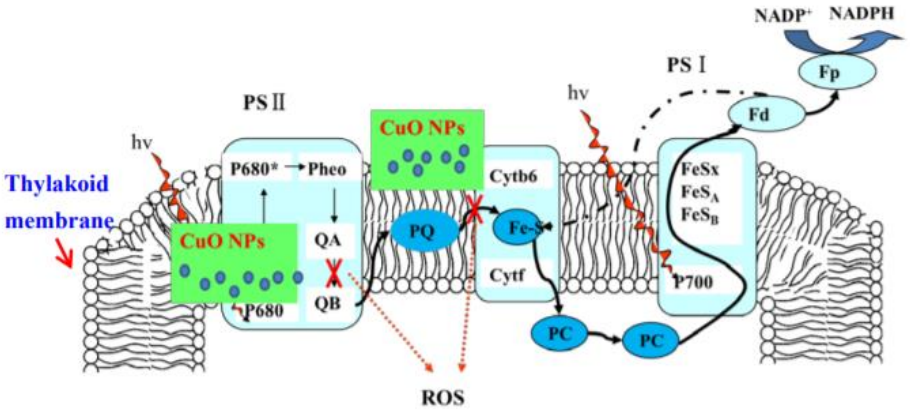

Figure 31. Schematic diagram of ROS generation sites in chloroplast electron transport chain after CuO NPs exposure (Wang *et al.* 2016).

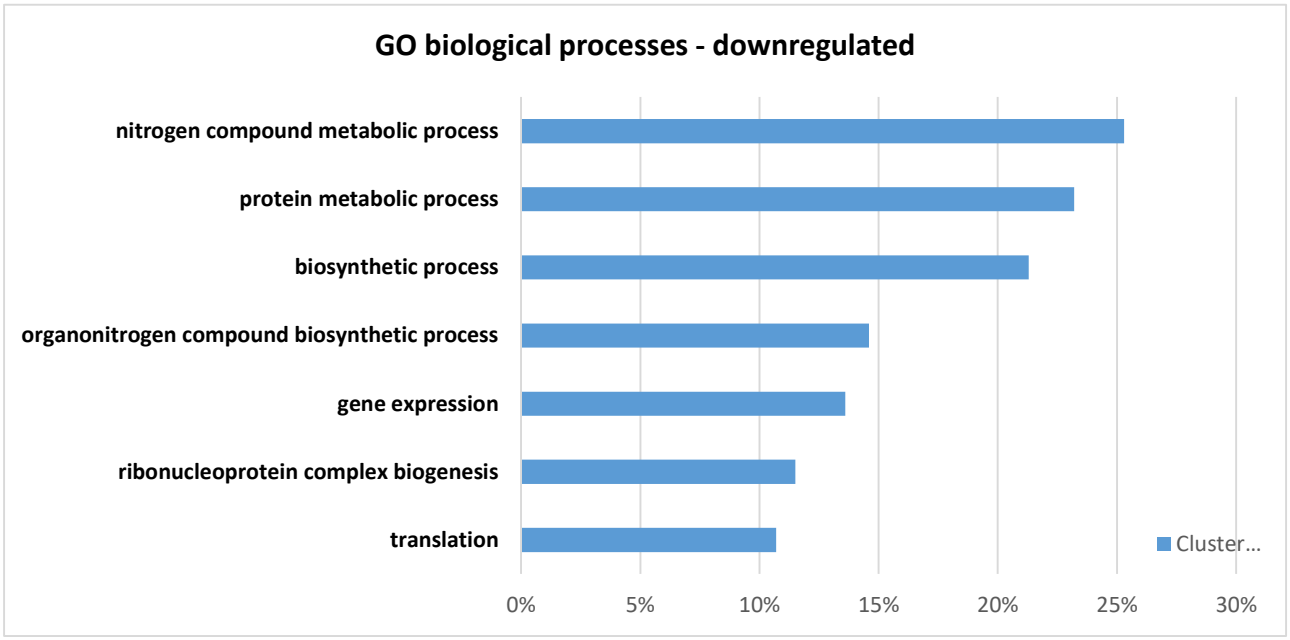

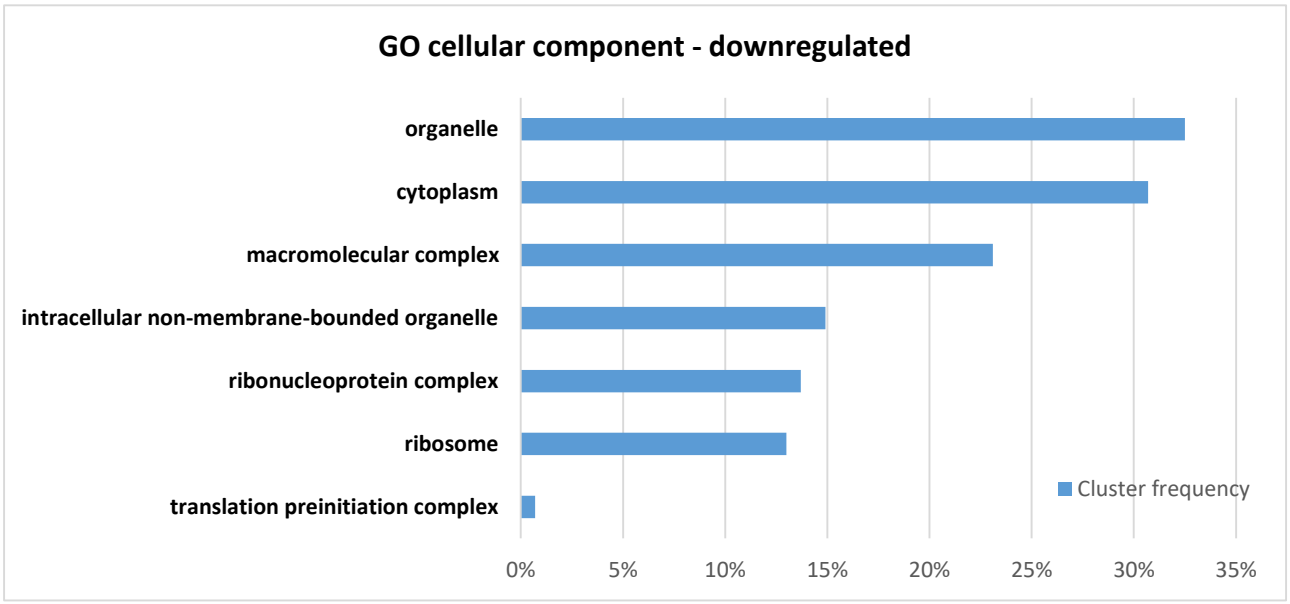

Figure 32. (Top) GO enrichment in the category of biological process of DEGs up-regulated in CuO NPs treatment in leaves (Down). GO enrichment in the category of cellular component of DEGs down-regulated in CuO NPs treatment.

Pollen

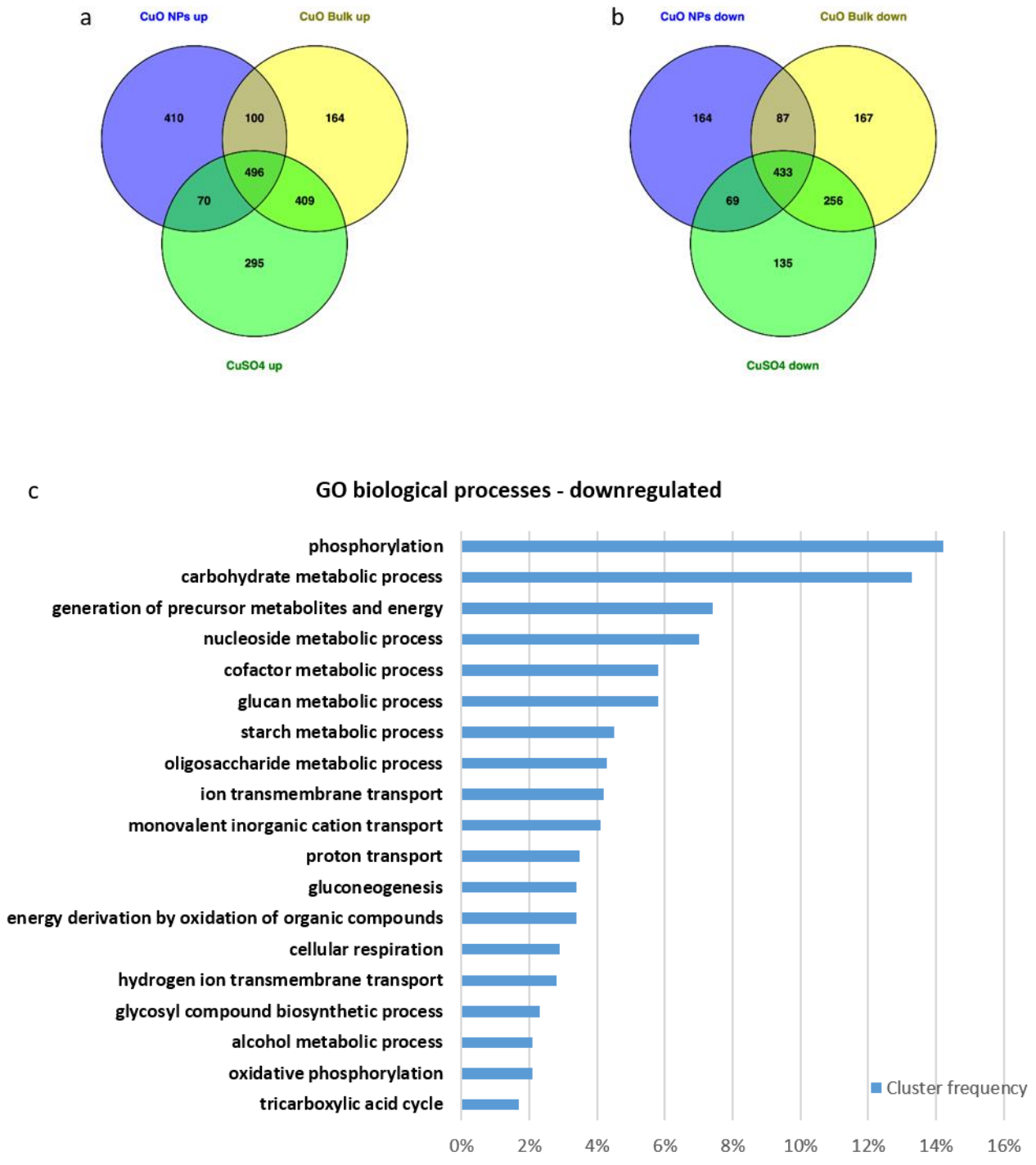

Figure 33. Venn diagrams of DEGs upregulated (a) and downregulated (b) in pollen: CuO NPs treatment (blue), CuO bulk (yellow), CuSO4 (green). (c) GO enrichment in the category of biological process of DEGs underexpressed in CuO NPs treatment.

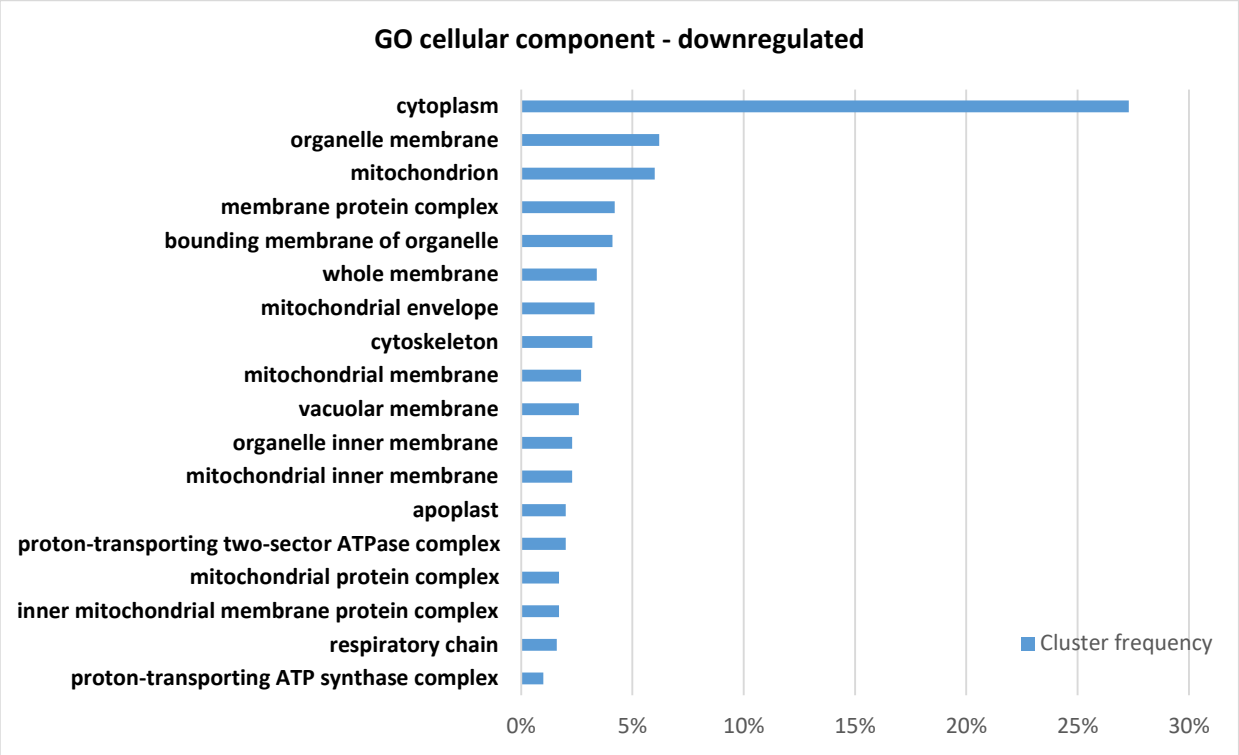

Figure 34. GO enrichment in the category of cellular component of DEGs down-regulated in CuO NPs treatment in pollen.

In pollen, the percentage of genes commonly up- or down-regulated in all treatments is once again increased if compared to leaves: 46% and 57% respectively (Fig. 33). This data enforced the idea that as CuO NPs translocated into apical parts of the plant, the percentage of copper ions dissociated increased, and as a consequence the unspecific response between the different formulations of copper. Nevertheless, CuO NPs still has a great percentage of DEGs, unlike the bulk or the ion form. This result suggests that even if a part of CuO NPs dissociates, releasing copper ions and giving rise of the unspecific response, part of CuO NPs remains stable, exerting a nanospecific response. Pollen has a significantly lower amount of expressed genes compared with other vegetative tissue, and it's known that some genes are pollen-specific and others are expressed only in sporophytic tissues (Honys and Twell 2003; Becker *et al.* 2003). The most marked difference compared to leaves was the low expression levels in pollen of genes implicated in energy metabolism (especially photosynthesis), this finding is not surprising, as pollen is not photosynthetically active. The other striking difference is the higher expression level of genes with proposed functions in ion transport,

cell-wall metabolism, and cytoskeletal dynamics in comparison with vegetative tissues. Previous studies showed the implication of polarized internal gradients and/or external fluxes of protons, potassium, and chloride in pollen tube growth (Hepler *et al.* 2001). Anyway, channels and transporters involved in ion fluxes across the plasma membrane in pollen tubes are still largely unknown. Starch biosynthesis during the final phases of pollen maturation is fundamental not only because starch is a reserve source of energy for pollen germination but it also acts as a checkpoint of pollen maturity. Frequently, pollen maturation seems to be prematurely aborted if starch levels remain lower than a threshold point where pollen inviability is associated with starch deficiency (Wen and Chase 1999). A key aspect of tip growth of pollen tubes is the constant deposition of new cell wall and plasma membrane at the tube apex. Vesicles delivering this material are mediated by the actin cytoskeleton (Da Costa-Nunes and Grossniklaus 2003).

Conclusions

Nanotechnology is a rapidly growing field having potential applications in many areas. Engineered NPs have been widely used in several fields from medical to electronics and possess unique chemico-physical properties as compared to their bulk counterparts. The increasing interest for these advanced materials has led to great excitement about their potential benefits, but little is known about the biological effects of NP exposure on the environment and human health. Although studies on NP toxicity already exist, few of them report *in vivo* data. In this work, two different organisms, *S. cerevisiae* and *C. pepo L.* were exposed to diverse metal-based NPs, to assess the effects on the production of gametes.

Sporulation in yeast provides an excellent model system to study the meiotic developmental pathway. This process is tightly regulated by a precise transcriptional program and the timing of gene expression strongly correlates with the sporulation progression. Moreover, although sporulation in yeast has specific peculiarities, such as the formation of stress-resistant spores, some key aspects of the process have been conserved from yeast to higher organisms.

The presence in the sporulation medium of a particular kind of metal-based NPs, cadmium sulfide quantum dots, caused an alteration of the meiotic nuclear divisions in combination with a strong inhibition of spore morphogenesis, resulting in the formation of asci containing the meiotic products, but with the absence of refractile spores (multinucleated cells). These morphological anomalies seem to be peculiar for this specific NPs, as the same effect was not seen using other types of metal-based NPs characterized by different particle dimensions and Zeta potentials (ZnO, CuO, CeO_2) or a cadmium salt ($CdSO_4$) that, conversely, blocks the gametogenesis process forming mononucleated cells. To determine if the morphological alterations induced by QDs were followed by a transcriptional reprogramming of the gametogenesis process, a set of specific sporulation genes was analyzed by Real time PCR. Accordingly with the phenotypic effects observed in response to CdS QD exposure, a down-regulation of regulatory genes expressed in the early-middle phase of the sporulation process and their downstream transcriptional targets was found. Among these genes, *IME2* is involved in nuclear replication and in the regulation of sporulation progression, and *SMK1*, that is regulated by the transcription factor Ndt80 (one of the most downregulated genes upon CdS QD treatment) is involved in the proper spore morphogenesis. Smk1 is required for the execution of multiple steps in spore morphogenesis that demand increasing thresholds of its activity. Analysis of DNA content by Fluorescence-activated cell sorting (FACS) showed that sporulated cells exposed to CdS QDs presented an altered DNA content profile, in line with the phenotypic observations obtained by fluorescence microscopy. Moreover, the viability analysis of

singles spores reveals a lower germination rate of spores derived from treated cells, even at very low concentrations. Finally, investigation of the hard corona protein composition showed that the most abundant proteins found in the analysis are involved in the energetic metabolism and cell wall synthesis, and the modulation of this proteins by the presence of CdS QDs suggests that energy metabolism could be impaired by the NP-induced stress.

In flowering plants, the pollen grains are the products of the meiotic division. They are formed in the male reproductive organs of the flower, the anthers. The first mitotic division of the meiotic products (unicellular pollen) gives rise to two cells, the generative cell and the vegetative cell. The pollen grain in *C. pepo* is bicellular, with a generative cell enclosed inside the vegetative cell.

Literature is giving increased relevance to the beneficial effects that some ENMs may have on edible plants, when used as fertilizer or pest control agents. However, the lack of knowledge to the potential environmental effects and health risks are still limiting the widespread commerce and application of ENMs. Furthermore, because of the poor data of metals translocation into flowers, it is unclear what fitness repercussion may emerge crop plants that are capable of translocating heavy metals to their reproductive organs. The ENMs taken into consideration in this project, together with their bulk counterparts, have potential application in agriculture as nanofertilizers or nanopesticides (CeO_2, CuO).

RNAseq analysis performed in different tissues on zucchini allows a transcriptional assessment of plant response to diverse forms of Cu. A comparison between genes differentially expressed in different parts of the plant revealed that the number of common genes between treatments increased during metal translocation from roots to shoots: in roots the common response was relatively low, only 11% and 35% of total genes up- and down- expressed in CuO NPs treated plants were in common with other conditions respectively. This percentage increased in the apical part of the plant, reaching a percentage of 46% and 57% in pollen. This enrichment in the non-specific response with increasing translocation, is probably due to the dissolution of copper ions from the bulk and the nano form, which is initially modest (Rotini *et al.* 2017). On the other hand, CuO NPs preserved also a nano-specific response, due to the coexistence of nano and ionic forms derived from NPs dissolution, suggesting that both NPs and dissolved ions will contribute to the transcriptomic response during plants exposure.

Analysing the enriched GO terms, the modulated genes related to oxidative stress, mitochondria and electron transport chain were found particularly enriched in all tissues analysed. It was

previously observed that internalized CuO NPs were mainly located on mitochondria of plant cells. CuO NPs could inhibit complexes I and III on mitochondrial electron transport chain, resulting in the over-production of ROS and oxidative stress-induced membrane damage (Wang *et al.* 2016; Dai *et al.* 2018). The transformation of CuO NPs firstly occurred on plant cell walls but also intracellularly, and mitochondria were the main locations for CuO NPs transformation, suggesting that mitochondria could play an important role in the toxicity of CuO NPs to plant cells (Dai et al. 2019). In leaves, GO terms related to chloroplast are highly represented. Alterations in photosynthetic activity have been commonly reported as an indicator of plant physiological response to ENMs exposure, and oxidative stress sensing and signalling pathways within chloroplasts are well-known. For example, Wang *et al.* (2016) demonstrated direct evidence of ENMs impacts on the two photosystems and on the thylakoid electron transport chain, and future works will be focused on the characterization of genes involved in mitochondrion and chloroplasts response to NPs. Lately, CuO NPs are tested as potential candidates for agrochemical fertilizer and pesticides to increase plant production, due to its beneficial effects in plant growth as well as defence. For instance, Elmer *et al.* (2018) showed that watermelon plants infested with *Fusarium oxysporum f. sp. Niveum* sprayed with CuO NPs suspension suppressed disease and increased biomass, while plants treated in field produced more fruit compared to control. Anyway, contradictory results are present in literature, because of the many variables involved: experimental conditions, time and way of exposure, the plant species used, and especially the concentration tested. In this work, no physiological changes have been observed on plant biomass and pollen morphology and vitality at the concentration tested. Cu has a fundamental role in many pathways in plants, including photosynthesis, respiration, and carbohydrate distribution, protein metabolism and is already present within cells at a certain level; but at high concentrations could negatively affect the plants. RNAseq data showed that at equivalent concentration tested, the number of differentially expressed genes in plant exposed to CuO NPs was lower when compared to other treatments, suggesting a lower impact of the nano form on gametes, designating this formulation as potentially employable for nanofertilization purposes.

Acknowledgements

I wish to thank Prof. Nelson Marmiroli for the coordination of this project. I also thank my tutor Prof. Roberta Ruotolo to help me during these years of work. Thanks to all the colleagues, in particular Prof. Marta Marmiroli and Prof. Luca Pagano, for their help and suggestion during these three years of PhD.

I would also like to thank the Connecticut Agricultural Experiment Station of New Haven, CT, for giving me the opportunity to spend six months of my PhD in their laboratories and allowing me to gain experience in an international work environment.

I wish to thank also Dr. Andrea Zappettini and Dr. Marco Villani of the IMEM-CNR (Parma, Italy) for providing certified CdS QDs, useful comments and suggestions on the physics of nanomaterials.

References

Adhikari T, Sarkar D, Mashayekhi H, Xing B. Growth and enzymatic activity of maize (*Zea mays* L.) plant: Solution culture test for copper dioxide nano particles. *J Plant Nutr*. 2016;39(1):99-115. doi:10.1080/01904167.2015.1044012

Ariga K., Hill JP., Lee MV., Vinu A., Charvet R., Acharya S. Challenges and breakthroughs in recent research on self-assembly. *Sci Technol Adv Mater* 2008; 9:014109

Bailey RE., Smith AM., Nie S. Quantum dots in biology and medicine. *Physica E*. 2004; 25:1–12

Balavi H, Samadanian-Isfahani S, Mehrabani-Zeinabad M, Edrissi M. Preparation and optimization of CeO_2 nanoparticles and its application in photocatalytic degradation of Reactive Orange 16 dye. *Powder Technol*. 2013;249(3):549-555. doi:10.1016/j.powtec.2013.09.021

Becker D, Boavida LC, Carneiro J, Haury M, Feijo A. Transcriptional profiling of *Arabidopsis* tissues reveals the unique characteristics of the pollen transcriptome. *Plant Physiol*. 2003;133(October):713-725. doi:10.1104/pp.103.028241

Becker J, Boavida LC, Carneiro J, Haury M, Feijó JA: Transcrip- tional profiling of *Arabidopsis* tissues reveals the unique characteristics of the pollen transcriptome. Plant Physiol 2003, 133:713-725

Bencivenni M, Faccini A, Zecchi R, et al. Electrospray MS and MALDI imaging show that non-specific lipid-transfer proteins (LTPs) in tomato are present as several isoforms and are concentrated in seeds. *J Mass Spectrom*. 2014;49(12):1264-1271. doi:10.1002/jms.3454

Blanca J, Cañizares J, Roig C, Ziarsolo P, Nuez F, Picó B. Transcriptome characterization and high throughput SSRs and SNPs discovery in *Cucurbita pepo* (Cucurbitaceae). *BMC Genomics*. 2011;12(1):104. doi:10.1186/1471-2164-12-104

Blum J.L, Edwards J.R, Prozialeck W.C, Xiong J.Q, Zelikoff J.T. Effects of Maternal Exposure to Cadmium Oxide Nanoparticles During Pregnancy on Maternal and Offspring Kidney Injury Markers Using a Murine Model. *J Toxicol Environ Health A.* 2015;78(12):711-24. doi: 10.1080/15287394.2015.1026622

Bondarenko O, Juganson K, Ivask A, Kasemets K, Mortimer M, Kahru A. Toxicity of Ag, CuO and ZnO nanoparticles to selected environmentally relevant test organisms and mammalian cells in vitro: A critical review. *Arch Toxicol*. 2013;87(7):1181-1200. doi:10.1007/s00204-013-1079-4

Borm PJA, Robbins D, Haubold S, et al. *The Potential Risks of Nanomaterials: A Review Carried out for ECETOC*. Vol 3.; 2006. doi:10.1186/1743-8977-3-11

Breygina M, Matveyeva N, Polevova S, et al. Ni2+ effects on *Nicotiana tabacum* L. pollen germination and pollen tube growth. *BioMetals*. 2012;25(6):1221-1233. doi:10.1007/s10534-012-9584-0

Brown PD, Tokuhisa JG, Reichelt M, Gershenzon J. Variation of glucosinolate accumulation among different organs and developmental stages of *Arabidopsis thaliana*. *Phytochemistry*. 2003;62(3):471-481. doi:10.1016/S0031-9422(02)00549-6

Burden N, Aschberger K, Chaudhry Q, et al. The 3Rs as a framework to support a 21st century approach for nanosafety assessment. *Nano Today*. 2017;12:10-13. doi:10.1016/j.nantod.2016.06.007

Buzea C, Pacheco II, Robbie K. Nanomaterials and nanoparticles: Sources and toxicity. *Biointerphases*. 2007;2(4):MR17-MR71. doi:10.1116/1.2815690

Carpenter K, Bell RB, Yunus J, Amon A, Berchowitz LE. Phosphorylation-Mediated Clearance of Amyloid-like Assemblies in Meiosis. *Dev Cell*. 2018;45(3):392-405.e6. doi:10.1016/j.devcel.2018.04.001

Carvajal F, Garrido D, Jamilena M, Rosales R. Cloning and characterisation of a putative pollen-specific polygalacturonase gene (CpPG1) differentially regulated during pollen development in zucchini (*Cucurbita pepo* L.). *Plant Biol*. 2014;16(2):457-466. doi:10.1111/plb.12070

Chang YN, Zhang M, Xia L, Zhang J, Xing G. The toxic effects and mechanisms of CuO and ZnO nanoparticles. *Materials (Basel)*. 2012;5(12):2850-2871. doi:10.3390/ma5122850

Cheki M, Moslehi M, Assadi M. Marvelous applications of quantum dots. *Eur Rev Med Pharmacol Sci*. 2013;17(9):1141-1148

Cherkasov A., Muratov EN., Fourches D., Varnek A., Baskin II., Cronin M., Dearden J., Gramatica P., Martin YC., Todeschini R., Consonni V., Kuz'min VE., Cramer R., Benigni R., Yang C., Rathman J., Terfloth L., Gasteiger J., Richard A., Tropsha A. QSAR modeling: where have you been? Where are you going to? *J. Med. Chem.* 2014; 57(12):4977-5010. doi: 10.1021/jm4004285

Coluccio A, Bogengruber E, Conrad MN, Dresser ME, Briza P, Neiman AM. Morphogenetic Pathway of Spore Wall Assembly in *Saccharomyces cerevisiae*. *Society*. 2004;3(6):1464-1475. doi:10.1128/EC.3.6.1464

Da Costa-Nunes JA, Grossniklaus U. Unveiling the gene-expression profile of pollen. *Genome Biol*. 2003;5(1):9-11. doi:10.1186/gb-2003-5-1-205

Da Costa-Nunes JA, Grossniklaus U. Unveiling the gene-expression profile of pollen. *Genome Biol*. 2003;5(1):9-11. doi:10.1186/gb-2003-5-1-205

Dai Y, Wang Z, Zhao J, et al. Interaction of CuO nanoparticles with plant cells: Internalization, oxidative stress, electron transport chain disruption, and toxicogenomic responses. *Environ Sci Nano*. 2018;5(10):2269-2281. doi:10.1039/c8en00222c

Dai Y, Zhao J, Liu X, et al. Transformation and species identification of CuO nanoparticles in plant cells (*Nicotiana tabacum*) . *Environ Sci Nano*. 2019;6(9):2724-2735. doi:10.1039/c9en00781d

de Carvalho SM, Mansur AAP, Mansur HS, Guedes MIMC, Lobato ZIP, Leite MF. In vitro and in vivo assessment of nanotoxicity of CdS quantum dot/aminopolysaccharide bionanoconjugates. *Mater Sci Eng C*. 2017;71:412-424. doi:10.1016/j.msec.2016.10.023

Dearden JC., Hewitt M., Bresnen GM., Gregg CN. Improved correlation between animal and human potency of non-steroidal anti-inflammatory drugs using quantitative structure-activity relationships (QSARs). *SAR QSAR Environ Res*. 2017; 28(7):557-565. doi: 10.1080/1062936X.2017.1351391

Dekkers S, Oomen AG, Bleeker EAJ, et al. Towards a nanospecific approach for risk assessment. *Regul Toxicol Pharmacol*. 2016;80:46-59. doi:10.1016/j.yrtph.2016.05.037

Deng C, Saunders W. RIM4 encodes a meiotic activator required for early events of meiosis in *Saccharomyces cerevisiae*. Mol Genet Genomics. 2001;266(3):497-504. doi:10.1007/s004380100571

Derfus A.M., Chan W.C.W. , Bhatia S.N. Probing the cytoxicity of semiconductor quantum dots Nano Lett., 4 (2004), pp. 11-18

Digonnet-Kerhoas C, Gay G, Duplan JC, Dumas C. Viability of Cururbita pepo pollen: biophysical and structural data. *Planta*. 1989;179(2):165-170. doi:10.1007/BF00393686

Djurišić AB, Leung YH, Ng AMC, et al. Toxicity of metal oxide nanoparticles: Mechanisms, characterization, and avoiding experimental artefacts. *Small*. 2015;11(1):26-44. doi:10.1002/smll.201303947

Dos Santos S. C., Sá-Correia I. Yeast toxicogenomics: lessons from a eukaryotic cell model and cell factory. *Curr Opin Biotechnol*. 2015; 33, 183-191

Dunnick KM, Pillai R, Pisane KL, Stefaniak AB, Sabolsky EM, Leonard SS. The Effect of Cerium Oxide Nanoparticle Valence State on Reactive Oxygen Species and Toxicity. *Biol Trace Elem Res*. 2015;166(1):96-107. doi:10.1007/s12011-015-0297-4

Dutta S, Mitra M, Agarwal P, et al. Oxidative and genotoxic damages in plants in response to heavy metal stress and maintenance of genome stability. *Plant Signal Behav*. 2018;13(8):1-17. doi:10.1080/15592324.2018.1460048

Dutta S, Mitra M, Agarwal P, et al. Oxidative and genotoxic damages in plants in response to heavy metal stress and maintenance of genome stability. *Plant Signal Behav*. 2018;13(8):1-17. doi:10.1080/15592324.2018.1460048

Elmer W, Latorre-Roche R De, Pagano L, et al. Effect of metalloid and metal oxide nanoparticles on fusarium wilt of watermelon. *Plant Dis*. 2018;102(7):1394-1401. doi:10.1094/PDIS-10-17-1621-RE

Fan J, Shao M, Lai L, Liu Y, Xie Z. Inhibition of autophagy contributes to the toxicity of cadmium telluride quantum dots in *Saccharomyces cerevisiae*. *Int J Nanomedicine*. 2016b;11:3371-3383. doi:10.2147/IJN.S108636

Fan J, Sun Y, Wang S, et al. Inhibition of autophagy overcomes the nanotoxicity elicited by cadmium-based quantum dots. *Biomaterials*. 2016;78:102-114. doi:10.1016/j.biomaterials.2015.11.029

Formisano G, Roig C, Esteras C, et al. Genetic diversity of Spanish *Cucurbita pepo* landraces: An unexploited resource for summer squash breeding. *Genet Resour Crop Evol*. 2012;59(6):1169-1184. doi:10.1007/s10722-011-9753-y

Futamura N, Mori H, Kouchi H, Shinohara K. Male flower-specific expression of genes for polygalacturonase, pectin methylesterase and β-1,3-glucanase in a dioecious willow (*Salix gilgiana* Seemen). *Plant Cell Physiol*. 2000;41(1):16-26. doi:10.1093/pcp/41.1.16

Gao S, Wang X, Wang S, Zhu S, Rong R, Xu X. Complex effect of zinc oxide nanoparticles on cadmium chloride-induced hepatotoxicity in mice: Protective role of metallothionein. *Metallomics*. 2017;9(6):706-714. doi:10.1039/c7mt00024c

Garrido D, Busscher J, Van Tunen AJ. Promoter activity of a putative pollen monosaccharide transporter in *Petunia hybrida* and characterisation of a transposon insertion mutant. *Protoplasma*. 2006;228(1-3):3-11. doi:10.1007/s00709-006-0171-5

Gates BD, Xu Q, Stewart M, Ryan D, Willson CG, Whitesides GM. New approaches to nanofabrication: Molding, printing, and other techniques. *Chem Rev*. 2005;105(4):1171-1196. doi:10.1021/cr030076o

Goffeau A, Barrell B.G, Bussey H, Davis R.W, Dujon B, Feldmann H, Galibert F, Hoheisel J.D, Jacq C, Johnston M, Louis E.J, Mewes H.W, Murakami Y, Philippsen P, Tettelin H, Oliver S.G. Life with 6000 genes. *Science.* 1996; Vol.274, Issue 5287, pp. 546-567; DOI: 10.1126/science.2745287.546

Grigore ME, Biscu ER, Holban AM, Gestal MC, Grumezescu AM. Methods of synthesis, properties and biomedical applications of CuO nanoparticles. *Pharmaceuticals*. 2016;9(4):1-14. doi:10.3390/ph9040075

Haddad P.S, Seabra A.B. Biomedical applications of magnetic nanoparticles. In Iron Oxides: Structure, Properties and Applications; Martinez, A.I., Ed.; Nova Science Publishers, Inc.: New York, NY, USA, 2012; Volume 1, pp. 165–188

Hardy A, Benford D, Halldorsson T, et al. Guidance on risk assessment of the application of nanoscience and nanotechnologies in the food and feed chain: Part 1, human and animal health. *EFSA J*. 2018;16(7). doi:10.2903/j.efsa.2018.5327

Hashimoto H, Sakakibara A, Yamasaki M, Yoda K. *Saccharomyces cerevisiae* VIG9 encodes GDP-mannose pyrophosphorylase, which is essential for protein glycosylation. *J Biol Chem*. 1997;272(26):16308-16314. doi:10.1074/jbc.272.26.16308

Hepler PK, Vidali L, Cheung AY (2001) Polarized cell growth in higher plants. Annu Rev Cell Dev Biol 17: 159‑187

Honys D, Twell D. Press release IMEC RR sensing. 2003;132(June):640-652. doi:10.1104/pp.103.020925

Honys D, Twell D: Comparative analysis of the *Arabidopsis* pollen transcriptome. Plant Physiol 2003, 132:640-652

Hou J, Wang X, Hayat T, Wang X. Ecotoxicological effects and mechanism of CuO nanoparticles to individual organisms. *Environ Pollut*. 2017;221:209-217. doi:10.1016/j.envpol.2016.11.066

Hua H, Namdar M, Ganier O, Gregan J, Mé chali M, Kearsey SE. Sequential steps in DNA replication are inhibited to ensure reduction of ploidy in meiosis. *Mol Biol Cell*. 2013;24(5):578-587. doi:10.1091/mbc.E12-11-0825

Javanbakht T, Laurent S, Stanicki D, Wilkinson KJ. Relating the Surface Properties of Superparamagnetic Iron Oxide Nanoparticles (SPIONs) to Their Bactericidal Effect towards a Biofilm of *Streptococcus mutans*. *PLoS One*. 2016;11(4):1-13. doi:10.1371/journal.pone.0154445

Jeevanandam J, Barhoum A, Chan YS, Dufresne A, Danquah MK. Review on nanoparticles and nanostructured materials: History, sources, toxicity and regulations. *Beilstein J Nanotechnol*. 2018;9(1):1050-1074. doi:10.3762/bjnano.9.98

Karlsson HL, Gustafsson J, Cronholm P et al. Size-dependent toxicity of metal oxide particles-A comparison between nano- and micrometer size. *Toxicol Lett. 2009;* 188:112–118

Keller AA, Lazareva A. Predicted Releases of Engineered Nanomaterials: From Global to Regional to Local. *Environ Sci Technol Lett*. 2013;1(1):65-70. doi:10.1021/ez400106t

Kreyling WG, Semmler-Behnke M, Seitz J, et al. Size dependence of the translocation of inhaled iridium and carbon nanoparticle aggregates fürom the lung of rats to the blood and secondary target organs. *Inhal Toxicol*. 2009;21(SUPPL. 1):55-60. doi:10.1080/08958370902942517

Kumbhakar DV, Datta AK, Mandal A, et al. Effectivity of copper and cadmium sulphide nanoparticles in mitotic and meiotic cells of *Nigella sativa* L. (black cumin) – can nanoparticles act as mutagenic agents? *J Exp Nanosci*. 2016;11(11):823-839. doi:10.1080/17458080.2016.1149236

Lu PJ, Huang SC, Chen YP, Chiueh LC, Shih DYC. Analysis of titanium dioxide and zinc oxide nanoparticles in cosmetics. *J Food Drug Anal*. 2015;23(3):587-594. doi:10.1016/j.jfda.2015.02.009

Ma C, White JC, Dhankher OP, Xing B. Metal-Based Nanotoxicity and Detoxification Pathways in Higher Plants. *Environ Sci Technol*. 2015;49(12):7109-7122. doi:10.1021/acs.est.5b00685

Mailly D. Nanofabrication techniques. *Eur Phys J Spec Top*. 2009;172(1):333-342. doi:10.1140/epjst/e2009-01058-x

Majumdar S, Ma C, Villani M, et al. Surface coating determines the response of soybean plants to cadmium sulfide quantum dots. *NanoImpact*. 2019;14(November 2018):100151. doi:10.1016/j.impact.2019.100151

Marmiroli M, Pagano L, Pasquali F, et al. A genome-wide nanotoxicology screen of *Saccharomyces cerevisiae* mutants reveals the basis for cadmium sulphide quantum dot tolerance and sensitivity. *Nanotoxicology*. 2016;10(1):84-93. doi:10.3109/17435390.2015.1019586

Marmiroli M, Pagano L, Savo Sardaro ML, Villani M, Marmiroli N. Genome-wide approach in *Arabidopsis thaliana* to assess the toxicity of cadmium sulfide quantum dots. *Environ Sci Technol*. 2014;48(10):5902-5909. doi:10.1021/es404958r

Marmiroli M., Imperiale D., Pagano L., Villani M., Zappettini A., Marmiroli N. The Proteomic Response of *Arabidopsis thaliana* to Cadmium Sulfide Quantum Dots, and Its Correlation with the Transcriptomic Response. *Front. Plant Sci*. 2015; 16; 6:1104. doi: 10.3389/fpls.2015.01104

Marmiroli, White S. *Exposure to Engineered Nanomaterials in the Environment*. Elsevier; 2019. doi:10.1016/B978-0-12-814835-8.00028-5

McCarthy J, Inkielewicz-Stępniak I, Corbalan JJ, Radomski MW. Mechanisms of toxicity of amorphous silica nanoparticles on human lung submucosal cells in vitro: Protective effects of fisetin. *Chem Res Toxicol*. 2012;25(10):2227-2235. doi:10.1021/tx3002884

McDonald CM, Wagner M, Dunham MJ, Shin ME, Ahmed NT, Winter E. The Ras/cAMP pathway and the CDK-like kinase Ime2 regulate the MAPK Smk1 and spore morphogenesis in *Saccharomyces cerevisiae*. *Genetics*. 2009;181(2):511-523. doi:10.1534/genetics.108.098434

McDonald CM, Wagner M, Dunham MJ, Shin ME, Ahmed NT, Winter E. The Ras/cAMP pathway and the CDK-like kinase Ime2 regulate the MAPK Smk1 and spore morphogenesis in *Saccharomyces cerevisiae*. *Genetics*. 2009;181(2):511-523. doi:10.1534/genetics.108.098434

Mcwilliams JNA. Nanoclays and Nanotubes : Global Markets to 2022. *BCC Res Rep NANO21H*. 2018.

Meindl GA, Ashman TL. Nickel Accumulation by *Streptanthus polygaloides* (*Brassicaceae*) Reduces Floral Visitation Rate. *J Chem Ecol*. 2014;40(2):128-135. doi:10.1007/s10886-014-0380-x

Meindl GA, Bain DJ, Ashman TL. Variation in nickel accumulation in leaves, reproductive organs and floral rewards in two hyperaccumulating *Brassicaceae* species. *Plant Soil*. 2014;383(1-2):349-356. doi:10.1007/s11104-014-2184-8

Montero-Pau J, Blanca J, Bombarely A, et al. De novo assembly of the zucchini genome reveals a whole-genome duplication associated with the origin of the Cucurbita genus. *Plant Biotechnol J*. 2018;16(6):1161-1171. doi:10.1111/pbi.12860

Musante W. Toxicity of Silver and Copper to *Cucurbita pepo*: Differential Effects of Nano and Bulk-Size Particles. *Environ Toxicol*. 2012;165:16. doi:10.1002/tox.20667

Oberdörster G, Oberdörster E, Oberdörster J. Nanotoxicology: An emerging discipline evolving from studies of ultrafine particles. *Environ Health Perspect*. 2005;113(7):823-839. doi:10.1289/ehp.7339

Obrero Á, Die J V., Román B, Gómez P, Nadal S, González-Verdejo CI. Selection of reference genes for gene expression studies in zucchini (*Cucurbita pepo*) using qPCR. *J Agric Food Chem*. 2011;59(10):5402-5411. doi:10.1021/jf200689r

Oh E., Liu R., Nel A., Gemill K.B., Bilal M., Cohen Y., Medintz I.L. Meta-analysis of cellular toxicity for cadmium-containing quantum dots. *Nature Nanotechnology.* 2016; 11, 479–486

Paesano L, Perotti A, Buschini A, et al. Markers for toxicity to HepG2 exposed to cadmium sulphide quantum dots; damage to mitochondria. *Toxicology*. 2016;374:18-28. doi:10.1016/j.tox.2016.11.012

Pagano L, Pasquali F, Majumdar S, et al. Exposure of: *Cucurbita pepo* to binary combinations of engineered nanomaterials: Physiological and molecular response. *Environ Sci Nano*. 2017;4(7):1579-1590. doi:10.1039/c7en00219j

Pagano L., Servin A.D., De La Torre-Roche R., Mukherjee A., Majumdar S., Hawthorne J., Marmiroli M., Maestri E., Marra R.E., Isch S.M., Dhankher O.P., White J.C., Marmiroli N. Molecular Response of Crop Plants to Engineered Nanomaterials. Environ Sci Technol. 2016; 5; 50(13):7198-207. doi: 10.1021/acs.est.6b01816

Pasquali F, Agrimonti C, Pagano L, et al. Nucleo-mitochondrial interaction of yeast in response to cadmium sulfide quantum dot exposure. *J Hazard Mater*. 2017;324:744-752. doi:10.1016/j.jhazmat.2016.11.053

Phizicky D V., Berchowitz LE, Bell SP. Multiple kinases inhibit origin licensing and helicase activation to ensure reductive cell division during meiosis. *Elife*. 2018;7:1-23. doi:10.7554/eLife.33309

Popov AP, Zvyagin A V., Lademann J, et al. Designing inorganic light-protective skin nanotechnology products. *J Biomed Nanotechnol*. 2010;6(5):432-451. doi:10.1166/jbn.2010.1144

Pramanik A, Datta AK, Das D, et al. Assessment of Nanotoxicity (Cadmium Sulphide and Copper Oxide) Using Cytogenetical Parameters in *Coriandrum sativum* L. (*Apiaceae*). *Cytol Genet*. 2018;52(4):299-308. doi:10.3103/S0095452718040084

Rocha TL, Mestre NC, Sabóia-Morais SMT, Bebianno MJ. Environmental behaviour and ecotoxicity of quantum dots at various trophic levels: A review. *Environ Int*. 2017;98:1-17. doi:10.1016/j.envint.2016.09.021

Rotini A, Tornambè A, Cossi R, et al. Salinity-based toxicity of CuO nanoparticles, CuO-bulk and Cu ion to vibrio anguillarum. *Front Microbiol*. 2017;8(OCT). doi:10.3389/fmicb.2017.02076

Ruotolo R, Pira G, Villani M, Zappettini A, Marmiroli N. Ring-shaped corona proteins influence the toxicity of engineered nanoparticles to yeast. *Environ Sci Nano*. 2018;5(6):1428-1440. doi:10.1039/c7en01226h

Ryu J, Girigoswami K, Ha C et al. Influence of multiple metal ions on β-amyloid aggregation and dissociation on a solid surface. Biochemistry. 2008; 47(19):5328–5335

Sabella S, Carney RP, Brunetti V et al (2014) A general mechanism for intracellular toxicity of metal-containing nanoparticles. Nanoscale 6:7052–7061

Sabrine H, Afif H, Mohamed B, Hamadi B, Maria H. Effects of Cadmium and Copper on Pollen Germination and Fruit Set in Pea (*Pisum sativum* L.). Scientia Horticulturae. 2010; 125. 551-555. 10.1016/j.scienta.2010.05.031

Sahu D, Kannan GM, Vijayaraghavan R. Size-dependent effect of zinc oxide on toxicity and inflammatory potential of human monocytes. *J Toxicol Environ Heal - Part A Curr Issues*. 2014;77(4):177-191. doi:10.1080/15287394.2013.853224

Sánchez-Mata D, De La Fuente V, Rufo L, Rodríguez N, Amils R. Localization of nickel in tissues of *Streptanthus polygaloides* gray (*Cruciferae*) and endemic nickel hyperaccumulators from california. *Biol Trace Elem Res*. 2014;157(1):75-83. doi:10.1007/s12011-013-9868-4

Sandbaken MG, Culbertson MR. Mutations in elongation factor EF-1 alpha affect the frequency of frameshifting and amino acid misincorporation in *Saccharomyces cerevisiae*. *Genetics*. 1988;120(4):923-934

Saquib Q, Faisal M, Al-Khedhairy AA, Alatar AA. *Cellular and Molecular Toxicity of Nanoparticles*.; 2012. doi:10.1007/978-90-481-9751-4_100120

Savolainen K, Pylkkänen L, Norppa H, et al. Nanotechnologies, engineered nanomaterials and occupational health and safety - A review. *Saf Sci*. 2010;48(8):957-963. doi:10.1016/j.ssci.2010.03.006

Seabra A.B, Haddad P.S. Cytotoxicity and Genotoxicity of Iron Oxides Nanoparticles. In Nanotoxicology: Materials, Methodologies, and Assessment; Durán, N., Guterres, S.S., Alves, O.L., Eds.; Springer: New York, NY, USA, 2014; Chapter 12, pp. 265–279

Seabra AB, Durán N. Nanotoxicology of metal oxide nanoparticles. 2015; Metals 5:934–975

Servin AD, Pagano L, Castillo-Michel H, et al. Weathering in soil increases nanoparticle CuO bioaccumulation within a terrestrial food chain. *Nanotoxicology*. 2017;11(1):98-111. doi:10.1080/17435390.2016.1277274

Sharafi Y. Effects of Copper and Leadon Pollen Germination Traits in Almond Cultivars. *J Nuts (International J Nuts Relat Sci*. 2014;5(2):67-73

Shvedova AA, Kisin ER, Mercer R, et al. Unusual inflammatory and fibrogenic pulmonary responses to single-walled carbon nanotubes in mice. *Am J Physiol - Lung Cell Mol Physiol*. 2005;289(5 33-5):1-37. doi:10.1152/ajplung.00084.2005

Silva G. A. Neuroscience nanotechnology: progress, opportunities and challenges. *Nat. Rev. Neurosci*. 2016; 7:65-74

Sirover MA. New nuclear functions of the glycolytic protein, glyceraldehyde-3-phosphate dehydrogenase, in mammalian cells. *J Cell Biochem*. 2005;95(1):45-52. doi:10.1002/jcb.20399

Smijs TG, Pavel S. Titanium dioxide and zinc oxide nanoparticles in sunscreens: Focus on their safety and effectiveness. *Nanotechnol Sci Appl*. 2011;4(1):95-112

Spahn CMT, Gomez-Lorenzo MG, Grassucci RA, et al. Domain movements of elongation factor eEF2 and the eukaryotic 80S ribosome facilitate tRNA translocation. *EMBO J*. 2004;23(5):1008-1019. doi:10.1038/sj.emboj.7600102

Stampoulis D, Sinha SK, White JC. Assay-dependent phytotoxicity of nanoparticles to plants. *Environ Sci Technol*. 2009; 43:9473–9479

Stone V., Johnstone H. J., Balharry D., Gernand JM., Gulumian M. Approaches to develop alternative testing strategies to inform human health risk assestement of nanomaterials. *Risk Anal*. 2016; 36(8)1535-50

Strtak A, Sathiamoorthy S, Tang PS, et al. Yeast Populations Evolve to Resist CdSe Quantum Dot Toxicity. *Bioconjug Chem*. 2017;28(4):1205-1213. doi:10.1021/acs.bioconjchem.7b00056

Sund J, Alenius H, Vippola M, Savolainen K, Puustinen A. Proteomic characterization of engineered nanomaterial-protein interactions in relation to surface reactivity. *ACS Nano*. 2011;5(6):4300-4309. doi:10.1021/nn101492k

Tamez C, Hernandez-Molina M, Hernandez-Viezcas J.A, Gardea-Torresday J.L. Uptake, transport, and effects of nano-copper exposure in zucchini (*Cucurbita pepo*). *Sci Total Environ*. 2019:1-7

Tang Y, He R, Zhao J, Nie G, Xu L, Xing B. Oxidative stress-induced toxicity of CuO nanoparticles and related toxicogenomic responses in *Arabidopsis thaliana*. *Environ Pollut*. 2016;212:605-614. doi:10.1016/j.envpol.2016.03.019

Thompson J, Bannigan J. Cadmium: Toxic effects on the reproductive system and the embryo. *Reprod Toxicol*. 2008;25(3):304-315. doi:10.1016/j.reprotox.2008.02.001

van Werven FJ, Amon A. Regulation of entry into gametogenesis. Philos Trans R Soc B Biol Sci. 2011;366(1584):3521-3531. doi:10.1098/rstb.2011.0081

Vance ME, Kuiken T, Vejerano EP, McGinnis SP, Hochella MF, Hull DR. Nanotechnology in the real world: Redeveloping the nanomaterial consumer products inventory. *Beilstein J Nanotechnol*. 2015;6(1):1769-1780. doi:10.3762/bjnano.6.181

Villani M., Calestani D., Lazzarini L., Zannotto L., Mosca R., Zappettini A. Extended functionality of ZnO nanotetrapods by solution-based coupling with CdS nanoparticles. J. *Mater. Chem*. 2012; 22, 5694

Vogel-Mikuš K, Pongrac P, Kump P, et al. Localisation and quantification of elements within seeds of Cd/Zn hyperaccumulator *Thlaspi praecox* by micro-PIXE. *Environ Pollut*. 2007;147(1):50-59. doi:10.1016/j.envpol.2006.08.026

Wagner M, Briza P, Pierce M, Winter E. Distinct steps in yeast spore morphogenesis require distinct SMK1 MAP kinase thresholds. *Genetics*. 1999;151(4):1327-1340

Wang Y, Lin Y, Xu Y, Yin Y, Guo H, Du W. Divergence in response of lettuce (var. ramosa Hort .) to copper oxide nanoparticles/microparticles as potential agricultural fertilizer . *Environ Pollut Bioavailab*. 2019;31(1):80-84. doi:10.1080/26395940.2019.1578187

Wang Y, Tang M. Review of in vitro toxicological research of quantum dot and potentially involved mechanisms. *Sci Total Environ*. 2018;625:940-962. doi:10.1016/j.scitotenv.2017.12.334

Wang Z, Xu L, Zhao J, Wang X, White JC, Xing B. CuO Nanoparticle Interaction with *Arabidopsis thaliana*: Toxicity, Parent-Progeny Transfer, and Gene Expression. *Environ Sci Technol*. 2016;50(11):6008-6016. doi:10.1021/acs.est.6b01017

Wang, Z., Gerstein, M., Snyder, M., 2009. RNA-Seq: a revolutionary tool for transcriptomics. Nat. Rev. Genet. 10, 57-63

Wani I. A., Ahmad T. Understanding toxicity of Nanomaterials in Biological Systems. In applying nanotechnology for environmental sustainability. *IGI global*. 2017; Sung Hee Joo (University of Miami, USA) (403-427); DOI: 10.4018/978-1-5225-0585-3

Wannige CT, Kulasiri D, Samarasinghe S. A nutrient dependant switch explains mutually exclusive existence of meiosis and mitosis initiation in budding yeast. *J Theor Biol*. 2014;341:88-101. doi:10.1016/j.jtbi.2013.09.030

Wen LY, Chase CD. Mitochondrial gene expression in developing male gametophytes of male-fertile and S male-sterile maize. *Sex Plant Reprod*. 1999;11(6):323-330. doi:10.1007/s004970050159

Wu H, Yin J, Wamer W.G, Zeng M, Lo Y.M. Reactive oxygen species-related activities of nano-iron metal and nano-iron oxides. *J. Food Drug Anal.* 2014; 22, 86–94

Wu T., Tang M. Toxicity of quantum dots on respiratory system. Inhal. Toxicol. 26 (2). 2014; 128e139. https://doi.org/10.3109/08958378.2013.871762

Wyatt LE, Strickler SR, Mueller LA, Mazourek M. An acorn squash (*Cucurbita pepo* ssp. *ovifera*) fruit and seed transcriptome as a resource for the study of fruit traits in Cucurbita. *Hortic Res*. 2015;2(October 2014):1-7. doi:10.1038/hortres.2014.70

Xanthopoulou A, Psomopoulos F, Ganopoulos I, et al. De novo transcriptome assembly of two contrasting pumpkin cultivars. *Genomics Data*. 2016;7:200-201. doi:10.1016/j.gdata.2016.01.006

Xing W., Chen Y., *Wang X., Lv L., Ouyang X., Ge Z., Huang H.* MoS_2 Quantum Dots with a Tunable Work Function for High-Performance Organic Solar Cells. *ACS Appl. Mater. Interfaces*. 2016; *8* (40): 26916–26923

Xun E, Zhang Y, Zhao J, Guo J. Translocation of heavy metals from soils into floral organs and rewards of *Cucurbita pepo*: Implications for plant reproductive fitness. *Ecotoxicol Environ Saf*. 2017;145(January):235-243. doi:10.1016/j.ecoenv.2017.07.045

Yan K, Liu Y, Yang Q, et al. Evaluation of the novel nanoparticle material – CdSe quantum dots on *Chlorella pyrenoidosa* and *Scenedesmus obliquus*: Concentration-time-dependent responses. *Ecotoxicol Environ Saf*. 2019;171(November 2018):728-736. doi:10.1016/j.ecoenv.2019.01.018

Zhai T., Fang X., *Xu J, Zhang Q., Bando Y, Golberg D., Ma Y., Zhai T*. One-dimensional CdS nanostructures: synthesis, properties, and applications. *Nanoscale*. 2010; 2, 168-187

Appendix

Descriptions of genes analyzed by Real time PCR in *S. cerevisiae* (retrieved from SGD)

IME1: master regulator of meiosis that activates transcription of early meiotic genes through interaction with Ume6; Ime1 was degraded by the 26S proteasome following phosphorylation by Ime2

IME2: serine/threonine protein kinase involved in activation of meiosis that associates with Ime1 and mediates its stability; Ime2 activates Ndt80; *IME2* expression is positively regulated by Ime1

RIM4: RNA-binding protein required for the expression of early and middle sporulation genes

NDT80: meiosis-specific transcription factor required for exit from pachytene and for full meiotic recombination; Ndt80 activates middle sporulation genes

SMK1: middle sporulation-specific mitogen-activated protein kinase (MAPK) required for production of the outer spore wall layers

SPO1: meiosis-specific prospore protein required for meiotic spindle pole body duplication and separation; Spo1 was required to produce bending force necessary for proper prospore membrane assembly during sporulation

DIT1: sporulation-specific enzyme required for spore wall maturation involved in the production of a soluble LL-dityrosine-containing precursor of the spore wall; *DIT1* transcripts accumulate at the time of prospore enclosure

DIT2: sporulation-specific N-formyltyrosine oxidase involved in the production of N,N-bisformyl dityrosine, that is required for spore wall maturation, homologous to cytochrome P-450s

SPO20: meiosis-specific subunit of the t-SNARE complex required for prospore membrane formation during sporulation; Spo20 is similar to (but not functionally redundant) with Sec9p and binds to phosphatidic acid

SPS100: protein required for spore wall maturation; expressed during the late stage of sporulation; Sps100 may be a component of the spore wall

List of primers for genes analyzed in *S. cerevisiae*

gene	SGD ID	fw	rev
IME1	SGD:S000003854	CGTTGAAAAATCACCACCGCCA	CTGAAGGAGTAAGCCGCAGCA
IME2	SGD:S000003642	ACGGCCTACGTTTCCACAAGAT	CCACGCACCCGAATGCCCAA
NDT80	SGD:S000001166	GCCATCAATGGCGCAGCCGT	CGAGATGGAGGCCCCAGAGT
SMK1	SGD:S000006258	TGACCAGCTCGCCCTATGACG	CCGAGAGCTGCACGGACGAAT
SPO1	SGD:S000004957	TGGATTATCAGGCGGAAGTTGG	TCCTCTTCAAGGTCCCACTCTT
RIM4	SGD:S000001016	GGCAAAACATTTACAGGGCCAG	GCTTTCCTGCTGGGATCCGC
DIT1	SGD:S000002811	GGTCGATGATGACGTCGTGAG	AGCCAATGGCGTCAACACCAG
DIT2	SGD:S000002810	CGTGCAAGTTGGGGGCGGAA	GCCCCAAGTTTTGGGATCGTG
SPO20	SGD:S000004619	TCACCCAAACTGTCGGTTCGATGA	GTAGCAAGGCCATCCCTTTCG
SPS100	SGD:S000001181	ACGCGGAAGGTAGAGGCACTT	CCTGTGGGCGTTTTGTCTGGT

Gene Ontology enrichment – Roots

CuO NPs up-regulated - Cellular Component		
GO term	**GO class**	**Cluster frequency**
GO:0071944	cell periphery	7.20%
GO:0005829	cytosol	4.80%
GO:0005911	cell-cell junction	2.40%
GO:0009506	plasmodesma	2.40%
GO:0030054	cell junction	2.40%
GO:0055044	symplast	2.40%

CuO NPs up-regulated - Biological Processes		
GO term	**Go class**	**Cluster frequency**
GO:0050896	response to stimulus	14.30%
GO:0019752	carboxylic acid metabolic process	10.30%
GO:0009755	hormone-mediated signaling pathway	2.10%

CuO bulk up-regulted - Biological processes		
GO term	**GO class**	**Cluster frequency**
GO:0043436	oxoacid metabolic process	9.70%
GO:0006082	organic acid metabolic process	9.70%
GO:0019752	carboxylic acid metabolic process	9.40%
GO:0046417	chorismate metabolic process	0.30%

CuSO4 up-regulated - Cellular component		
GO term	**GO class**	**Cluster frequency**
GO:0000785	chromatin	1.50%
GO:0000786	nucleosome	1.20%
GO:0044815	DNA packaging complex	1.20%
GO:0032993	protein-DNA complex	1.20%

CuSO4 up-regulated - Biological processes		
GO term	**GO class**	**Cluster frequency**
GO:0055114	oxidation-reduction process	10.00%

CuO bulk down-regulated - Biological processes		
GO term	**GO class**	**Cluster frequency**
GO:0019538	protein metabolic process	20.10%
GO:0009058	biosynthetic process	16.80%
GO:1901564	organonitrogen compound metabolic process	15.80%
GO:0050896	response to stimulus	13.40%
GO:0006793	phosphorus metabolic process	13.40%
GO:0006810	transport	11.70%
GO:0010467	gene expression	8.80%
GO:0022613	ribonucleoprotein complex biogenesis	5.90%
GO:0019637	organophosphate metabolic process	5.60%
GO:0007154	cell communication	5.40%
GO:0055086	nucleobase-containing small molecule metabolic process	4.80%
GO:0006812	cation transport	3.80%
GO:0019693	ribose phosphate metabolic process	3.70%
GO:1901657	glycosyl compound metabolic process	3.50%
GO:0006091	generation of precursor metabolites and energy	3.30%
GO:0046034	ATP metabolic process	2.90%
GO:0015672	monovalent inorganic cation transport	2.30%
GO:0006818	hydrogen transport	1.90%
GO:0006970	response to osmotic stress	1.60%
GO:0006119	oxidative phosphorylation	1.20%
GO:0009853	photorespiration	0.70%

CuO bulk down-regulated - Cellular component		
GO term	**GO class**	**Cluster frequency**
GO:0043226	organelle	27.50%
GO:0005737	cytoplasm	25.40%
GO:0032991	macromolecular complex	19.40%
GO:0044446	intracellular organelle part	12.10%
GO:1990904	ribonucleoprotein complex	8.10%
GO:0005840	ribosome	7.30%
GO:0005886	plasma membrane	4.90%
GO:1902494	catalytic complex	4.80%
GO:0005739	mitochondrion	4.00%
GO:0031967	organelle envelope	3.40%
GO:0098796	membrane protein complex	2.80%
GO:0005773	vacuole	2.50%
GO:0005774	vacuolar membrane	1.80%
GO:0098798	mitochondrial protein complex	1.30%
GO:1903293	phosphatase complex	1.20%
GO:0015935	small ribosomal subunit	1.00%
GO:0070469	respiratory chain	0.90%
GO:0033176	proton-transporting V-type ATPase complex	0.60%
GO:0030964	NADH dehydrogenase complex	0.60%

CuSO4 down-regulated - Biological processes		
GO term	**GO class**	**Cluster frequency**
GO:0071704	organic substance metabolic process	38.00%
GO:0006807	nitrogen compound metabolic process	26.00%
GO:0009058	biosynthetic process	22.20%
GO:0019538	protein metabolic process	20.20%
GO:0006139	nucleobase-containing compound metabolic process	12.10%
GO:0006412	translation	9.80%
GO:1901135	carbohydrate derivative metabolic process	7.30%
GO:0019637	organophosphate metabolic process	7.10%
GO:0009056	catabolic process	6.60%
GO:0019693	ribose phosphate metabolic process	5.30%
GO:0006811	ion transport	5.10%
GO:0006091	generation of precursor metabolites and energy	4.90%
GO:0046034	ATP metabolic process	4.30%
GO:0008104	protein localization	4.30%
GO:0015672	monovalent inorganic cation transport	3.10%
GO:0006733	oxidoreduction coenzyme metabolic process	2.90%
GO:0005996	monosaccharide metabolic process	2.80%
GO:0010608	posttranscriptional regulation of gene expression	2.70%
GO:0015980	energy derivation by oxidation of organic compounds	2.40%
GO:0098655	cation transmembrane transport	2.20%
GO:0046939	nucleotide phosphorylation	2.10%
GO:0006006	glucose metabolic process	2.10%
GO:0006119	oxidative phosphorylation	2.00%
GO:0006457	protein folding	2.00%
GO:0006094	gluconeogenesis	1.80%
GO:0022900	electron transport chain	1.40%
GO:0051169	nuclear transport	1.40%
GO:0042775	mitochondrial ATP synthesis coupled electron transport	1.10%
GO:0006164	purine nucleotide biosynthetic process	1.10%
GO:0006413	translational initiation	0.70%

CuSO4 down-regulated – Cellular component		
GO term	**GO class**	**Cluster frequency**
GO:0043226	organelle	35.30%
GO:0005737	cytoplasm	33.60%
GO:0032991	macromolecular complex	24.60%
GO:0043231	intracellular membrane-bounded organelle	23.70%
GO:1990904	ribonucleoprotein complex	13.70%
GO:0005840	ribosome	12.60%
GO:0043234	protein complex	9.60%
GO:0005739	mitochondrion	6.70%
GO:0098796	membrane protein complex	3.90%
GO:0043233	organelle lumen	3.70%
GO:0005740	mitochondrial envelope	3.20%
GO:0005783	endoplasmic reticulum	3.10%
GO:0005773	vacuole	2.90%
GO:0031981	nuclear lumen	2.80%
GO:0044391	ribosomal subunit	2.40%
GO:0005774	vacuolar membrane	2.20%
GO:0098798	mitochondrial protein complex	1.80%
GO:1990204	oxidoreductase complex	1.50%
GO:0015935	small ribosomal subunit	1.40%
GO:0015934	large ribosomal subunit	1.00%
GO:0030964	NADH dehydrogenase complex	0.90%
GO:0045259	proton-transporting ATP synthase complex	0.70%
GO:0005852	eukaryotic translation initiation factor 3 complex	0.60%
GO:0070993	translation preinitiation complex	0.60%
GO:0070069	cytochrome complex	0.60%
GO:0022627	cytosolic small ribosomal subunit	0.50%
GO:0033179	proton-transporting V-type ATPase, V0 domain	0.40%

Gene Ontology enrichment – Leaves

CuO bulk up-regulated - Biological processes		
GO term	**GO class**	**Cluster frequency**
GO:0071704	organic substance metabolic process	42.50%
GO:0019538	protein metabolic process	20.70%
GO:0006139	nucleobase-containing compound met. process	12.90%
GO:0005975	carbohydrate metabolic process	8.40%
GO:0022613	ribonucleoprotein complex biogenesis	7.70%
GO:0006412	translation	7.20%
GO:0006520	cellular amino acid metabolic process	6.70%
GO:0006996	organelle organization	6.40%
GO:0006629	lipid metabolic process	5.90%
GO:0009056	catabolic process	5.90%
GO:0009117	nucleotide metabolic process	5.50%
GO:0032787	monocarboxylic acid metabolic process	4.90%
GO:0006508	proteolysis	4.40%
GO:0009628	response to abiotic stimulus	4.20%
GO:0006790	sulfur compound metabolic process	3.60%
GO:0006733	oxidoreduction coenzyme metabolic process	3.30%
GO:0006396	RNA processing	3.20%
GO:0006090	pyruvate metabolic process	2.90%
GO:0015979	photosynthesis	2.80%
GO:0005982	starch metabolic process	2.60%
GO:0019682	glyceraldehyde-3-phosphate metabolic process	2.20%
GO:0071555	cell wall organization	2.10%
GO:0000271	polysaccharide biosynthetic process	2.00%
GO:0006006	glucose metabolic process	1.80%
GO:0006457	protein folding	1.80%
GO:0042440	pigment metabolic process	1.60%
GO:0006970	response to osmotic stress	1.40%
GO:0007010	cytoskeleton organization	1.40%
GO:0010628	positive regulation of gene expression	1.20%
GO:0009668	plastid membrane organization	1.10%
GO:0009651	response to salt stress	1.10%
GO:0030243	cellulose metabolic process	0.80%
GO:0019750	chloroplast localization	0.60%
GO:0072598	protein localization to chloroplast	0.50%
GO:0016129	phytosteroid biosynthetic process	0.40%

CuO bulk up-regulated - Biological processes		
GO term	**GO class**	**Cluster frequency**
GO:0043227	membrane-bounded organelle	27.10%
GO:0016020	membrane	20.40%
GO:0009507	chloroplast	12.50%
GO:0043228	non-membrane-bounded organelle	11.80%
GO:1990904	ribonucleoprotein complex	8.80%
GO:0005840	ribosome	8.10%
GO:0012505	endomembrane system	5.50%
GO:0009532	plastid stroma	5.00%
GO:0005829	cytosol	4.90%
GO:0005886	plasma membrane	4.90%
GO:0009570	chloroplast stroma	4.80%
GO:0009579	thylakoid	4.50%
GO:0009526	plastid envelope	3.80%
GO:0005739	mitochondrion	3.80%
GO:0005794	Golgi apparatus	3.10%
GO:0034357	photosynthetic membrane	2.80%
GO:0005618	cell wall	2.20%
GO:0005773	vacuole	2.20%
GO:0030054	cell junction	2.00%
GO:0031982	vesicle	1.70%
GO:0044391	ribosomal subunit	1.50%
GO:0048046	apoplast	1.50%
GO:0009521	photosystem	1.20%
GO:0015935	small ribosomal subunit	0.90%
GO:0015934	large ribosomal subunit	0.70%
GO:0016469	proton-transporting two-sector ATPase complex	0.60%
GO:0000786	nucleosome	0.60%

CuSO4 up-regulated - Biological processes		
GO term	**GO class**	**Cluster frequency**
GO:1901576	organic substance biosynthetic process	20.20%
GO:0019538	protein metabolic process	17.40%
GO:0006793	phosphorus metabolic process	14.00%
GO:0006139	nucleobase-containing compound met. process	12.50%
GO:0019752	carboxylic acid metabolic process	11.70%
GO:0010467	gene expression	8.90%
GO:0005975	carbohydrate metabolic process	8.30%
GO:0006629	lipid metabolic process	6.90%
GO:0006996	organelle organization	6.40%
GO:0022613	ribonucleoprotein complex biogenesis	5.40%
GO:0032787	monocarboxylic acid metabolic process	5.40%
GO:0009117	nucleotide metabolic process	5.00%
GO:0009628	response to abiotic stimulus	4.60%
GO:0006412	translation	4.50%
GO:0006790	sulfur compound metabolic process	3.90%
GO:0015979	photosynthesis	3.80%
GO:0090407	organophosphate biosynthetic process	3.80%
GO:0006396	RNA processing	3.70%
GO:0006733	oxidoreduction coenzyme metabolic process	3.30%
GO:0006090	pyruvate metabolic process	3.00%
GO:0005982	starch metabolic process	3.00%
GO:0019682	glyceraldehyde-3-phosphate metabolic process	2.80%
GO:0042440	pigment metabolic process	2.30%
GO:0051156	glucose 6-phosphate metabolic process	2.00%
GO:0006457	protein folding	2.00%
GO:0009668	plastid membrane organization	1.50%
GO:0019252	starch biosynthetic process	1.10%
GO:0019750	chloroplast localization	0.90%
GO:0042793	transcription from plastid promoter	0.70%
GO:0031163	metallo-sulfur cluster assembly	0.70%
GO:0072598	protein localization to chloroplast	0.60%
GO:0046471	phosphatidylglycerol metabolic process	0.50%

CuSO4 up-regulated – Cellular component		
GO term	**GO class**	**Cluster frequency**
GO:0043226	organelle	32.10%
GO:0005737	cytoplasm	30.30%
GO:0016020	membrane	18.90%
GO:0032991	macromolecular complex	15.70%
GO:0009507	chloroplast	15.20%
GO:0009532	plastid stroma	6.20%
GO:0009579	thylakoid	5.70%
GO:1990904	ribonucleoprotein complex	5.60%
GO:0005840	ribosome	4.80%
GO:0009941	chloroplast envelope	4.60%
GO:0034357	photosynthetic membrane	3.90%
GO:0098796	membrane protein complex	2.80%
GO:0009523	photosystem II	1.20%
GO:0009522	photosystem I	0.90%
GO:0044391	ribosomal subunit	0.90%
GO:0009295	nucleoid	0.50%

CuO bulk down-regulated - Cellular component		
GO term	**GO class**	**Cluster frequency**
GO:0008287	protein serine/threonine phosphatase complex	1.10%
GO:1903293	phosphatase complex	1.10%
GO:0005777	peroxisome	1.00%
GO:0042579	microbody	1.00%

CuO bulk down-regulated - Biological processes		
GO term	**GO class**	**Cluster frequency**
GO:0050896	response to stimulus	12.80%
GO:0051179	localization	12.20%
GO:0051234	establishment of localization	12.00%
GO:0006810	transport	11.80%
GO:0036211	protein modification process	10.90%
GO:0009628	response to abiotic stimulus	4.20%
GO:0016311	dephosphorylation	2.30%
GO:0001101	response to acid chemical	2.30%
GO:0006470	protein dephosphorylation	2.10%
GO:0007034	vacuolar transport	0.90%

CuSO4 down-regulated - Biological processes		
GO term	**GO class**	**Cluster frequency**
GO:0051179	localization	12.90%
GO:0051234	establishment of localization	12.70%
GO:0006810	transport	12.50%
GO:0050896	response to stimulus	12.40%
GO:0055085	transmembrane transport	5.00%
GO:0006811	ion transport	4.70%
GO:0023052	signaling	4.70%

CuSO4 down-regulated - Cellular component		
GO term	**GO class**	**Cluster frequency**
GO:0005623	cell	35.80%
GO:0044464	cell part	35.20%
GO:0005622	intracellular	32.60%
GO:0005737	cytoplasm	20.30%
GO:0005777	peroxisome	1.00%
GO:0042579	microbody	1.00%

Gene Ontology enrichment – Pollen

CuO bulk up-regulated - Biological processes		
GO term	**GO class**	**Cluster frequency**
GO:0005975	carbohydrate metabolic process	12.40%
GO:0016310	phosphorylation	11.30%
GO:0019637	organophosphate metabolic process	9.20%
GO:0006811	ion transport	6.20%
GO:0046034	ATP metabolic process	6.10%
GO:0051186	cofactor metabolic process	5.70%
GO:0005982	starch metabolic process	4.50%
GO:0005984	disaccharide metabolic process	4.20%
GO:0005985	sucrose metabolic process	4.10%
GO:0046496	nicotinamide nucleotide metabolic process	3.50%
GO:0045333	cellular respiration	3.20%
GO:0015992	proton transport	3.20%
GO:0006094	gluconeogenesis	3.00%
GO:0098660	inorganic ion transmembrane transport	2.80%
GO:0006119	oxidative phosphorylation	2.20%
GO:1902600	hydrogen ion transmembrane transport	2.20%
GO:0006099	tricarboxylic acid cycle	2.10%
GO:0006012	galactose metabolic process	1.60%
GO:0015977	carbon fixation	1.10%

CuO bulk up-regulated - Cellular component		
GO term	**GO class**	**Cluster frequency**
GO:0005737	cytoplasm	24.40%
GO:0016020	membrane	20.40%
GO:0005739	mitochondrion	5.30%
GO:0031090	organelle membrane	5.00%
GO:0005773	vacuole	3.30%
GO:0005740	mitochondrial envelope	2.80%
GO:0005743	mitochondrial inner membrane	2.10%
GO:0048046	apoplast	2.10%
GO:0016469	proton-transporting two-sector ATPase complex	1.70%
GO:0070469	respiratory chain	1.50%
GO:0098800	inner mitochondrial membrane protein complex	1.40%
GO:0033178	proton-transporting two-sector ATPase complex, catalytic domain	0.90%
GO:0005753	mitochondrial proton-transporting ATP synthase complex	0.80%

CuOSO4 up-regulated – Biological processes		
GO term	**GO class**	**Cluster frequency**
GO:1901564	organonitrogen compound metabolic process	15.40%
GO:0043436	oxoacid metabolic process	12.00%
GO:0006082	organic acid metabolic process	12.00%
GO:0019752	carboxylic acid metabolic process	11.60%
GO:0005975	carbohydrate metabolic process	10.80%
GO:0009056	catabolic process	7.90%
GO:0009259	ribonucleotide metabolic process	4.70%
GO:0046034	ATP metabolic process	4.40%
GO:0015980	energy derivation by oxidation of organic compounds	2.90%
GO:0006006	glucose metabolic process	2.70%
GO:0045333	cellular respiration	2.40%
GO:0006099	tricarboxylic acid cycle	1.70%
GO:0006101	citrate metabolic process	1.70%
GO:0009060	aerobic respiration	1.70%
GO:0072350	tricarboxylic acid metabolic process	1.70%

CuSO4 up-regulated - Cellular component		
GO term	**GO class**	**Cluster frequency**
GO:0005737	cytoplasm	23.50%
GO:0031090	organelle membrane	5.20%
GO:0005739	mitochondrion	4.70%
GO:0098588	bounding membrane of organelle	3.50%
GO:0005773	vacuole	3.10%
GO:0005740	mitochondrial envelope	2.50%
GO:0005774	vacuolar membrane	2.50%
GO:0031966	mitochondrial membrane	2.30%
GO:0005743	mitochondrial inner membrane	1.70%
GO:0016469	proton-transporting two-sector ATPase complex	1.30%